DD&T

Drug Discoveries & Therapeutics

IRCA BSSA

IACMHR

www.ddtjournal.com

Drug Discoveries & Therapeutics is one of a series of peer-reviewed journals of the International Research and Cooperation Association for Bio & Socio-Sciences Advancement (IRCA-BSSA) Group and is published bimonthly by the International Advancement Center for Medicine & Health Research Co., Ltd. (IACMHR Co., Ltd.) and supported by the IRCA-BSSA and Shandong University China-Japan Cooperation Center for Drug Discovery & Screening (SDU-DDSC).

Drug Discoveries & Therapeutics publishes contributions in all fields of pharmaceutical and therapeutic research such as medicinal chemistry, pharmacology, pharmaceutical analysis, pharmaceutics, pharmaceutical administration, and experimental and clinical studies of effects, mechanisms, or uses of various treatments. Studies in drug-related fields such as biology, biochemistry, physiology, microbiology, and immunology are also within the scope of this journal.

Drug Discoveries & Therapeutics publishes Original Articles, Brief Reports, Reviews, Policy Forum articles, Case Reports, News, and Letters on all aspects of the field of pharmaceutical research. All contributions should seek to promote international collaboration in pharmaceutical science.

Editorial Board

Drug Discoveries & Therapeutics

Editorial and Head Office

Pearl City Koishikawa 603, 2-4-5 Kasuga, Bunkyo-ku,
Tokyo 112-0003, Japan

Tel: 03-5840-9697, Fax: 03-5840-9698
E-mail: office@ddtjournal.com
URL: www.ddtjournal.com

Editorial Board Members

(*As of February 2011*)

CONTENTS

Volume 5, Number 1, 2011

Editorial

Review

Brief Report

Original Articles

CONTENTS   (*Continued*)

Guide for Authors

Copyright

Editorial

Drug Discoveries & Therapeutics: A platform for promoting pharmaceutical sciences and clinical therapeutics

Yun Yen

Co-Editor-in-Chief
Drug Discoveries & Therapeutics

Yun Yen, *M.D., Ph.D.*
Professor and Chair of Molecular Pharmacology
City of Hope Beckman Center
Duarte, CA, USA
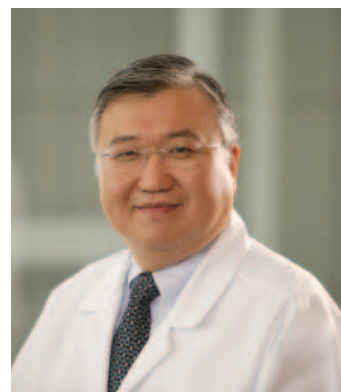
In 2011, the world is filled with both challenges and opportunities across disciplines. Around the world, all look for opportunities to improve the economy by investing in eco-industry as well as biotechnology. Within biotechnology, drug discovery and therapeutics remain the mainstays of biomedical research.

Drug discovery bridges the gap between pre-clinical research and clinical therapeutics to benefit human health. The three main tenets of drug discovery and therapeutics, molecular diagnostics, targeted therapy, and personalized medicine, will be our focuses as well in *Drug Discoveries & Therapeutics* in the present and near future. To do so, *Drug Discoveries & Therapeutics* must welcome new topics that align themselves with traditional areas of research in drug development and therapeutics. We must continue to emphasize topics on biomarker-guided therapies in proteomics, metabolomics, genomics, and genetics as well as up-and-coming areas of research such as autophagy, exosomes, and RNA spliceosomes. Research on small molecules, peptides, monoclonal antibodies, nano-particles, will and should be covered by this journal's scope alongside pharmacokinetics, pharmacodynamics, and drug delivery systems.

The journal will continue to invite outstanding review articles, original research papers, and frontier discoveries, while simultaneously attracting a greater readership. Our immediate goal is to become a leading authority in the biomedical research field of drug discovery and therapeutics. Allongside editorial colleagues, I will continue to bring high quality, efficient publications to our readership.

(February 5, 2011)

c-Met: A potential therapeutic target for hepatocellular carcinoma

Jianjun Gao[1,2], Yoshinori Inagaki[1], Xia Xue[2], Xianjun Qu[2], Wei Tang[1,2,*]

[1] *Hepato-Biliary-Pancreatic Surgery Division, Department of Surgery, Graduate School of Medicine, The University of Tokyo, Tokyo, Japan;*
[2] *School of Pharmaceutical Sciences, Shandong University, Ji'nan, China.*

ABSTRACT: The approval of receptor tyrosine kinase (RTK) targeted agent sorafenib as the first effective drug for the systemic treatment of advanced hepatocellular carcinoma (HCC) represents a milestone in the treatment of this disease. A better understanding of HCC pathogenesis will lead to development of novel targeted treatments. As a typical member of the RTK family, c-Met represents an intriguing target for cancer therapy. The c-Met signaling pathway has been shown to be deregulated and to correlate with poor prognosis in a number of major human cancers. This review discusses the possibility of c-Met as a target in HCC treatment from the following respects: *i*) c-Met expression and activation profile in HCC, *ii*) relationship between c-Met and clinicopathologic state and prognosis of HCC, *iii*) role of c-Met signaling activity in HCC genesis and progression, and *iv*) strategy of c-Met pathway targeting therapy in HCC treatment.

Keywords: Receptor tyrosine kinases, cancer therapy, clinicopathological features, prognosis, hepatocellular carcinoma

1. Introduction

Liver cancer ranked fifth in incidence and third in mortality in global cancer burden in 2008 according to the statistics published by World Health Organization (*1*). Among the diverse, histologically distinct primary hepatic neoplasms, hepatocellular carcinoma (HCC) is the most common type of liver cancer, accounting for 83% of all cases (*2*). Therapeutic approaches including hepatic resection, liver transplantation, and loco-regional therapies play a major role in the clinical management of HCC (*3*). In recent years, introduction of molecular

Address correspondence to:
Dr. Wei Tang, Hepato-Biliary-Pancreatic Surgery Division, Department of Surgery, Graduate School of Medicine, The University of Tokyo, 7-3-1 Hongo, Bunkyo-ku, Tokyo 113-8655, Japan.
e-mail: TANG-SUR@h.u-tokyo.ac.jp

targeted therapies has opened new prospects in treatment of HCC. Systemic treatment with sorafenib, a multikinase inhibitor targeting Raf kinase and receptor tyrosine kinases (RTKs) including platelet-derived growth factor receptor (PDGFR), vascular endothelial growth factor (VEGF) receptor (VEGFR) and c-kit (receptor specific for stem cell factor), is recommended for patients at a more advanced stage of HCC (*4*). In addition, several other RTKs targeted drugs such as evacizumab, erlotinib, gefitinib, lapatinib, cetuximab, sunitinib, and brivanib have entered into clinical trials for treatment of advanced HCC (*5*). These studies illustrate the utility of targeting the protein class RTKs in HCC management.

c-Met is a prototypic member of RTKs. The ligand for c-Met is a growth factor known as hepatocyte growth factor (HGF) (*6*). c-Met signaling pathway is involved in diverse cellular responses such as mitogenesis, motogenesis, or morphogenesis depending on the particular cell type and the microenvironment (*7,8*). In circumstances of tissue removal or damage such as liver regeneration or renal and lung injury, c-Met expression is induced as an important mediator in the wound healing and tissue repair processes (*9-11*). Deregulation and activation of c-Met may result in unregulated cell growth and differentiation, contributing to malignant transformation (*12*). c-Met overexpression or enhanced activation relative to normal tissues is demonstrated in several human cancers including gastric, colorectal, pancreatic, lung, head and neck, ovarian, renal, glioma, melanoma, prostatic and breast carcinoma (*13-15*). This review provides a systematic retrospective about the role of c-Met in HCC pathogenesis and discusses the possibility of molecular targeting of c-Met as a potential therapeutic strategy for HCC.

2. c-Met expression and activation profile in HCC

2.1. *c-Met expression*

c-Met expression in human HCC and non-HCC liver tissues was examined in a number of studies in the past twenty years. c-Met positive rates and expression levels in HCCs are usually higher than those in normal or adjacent non-tumorous liver tissue either at the mRNA or protein level (Tables 1 and 2) (*16-30*). These studies

Table 1. c-Met positive rates in human HCC and non-HCC liver tissues in various studies

Authors	Level	HCC tissues			Non-HCC tissues		
		Sample tested (*n*)	Positive (*n*)	Positive rate (%)	Sample tested (*n*)	Positive (*n*)	Positive rate (%)
Annen (*16*)	protein	18	12	66.7	18[a]	8	44.4
Xie *et al.* (*17*)	protein	47	18	38.3	25[b]	3	12.0
Wu *et al.* (*18*)	protein	25	21	84.0	25[c]	5	20.0
	mRNA	25	25	100.0	25[c]	6	24.0
Ueki *et al.* (*19*)	protein	62	40	64.5	62[d]	4	6.4
Ljubimova *et al.* (*22*)	protein	6	6	100.0	9[e]	9	100.0
	mRNA	12	10	83.3	30[f]	13	43.3
Chau *et al.* (*20*)	protein	40	35	87.5	40[g]	34	85.0
Kiss *et al.* (*21*)	protein	86	83	96.5	86[h]	86	100.0
D'Errico *et al.* (*26*)	protein	20	20	100.0	10[i]	10	100.0

[a] adjacent non-cancerous tissues; [b] adjacent non-cancerous tissues; [c] adjacent non-cancerous tissues; [d] adjacent non-cancerous tissues; [e] 3 normal, 3 HCV, and 3 alcoholic liver disease (ALD) cirrhotic specimens; [f] 7 normal, 9 HCV cirrhosis, 8 ALD, 4 ALD/HCV, 2 liver adenoma specimens; [g] adjacent non-cancerous tissues; [h] adjacent non-cancerous tissues; [i] 5 focal nodularhyperplasias, 4 fulminant hepatitis, 1 regenerated liver.

Table 2. Expression levels of c-Met in human HCC and non-HCC liver tissues

Authors	Level	c-Met expression	Method of detection
Ueki *et al.* (*19*)	protein	The mean expression level of c-Met was significantly higher in HCC tissues than in non-tumorous tissue.	Western blot
Kiss *et al.* (*21*)	protein	Overexpression in 20% of 86 HCC specimens when compared to the surrounding hepatic tissue.	Immunohistochemistry
Ljubimova *et al.* (*22*)	protein	In normal liver the staining intensity was usually weaker compared with HCC and some areas of cirrhotic livers.	Immunohistochemistry
Osada *et al.* (*23*)	protein	Expression at higher levels in 19 of 30 HCCs compared with non-tumorous tissue.	Western blot
Suzuki *et al.* (*24*)	protein	Detection in 16 of 23 patients (69.6%), overexpression in HCC compared with the surrounding normal liver.	Immunohistochemistry
	mRNA	c-Met mRNA was detected in 6 of 19 HCCs (31.6%); c-Met mRNA was overexpressed in HCC compared with the surrounding normal liver.	Northern blot
Zhang *et al.* (*25*)	protein	9 of the 20 HCCs exhibited c-Met overexpression, with an increase ranging between 2- and 7-fold when compared by densitometry with the surrounding non-tumor liver.	Immunohistochemistry
D'Errico *et al.* (*26*)	protein	The c-Met protooncogene product was expressed in all cases (20 HCCs, 5 focal nodularhyperplasias, 4 fulminant hepatitis, 1 regenerated liver), with marked overexpression in the HCCs.	Immunohistochemistry
Osada *et al.* (*27*)	protein	The mean value of c-Met in tumor tissue, 1.36 ± 0.12*, was clearly higher than in non-tumor tissue, 1.07 ± 0.06*. Data was obtained from specimens of 30 HCC patients.	Western blot
Boix *et al.* (*28*)	mRNA	c-Met overexpressed in 8 of 18 HCCs, with an increase ranging between 2- and 10-fold when compared by densitometry with the surrounding liver.	Northern blot
Noguchi *et al.* (*29*)	mRNA	Overall level of c-Met mRNA was significantly higher in HCC tissues than that in non-HCC surrounding regions (0.41 ± 0.20 *vs.* 0.08 ± 0.02 pg/μg total RNA) in 11 HCC specimens.	Competitive RT-PCR
Okano *et al.* (*30*)	protein	The expression of c-Met protein was higher in patients with HCC and acute hepatitis than in those with chronic hepatitis.	Immunohistochemistry

* The expression level of c-Met was presented as the optical density (OD) ratio of c-Met/β-actin.

suggested that c-Met expression, at least in part, was deregulated in the genesis and progression of HCC.

2.2. *Mechanisms underlying aberrant c-Met expression in HCC*

Mechanisms involved in c-Met aberrant expression are commonly found in the following repects.

Inducible endogenous or exogenous factors c-Met gene expression is inducible by its own ligand HGF (*31*). Besides HGF, other cytokines including epidermal growth factor (EGF), interleukin (IL)-1, IL-6, and tumor necrosis factor-α can induce c-Met expression in HCC cells *in vitro* (*31*). In HepG2 cells, *c-Met* gene promoter activity was up-regulated when treated with HGF, IL-1, and IL-6. The activator protein (AP)-1 was considered to participate in HGF and IL-6-induced *c-Met* gene transcription (*31,32*). In addition to the above endogenous

factors, hepatitis B virus X protein (HBX) which acted as a weak to moderately strong transcriptional transactivator was proven to be an exogenous inducible factor for c-Met expression (*33*). Activation of transcription factors AP-2 and specificity protein (SP)-1 at the promoter region of the *c-Met* gene contributed to transcriptional regulation of c-Met expression by HBX (*33*).

MicroRNAs (miRNAs) miRNAs are small RNA molecules which are approximately 22 nucleotides long and negatively control their target genes expression posttranscriptionally (*34*). miRNAs including miR-34a, miR-23b and miR-199a-3p targeting c-Met are dysregulated in HCC tissues (*35*). Li *et al.* demonstrated that down-regulation of miR-34a expression was highly significant in 19 of 25 (76%) HCC tissues compared with adjacent normal tissues and an inverse correlation between miR-34a and c-Met expression was observed in resected normal/tumor tissues (*36*). miR-23b was found down-regulated in 82% (14/17) HCC tissues compared with adjacent non-HCC tissues as indicated by Salvi *et al.* (*37*). Similarly, a significant down-regulation of miR-199a-3p expression was observed in HCC tissues (*38*). Thus, overexpression of c-Met may be partially ascribed to down-regulaton of miRNAs targeting c-Met in HCC.

Amplified maturation process During the maturation of c-Met, the primary single chain precursor protein (p170^{met}) is cleaved to produce the α subunit (p50^{met}) and β subunit (p140^{met}) which are disulfide linked to form the mature receptor (*6*). This process is probably amplified in carcinogenesis of the liver. Annen *et al.* showed that expression of p170^{met} precursor was significantly higher in non-cancerous regions than in cancerous regions, while the p140^{met} signal was obviously stronger in cancerous regions than in non-cancerous regions. These results imply that the processing pathway from the pro-receptor to the mature receptor is possibly facilitated in HCC (*16*).

2.3. *c-Met activation*

The classical mode of c-Met activation requires the binding of HGF to c-Met. In addition to this HGF-dependent form, an HGF-independent pattern of c-Met activation, especially found in tumor development, has also been reported.

2.3.1. *HGF-dependent activation*

Under physiological conditions, c-Met expression is mainly observed in the epithelial compartment of various tissues, while its ligand HGF is expressed in cells of mesenchymal origin (*39,40*). Accordingly, HGF and c-Met constitute a paracrine signaling system which plays a critical role in development and organogenesis (*40*). In normal human liver, HGF was detected in bile duct epithelia and in endothelial cells of both the central-lobular vein and portal tract vessels whereas c-Met was identified in mature hepatocytes (*41-43*). In HCC, a somewhat different

Table 3. c-Met mutations detected in HCC

Exon	Codon	Nucletide	Amino acid
17	1191	ACT → ATT	Thr → Ile
19	1268	ATG → ATA	Met → Ile
19	1262	AAG → AGG	Lys → Arg

scenario exists. In addition to paracrine activation, intracytoplasmic positivity for HGF was also evident in a large number of neoplastic cells in some cases of HCCs, which supported that an autocrine pattern of action of HGF also existed in HCC (*19,26*). Thus, c-Met can be activated in both autocrine and paracrine patterns in HCC.

2.3.2. *HGF-independent activation*

In addition to the HGF-dependent pattern, c-Met activation can occur through alternative mechanisms in HCCs including: *i*) active mutants of c-Met constitutively phosphorylating the downstream kinases; *ii*) activation by cell attachment; *iii*) transactivation by EGF receptor (EGFR); and *iv*) activation by des-γ-carboxy prothrombin (DCP).

Mutations that either promote receptor dimerization/oligomerization or alter catalytic activity or substrate specificity, would possibly activate RTKs. Constitutive activating mutations of c-Met may play an important role in the development of HCC by conferring cells a selective growth advantage. In HCC, three missense mutations K1262R, M1268I, and T1191I in the tyrosine kinase domain were exclusively detected in childhood HCCs (Table 3) (*44*). Missense mutations K1262R and M1268I in the kinase domain of c-Met are located in a specific region which is believed to act as an intramolecular substrate that, in the absence of ligand, functions to inhibit enzymatic activity by blocking the active site (*44*). It is speculated that these mutations stimulate the kinase activity of c-Met by altering the structure of the intramolecular substrate such that it is constitutively disengaged from the active site (*44*).

A mechanism of activation of c-Met that did not rely on mutation but depended on cell adhesion was demonstrated by Wang *et al.* (*45*). In their study, overexpression of the human wild-type c-Met which could not respond to murine HGF but was enzymatically active in mice hepatocytes allowed activation of the receptor (*46,47*). The activation of c-Met in this case was considered to be dependent on cell adherence, but not HGF (*45*). Furthermore, this style of activation might depend on overexpression of c-Met (*45*). These results indicate that cell adherence may be an alternative activation mechanism for tumor development in cancers related to hyperactivation or overexpression of wild-type tyrosine kinase receptors.

Cross-talk can occur between different growth factor receptors, which may induce mitogenic or motogenic

signal amplification. EGFR exists on the cell surface and is activated by binding of its specific ligands including EGF and transforming growth factor α (TGFα) (*48*). It has been shown that cross-talk between c-Met and EGFR occur in HCC. HCC cell lines expressing TGFα in an autocrine manner displayed constitutive phosphorylation of EGFR and c-Met in the absence of HGF (*49*). The association between these two receptors was demonstrated to happen either directly, or *via* adapter molecules, before or during tumorigenesis, and might enable TGFα or EGF to phosphorylate c-Met through EGFR (*49*).

DCP is employed as a tumor marker in the clinic for its high sensitivity and specificity in the screening and diagnosis of HCC (*50-52*). Two kringle domains in the structure of DCP are similar to those of HGF which are considered to be mandatory for HGF to bind to c-Met (*53*). Based on this similarity, DCP binds and induces the phosphorylation of c-Met (*54*). However, the manner of activation of c-Met by DCP is different from that by HGF. Tyrosines-1234 and -1235 in the tyrosine kinase domain and tyrosines-1349 and -1356 in the multifunctional docking site were phosphorylated when c-Met was activated by HGF (*55-57*). However, when binding DCP to c-Met phosphorylation occurred in those tyrosine residues located in the kinase activation loop (Tyr1234/1235) but not in the C-terminal tail (Tyr1349) (*54*).

3. c-Met as an indicator for clinicopathologic state and prognosis of HCC

3.1. *c-Met and clinicopathologic characteristics of HCC*

The relationship between c-Met protein expression in HCC tissues and clinicopathologic characteristics is indicated in Table 4. Generally, tumor proliferative index was high in HCCs with c-Met expression (*24,26*). In addition, HCCs with multiple nodular tumors showed higher c-Met expression (*58*). On the other hand, no relevance was observed between c-Met expression and serum alpha fetoprotein (AFP) level, sex, or age (*17,19,30,58*). Conflicting results were reported regarding characteristics such as tumor size, differentiation degree, stage, invasion, and metastasis

(*17,19,24,26,27,30,58*). However, characteristics like tumor invasion and metastasis, and differentiation degree were more frequently reported to be correlated with c-Met expression. In those studies, level of c-Met expression was significantly higher in invasive or poorly differentiated HCCs. With respect to tumor size, most studies suggested it was unrelated to c-Met expression. When referring to tumor stage, contradictory results were obtained by Ke *et al.* and Xie *et al.* (*17,58*). The former study demonstrated that c-Met expression was obviously higher in advanced HCCs (TNM stage III or IV), whereas the latter one indicated that no difference of c-Met expression existed in early and advanced stages of HCCs. The sample size which is 520 in the former study and 20 in the latter study may influence the consistency of results. Taken together, the expression of c-Met in HCC may be important to evaluate the status of this disease, especially to caution for tumor cells actively proliferating and the presence of intrahepatic metastasis or multiple nodular tumors.

3.2. *c-Met and prognosis of HCC*

Currently much work is underway to determine molecular predictors of the outcome of HCC (*59*). Expression of c-Met in HCC tissue was considered to be one of the independent prognostic factors indicating metastasis and recurrence in patients with HCC (*60*). Patients with high c-Met expression HCC usually had a significantly shorter 5-year survival than patients with low c-Met expression HCC after curative surgical resections (*19*). In addition, the sustained high level of serum HGF after hepatectomy was suggested to be related to early tumor recurrence and metastasis (*18*). Using transcriptome analysis, a group of HCCs (27%) with potentially activated c-Met signaling were classified based on a c-Met induced transcription signature (*61*). These tumors were characterized by higher vascular invasion rate, increased microvessel density, and shortened survival. Moreover, a predictive model was established according to *c-Met* gene signatures, which was able to diversify HCC patients into good and bad prognostic groups with 83-95% accuracy (*61*). These results suggest that expression and

Table 4. The relationship between c-Met protein expression and clinicopathologic characteristics of HCC

Studies	No. of cases	Tumor size	Proliferation activity	Differentiation degree	Tumor stage	Invasion and metastasis	Sex	Age	Serum AFP level
Xie *et al.* (*17*)	47	--	ND	+	--	+	--	--	ND
Ueki *et al.* (*19*)	62	--	ND	--	ND	+	--	--	ND
Suzuki *et al.* (*24*)	23	ND	NS	+	ND	ND	ND	ND	ND
D'Errico *et al.* (*26*)	50	ND	+	+	ND	ND	ND	ND	ND
Osada *et al.* (*27*)	30	ND	ND	ND	ND	+	ND	ND	ND
Okano *et al.* (*30*)	26	--	ND	--	ND	--	ND	ND	--
Ke *et al.* (*58*)	520	+	ND	+	+	+	--	--	--

ND: not determined; NS: not significant; +: positive; --: negative.

activation of c-Met in HCC tissues indicate an adverse prognosis for HCC patients.

4. c-Met signaling in HCC tumorigenesis and progression

Signal transduction is the communication process utilized by regulatory cytokines to mediate essential cell processes (including growth, differentiation, and survival) in response to stimuli. Enhanced signal transduction may lead to increased cell proliferation, sustained angiogenesis, tissue invasion and metastases, and inhibition of apoptosis during tumor development and progression. On the other hand, blocking tumor-dependent signal transduction pathways might slow down tumor progression.

4.1. *c-Met signaling in HCC*

The c-Met protein is first synthesized in the hepatocytes as a single chain precursor (p170^{met}), and then processed to a mature glycosylated heterodimer receptor (p190^{met}) which consists of an extracellular α subunit (p50^{met}) and a transmembrane β subunit (p140^{met}) (*6,62*). The β subunit has a protein kinase domain and a docking site for cell-signaling molecules (*55,63*). c-Met signal transduction involved in HCC is illustrated in Figure 1. When activated by HGF, the intracellular tyrosine kinase domain of c-Met is highly phosphorylated at two tyrosine residues (Tyr-1234 and Tyr-1235) that are essential for the catalytic activity of the enzyme (*64,65*). Phosphorylation also occurs at two tyrosine residues (Tyr-1349 and Tyr-1356) located in the
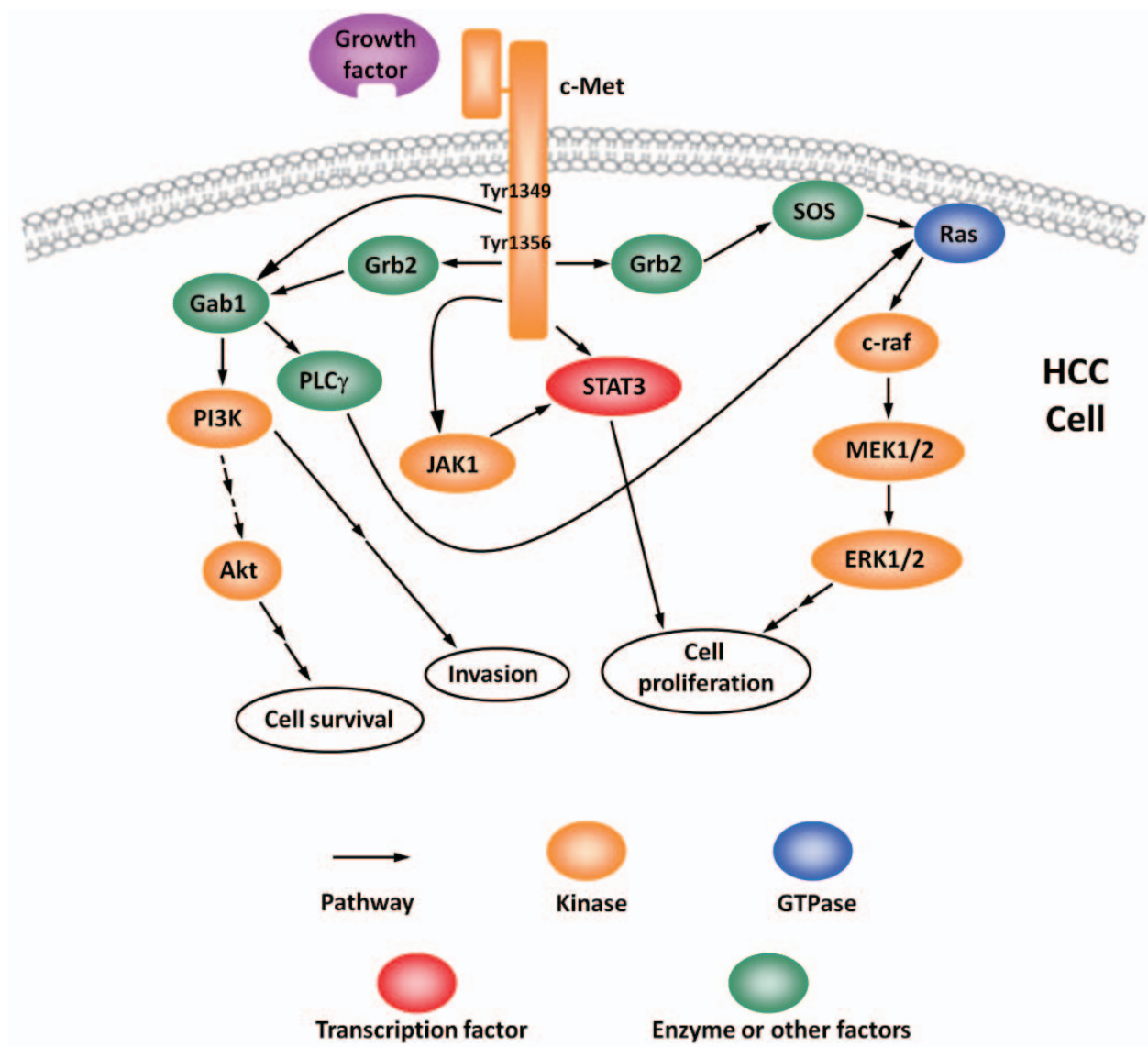

Figure 1. Schematic representation of the c-Met signaling pathway suggested in HCC cells. The activation of c-Met in HGF-dependent and/or HGF-independent ways induces phosphorylation of specific tyrosine residues within the c-Met intracellular domain and, in turn, initiates activation of the downstream signaling cascades.

carboxyl-terminal region of the β-subunit which acts as a multifunctional docking site and binds numerous srchomology 2 (SH2) domain-containing effectors such as the growth factor receptor-bound protein 2 (Grb2) and transcription factor STAT3 (*55,66,67*). Upon phosphorylation, this docking motif can also associate with Grb2-associated binding protein 1 (Gab-1), a multi-adaptor protein that provides binding sites for molecules such as phosphatidylinositol 3 kinase (PI3K) and phospholipase Cγ1 (PLCγ1) (*68*). It was suggested that Gab-1 interacted with the c-Met multifunctional docking site both directly and indirectly (*68*). On one side, Gab1 might interact directly with tyrosine-1349 of c-Met. On the other side, Gab1 indirectly associated with c-Met, in which Grb2 acted as an adapter by binding tyrosine-1356 of c-Met with the SH2 domain and the proline rich sequences of Gab1 with the srchomology 3 (SH3) domain (*68*). Downstream of adaptors the regulation of cell proliferation, invasion and metastasis by c-Met was related with extracellular signal-regulated protein kinase (ERK) and PI3K pathways. In addition, Suzuki *et al*. demonstrated DCP induced the JAK1-STAT3 signaling pathway, while it did not affect the ERK or PI3K pathway (*54*).

4.2. *Role of c-Met signaling in hepatocarcinogenesis*

As the natural ligand of c-Met, HGF is a potent mitogen for hepatocytes and various epithelial cells and activation of the ERK pathway plays an important role in the regulation of cell proliferation by HGF (*69*). That c-Met signaling is involved in hepatocarcinogenesis is evidenced by the fact that c-Met transgenic mice would develop HCC (*45*). In these mice, inactivation of the transgene led to regression of even highly advanced tumors, apparently mediated by apoptosis and cessation of cellular proliferation (*45*). HCC could also be initiated by hydrodynamic transfection of c-Met in combination with constitutively active versions of β-catenin into the livers of adult mice (*70*). Inactivation of c-Met transgene led to regression of hepatocellular carcinomas despite the persistence of activated β-catenin. The tumors eventually recurred in the absence of c-Met expression, however, presumably after the occurrence of one or more events that cooperated with activated β-catenin in lieu of c-Met (*70*). These studies implied that enhanced c-Met signal transduction played a critical role in the malignant transformation of normal hepatocytes.

4.3. *Role of c-Met signaling in HCC invasion and metastasis*

Tumor metastasis is a continuous dynamic process involving releasing of tumor cells, their migrating and crossing the blood vessel barriers, and colonizing at distant sites. The motility of HCC cell lines (Hep3B,

HepG2, PLC, and Huh-7) and HCC cells harvested from patients was stimulated by HGF (*71*). Tyrosine phosphorylation of c-Met and activation of PI3K were regarded to play a critical role in these processes (*71*). Neaud *et al*. showed that addition of human liver myofibroblasts (MF) conditioned medium induced cell scattering and increased about 100-fold the ability of HepG2 to invade Matrigel, and that the HGF secreted by MF played a critical role in these processes (*72*). Up-regulating of urokinase type plasminogen activator (uPA) induced by c-Met signaling was thought to contribute to the invasion and metastasis of HCC cells (*73*). Angiogenesis is the physiological process involving the growth of new blood vessels from pre-existing vessels, which is a fundamental step in the transition of tumors from a dormant state to a malignant one. Enhanced angiogenesis was observed in HCCs developed in HGF transgenic mice in which expression of VEGF was up-regulated in parallel with HGF transgene expression (*74*). Moreover, HGF as well as inducible nitric oxide synthase are involved in multidrug resistance (MDR) induced angiogenesis in HCC cell lines (*75*). Thus, HGF/c-Met signaling is possibly implicated in HCC metastasis through promoting cell motility, stimulating protease production that facilitates cellular invasion and strengthening angiogenesis which helps HCC cells colonize in other organs.

5. The strategy of c-Met signaling targeting therapy for HCC treatment

Based on the current understanding of the c-Met pathway in HCC, several strategies to intervene in the pathway could be proposed at different levels: *i*) inhibition of HGF expression or activity; *ii*) inhibition of c-Met expression or kinase activity; and *iii*) interference with downstream effector functions.

Even though HGF is a potent mitogen for hepatocytes, the effect of HGF on the growth of HCC cells is controversial. In addition to stimulating HCC cells proliferation, HGF also exhibits anti-proliferative effects on HCC cells (*76*). Besides that, both HCC stimulatory and inhibitory effects of exogenous administration of HGF on carcinogen-treated rats have been reported (*77-79*). There are also conflicting reports in HGF transgenic mice. Mice harboring a full-length mouse HGF cDNA under the control of the mouse metallothionein gene promoter induced liver tumors, which arose spontaneously in six independent transgenic lines after 17 months (*80*). In contrast, overexpression of a human HGF cDNA under the regulation of the albumin promoter in transgenic mice did not induce HCC (*81*). Moreover, the HGF transgene appeared to inhibit hepatocarcinogenesis in bitransgenic mice overexpressing c-Myc or TGF-α (*82*). In addition, D'Errico *et al*. reported that liver HGF did not always correlate with hepatocellular proliferation in human HCC, while its specific receptor c-Met did (*26*). Therefore,

whether or how HGF participates in hepatocarcinogenesis remains to be clarified. Subsequently the feasibility of HGF targeting therapies for HCC treatment needs to be futher studied.

The antitumor effects of reducing and/or silencing of c-Met expression in HCC cells using antisense or RNAi sequences targeting c-Met mRNA have been examined in various studies (*25,36-38,83,84*). These studies showed that down-regulation of c-Met significantly decreased the proliferation, motility, and invasive ability of HCC cells both *in vitro* and *in vivo*. The efficacy of inhibition of c-Met in HCC treatments is verified. So far, many approaches including biologic inhibitors (ribozymes, dominant-negative receptors, decoy receptors, peptides, and c-Met antagonist antibodies) and small-molecule c-Met inhibitors have been designed to inhibit c-Met expression or activity. Recently, small-molecule kinase inhibitors emerged as a major approach being investigated in the clinic. Several c-Met kinase inhibitors such as ARQ197, SGX523, and PF2341066 are rapidly progressing through various stages of development, with those in clinical trials having already demonstrated convincing early evidence of clinical activity in many types of human cancers (*85-87*). Agents that may interfere with c-Met downstream effector functions, including the MAPK and PI3K pathways may serve as an option for HCC treatment. However, targeting these downstream effectors might not be c-Met pathway-specific. Taken together we suggest that c-Met selective targeting therapies are possibly a promising strategy for HCC treatment. Finally, it should be noted that the intact HGF/c-Met signaling pathway was suggested to be essential for maintaining normal redox homeostasis in the liver and had tumor suppressor effects during the early stages of nitrosodiethylamine-induced hepatocarcinogenesis (*88*). Thus, the level of c-Met signaling activity has a range suitable for maintaining normal cell activity.

6. Conclusion

The demonstrated role of c-Met in experimental oncogenesis, its dysregulation and correlation with disease prognosis, and antitumor effects by suppression of its activity may suggest the potential of c-Met as a therapeutic target in HCC. However, identification of the subclass of patients with c-Met signaling dependent HCCs is of special importance in predicting drug efficiency and reducing side effects. So far, the efficacy of these approaches has not nearly been verified in HCC. It is necessary to apply these approaches to HCC treatments in the future.

Acknowledgements

References

1. International Agency for Research on Cancer. Cancer Incidence and Mortality Worldwide in 2008 (GLOBOCAN 2008). *http://globocan.iarc.fr* (accessed November 21, 2010).
2. American Cancer Society. Cancer Facts and FIGS 2005. *http://www.cancer.org/docroot/home/index.asp* (accessed November 21, 2010).
3. Song PP, Tang W, Tamura S, Hasegawa K, Sugawara Y, Dong JH, Kokudo N. The management of hepatocellular carcinoma in Asia: A guideline combining quantitative and qualitative evaluation. Biosci Trends. 2010; 4:283-287.
4. Llovet JM, Di Bisceglie AM, Bruix J, Kramer BS, Lencioni R, Zhu AX, Sherman M, Schwartz M, Lotze M, Talwalkar J, Gores GJ. Design and endpoints of clinical trials in hepatocellular carcinoma. J Natl Cancer Inst. 2008; 100:698-711.
5. Wörns MA, Galle PR. Future perspectives in hepatocellular carcinoma. Dig Liver Dis. 2010; 42 (Suppl 3):S302-S309.
6. Gonzatti-Haces M, Seth A, Park M, Copeland T, Oroszlan S, Vande Woude GF. Characterization of the TPR-MET oncogene p65 and the MET protooncogene p140 protein-tyrosine kinases. Proc Natl Acad Sci U S A. 1988; 85:21-25.
7. Uehara Y, Minowa O, Mori C, Shiota K, Kuno J, Noda T, Kitamura N. Placental defect and embryonic lethality in mice lacking hepatocyte growth factor/scatter factor. Nature. 1995; 373:702-705.
8. Sonnenberg E, Meyer D, Weidner KM, Birchmeier C. Scatter factor/hepatocyte growth factor and its receptor, the c-met tyrosine kinase, can mediate a signal exchange between mesenchyme and epithelia during mouse development. J Cell Biol. 1993; 123:223-235.
9. Joannidis M, Spokes K, Nakamura T, Faletto D, Cantley LG. Regional expression of hepatocyte growth factor/ c-met in experimental renal hypertrophy and hyperplasia. Am J Physiol. 1994; 267:F231-F236.
10. Tsuji S, Kawano S, Tsujii M, Fusamoto H, Kamada T. Roles of hepatocyte growth factor and its receptor in gastric mucosa. A cell biological and molecular biological study. Dig Dis Sci. 1995; 40:1132-1139.
11. Yanagita K, Matsumoto K, Sekiguchi K, Ishibashi H, Niho Y, Nakamura T. Hepatocyte growth factor may act as a pulmotrophic factor on lung regeneration after acute lung injury. J Biol Chem. 1993; 268:21212-21217.
12. Trusolino L, Bertotti A, Comoglio PM. MET signalling: Principles and functions in development, organ regeneration and cancer. Nat Rev Mol Cell Biol. 2010; 11:834-848.
13. Eder JP, Vande Woude GF, Boerner SA, LoRusso PM. Novel therapeutic inhibitors of the c-Met signaling pathway in cancer. Clin Cancer Res. 2009; 15:2207-2214.
14. Nakopoulou L, Gakiopoulou H, Keramopoulos A, Giannopoulou I, Athanassiadou P, Mavrommatis J, Davaris PS. c-Met tyrosine kinase receptor expression is associated with abnormal beta-catenin expression and favourable prognostic factors in invasive breast carcinoma. Histopathology. 2000; 36:313-325.
15. Birchmeier C, Birchmeier W, Gherardi E, Vande Woude GF. Met, metastasis, motility and more. Nat Rev Mol

Cell Biol. 2003; 4:915-925.

16. Annen K. Analysis of the hepatocyte growth factor receptor in regeneration and oncogenesis of hepatocytes. Hokkaido Igaku Zasshi. 1994; 69:301-311. (in Japanese)

17. Xie B, Li XW, Dong JH. Expression and clinical significance of c-Met, E-cadherin, β-catenin in metastasis of human hepatocellular carcinoma. Chinese Journal of Digestive Surgery. 2006; 5:62-66. (in Chinese)

18. Wu FS, Zheng SS, Wu LJ, Ding W, Ma ZM, Wang ZM, Teng LS, Zhao WH. Study on the prognostic value of hepatocyte growth factor and c-met for patients with hepatocellular carcinoma. Zhonghua Wai Ke Za Zhi. 2006; 44:603-608. (in Chinese)

19. Ueki T, Fujimoto J, Suzuki T, Yamamoto H, Okamoto E. Expression of hepatocyte growth factor and its receptor c-met proto-oncogene in hepatocellular carcinoma. Hepatology. 1997; 25:862-866.

20. Chau GY, Lui WY, Chi CW, Chau YP, Li AF, Kao HL, Wu CW. Significance of serum hepatocyte growth factor levels in patients with hepatocellular carcinoma undergoing hepatic resection. Eur J Surg Oncol. 2008; 34:333-338.

21. Kiss A, Wang NJ, Xie JP, Thorgeirsson SS. Analysis of transforming growth factor (TGF)-alpha/epidermal growth factor receptor, hepatocyte growth factor/c-met, TGF-beta receptor type II, and p53 expression in human hepatocellular carcinomas. Clin Cancer Res. 1997; 3:1059-1066.

22. Ljubimova JY, Petrovic LM, Wilson SE, Geller SA, Demetriou AA. Expression of HGF, its receptor c-met, c-myc, and albumin in cirrhotic and neoplastic human liver tissue. J Histochem Cytochem. 1997; 45:79-87.

23. Osada S, Kanematsu M, Imai H, Goshima S, Sugiyama Y. Evaluation of extracellular signal regulated kinase expression and its relation to treatment of hepatocellular carcinoma. J Am Coll Surg. 2005; 201:405-411.

24. Suzuki K, Hayashi N, Yamada Y, *et al*. Expression of the c-met protooncogene in human hepatocellular carcinoma. Hepatology. 1994; 20:1231-1236.

25. Zhang SZ, Pan FY, Xu JF, Yuan J, Guo SY, Dai G, Xue B, Shen WG, Wen CJ, Zhao DH, Li CJ. Knockdown of c-Met by adenovirus-delivered small interfering RNA inhibits hepatocellular carcinoma growth *in vitro* and *in vivo*. Mol Cancer Ther. 2005; 4:1577-1584.

26. D'Errico A, Fiorentino M, Ponzetto A, Daikuhara Y, Tsubouchi H, Brechot C, Scoazec JY, Grigioni WF. Liver hepatocyte growth factor does not always correlate with hepatocellular proliferation in human liver lesions: Its specific receptor c-met does. Hepatology. 1996; 24:60-64.

27. Osada S, Kanematsu M, Imai H, Goshima S. Clinical significance of serum HGF and c-Met expression in tumor tissue for evaluation of properties and treatment of hepatocellular carcinoma. Hepatogastroenterology. 2008; 55:544-549.

28. Boix L, Rosa JL, Ventura F, Castells A, Bruix J, Rodes J, Bartrons R. c-met mRNA overexpression in human hepatocellular carcinoma. Hepatology. 1994; 19:88-91.

29. Noguchi O, Enomoto N, Ikeda T, Kobayashi F, Marumo F, Sato C. Gene expressions of c-met and hepatocyte growth factor in chronic liver disease and hepatocellular carcinoma. J Hepatol. 1996; 24:286-292.

30. Okano J, Shiota G, Kawasaki H. Expression of hepatocyte growth factor (HGF) and HGF receptor (c-met) proteins in liver diseases: An immunohistochemical study. Liver.

1999; 19:151-159.

31. Chen Q, Seol DW, Carr B, Zarnegar R. Co-expression and regulation of Met and Ron proto-oncogenes in human hepatocellular carcinoma tissues and cell lines. Hepatology. 1997; 26:59-66.

32. Seol DW, Chen Q, Zarnegar R. Transcriptional activation of the hepatocyte growth factor receptor (c-met) gene by its ligand (hepatocyte growth factor) is mediated through AP-1. Oncogene. 2000; 19:1132-1137.

33. Xie B, Tang C, Chen P, Gou YB, Xiao J, Du H. The effect of hepatitis B virus X protein on the c-met promoter activity in HepG2 cells. Zhonghua Gan Zang Bing Za Zhi. 2009; 17:292-296. (in Chinese)

34. Zamore PD, Haley B. Ribo-gnome: The big world of small RNAs. Science. 2005; 309:1519-1524.

35. Budhu A, Jia HL, Forgues M, Liu CG, Goldstein D, Lam A, Zanetti KA, Ye QH, Qin LX, Croce CM, Tang ZY, Wang XW. Identification of metastasis-related microRNAs in hepatocellular carcinoma. Hepatology. 2008; 47:897-907.

36. Li N, Fu H, Tie Y, Hu Z, Kong W, Wu Y, Zheng X. miR-34a inhibits migration and invasion by down-regulation of c-Met expression in human hepatocellular carcinoma cells. Cancer Lett. 2009; 275:44-53.

37. Salvi A, Sabelli C, Moncini S, Venturin M, Arici B, Riva P, Portolani N, Giulini SM, De Petro G, Barlati S. MicroRNA-23b mediates urokinase and c-met downmodulation and a decreased migration of human hepatocellular carcinoma cells. FEBS J. 2009; 276:2966-2982.

38. Fornari F, Milazzo M, Chieco P, Negrini M, Calin GA, Grazi GL, Pollutri D, Croce CM, Bolondi L, Gramantieri L. MiR-199a-3p regulates mTOR and c-Met to influence the doxorubicin sensitivity of human hepatocarcinoma cells. Cancer Res. 2010; 70:5184-5193.

39. Rubin JS, Chan AM, Bottaro DP, Burgess WH, Taylor WG, Cech AC, Hirschfield DW, Wong J, Miki T, Finch PW, Aaronson SA. A broad-spectrum human lung fibroblast-derived mitogen is a variant of hepatocyte growth factor. Proc Natl Acad Sci U S A. 1991; 88:415-419.

40. Montesano R, Matsumoto K, Nakamura T, Orci L. Identification of a fibroblast-derived epithelial morphogen as hepatocyte growth factor. Cell. 1991; 67:901-908.

41. Bottaro DP, Rubin JS, Faletto DL, Chan AM, Kmiecik TE, Vande Woude GF, Aaronson SA. Identification of the hepatocyte growth factor receptor as the c-met proto-oncogene product. Science. 1991; 251:802-804.

42. Sakaguchi H, Seki S, Tsubouchi H, Daikuhara Y, Niitani Y, Kobayashi K. Ultrastructural location of human hepatocyte growth factor in human liver. Hepatology. 1994; 19:1157-1163.

43. Wolf HK, Zarnegar R, Michalopoulos GK. Localization of hepatocyte growth factor in human and rat tissues: An immunohistochemical study. Hepatology. 1991; 14:488-494.

44. Park WS, Dong SM, Kim SY, *et al*. Somatic mutations in the kinase domain of the Met/hepatocyte growth factor receptor gene in childhood hepatocellular carcinomas. Cancer Res. 1999; 59:307-310.

45. Wang R, Ferrell LD, Faouzi S, Maher JJ, Bishop JM. Activation of the Met receptor by cell attachment induces and sustains hepatocellular carcinomas in transgenic mice. J Cell Biol. 2001; 153:1023-1034.

46. Bhargava M, Joseph A, Knesel J, Halaban R, Li Y, Pang S, Goldberg I, Setter E, Donovan MA, Zarnegar R, Michalopoulos GA, Nakamura T, Faletto D, Rosen EM.

Scatter factor and hepatocyte growth factor: Activities, properties, and mechanism. Cell Growth Differ. 1992; 3:11-20.

47. Rong S, Bodescot M, Blair D, Dunn J, Nakamura T, Mizuno K, Park M, Chan A, Aaronson S, Vande Woude GF. Tumorigenicity of the met proto-oncogene and the gene for hepatocyte growth factor. Mol Cell Biol. 1992; 12:5152-5158.

48. Herbst RS. Review of epidermal growth factor receptor biology. Int J Radiat Oncol Biol Phys. 2004; 59:21-26.

49. Jo M, Stolz DB, Esplen JE, Dorko K, Michalopoulos GK, Strom SC. Cross-talk between epidermal growth factor receptor and c-Met signal pathways in transformed cells. J Biol Chem. 2000; 275:8806-8811.

50. Inagaki Y, Tang W, Xu H, Wang F, Nakata M, Sugawara Y, Kokudo N. Des-gamma-carboxyprothrombin: Clinical effectiveness and biochemical importance. Biosci Trends. 2008; 2:53-60.

51. Inagaki Y, Tang W, Makuuchi M, Hasegawa K, Sugawara Y, Kokudo N. Clinical and molecular insights into the hepatocellular carcinoma tumour marker des-gamma-carboxyprothrombin. Liver Int. 31:22-35.

52. Tang W, Kokudo N, Sugawara Y, Guo Q, Imamura H, Sano K, Karako H, Qu X, Nakata M, Makuuchi M. Des-gamma-carboxyprothrombin expression in cancer and/or non-cancer liver tissues: Association with survival of patients with resectable hepatocellular carcinoma. Oncol Rep. 2005; 13:25-30.

53. Nakamura T, Nishizawa T, Hagiya M, Seki T, Shimonishi M, Sugimura A, Tashiro K, Shimizu S. Molecular cloning and expression of human hepatocyte growth factor. Nature. 1989; 342:440-443.

54. Suzuki M, Shiraha H, Fujikawa T, Takaoka N, Ueda N, Nakanishi Y, Koike K, Takaki A, Shiratori Y. Des-gamma-carboxy prothrombin is a potential autologous growth factor for hepatocellular carcinoma. J Biol Chem. 2005; 280:6409-6415.

55. Ponzetto C, Bardelli A, Zhen Z, Maina F, dalla Zonca P, Giordano S, Graziani A, Panayotou G, Comoglio PM. A multifunctional docking site mediates signaling and transformation by the hepatocyte growth factor/scatter factor receptor family. Cell. 1994; 77:261-271.

56. Bardelli A, Longati P, Williams TA, Benvenuti S, Comoglio PM. A peptide representing the carboxyl-terminal tail of the met receptor inhibits kinase activity and invasive growth. J Biol Chem. 1999; 274:29274-29281.

57. Ferracini R, Longati P, Naldini L, Vigna E, Comoglio PM. Identification of the major autophosphorylation site of the Met/hepatocyte growth factor receptor tyrosine kinase. J Biol Chem. 1991; 266:19558-19564.

58. Ke AW, Shi GM, Zhou J, Wu FZ, Ding ZB, Hu MY, Xu Y, Song ZJ, Wang ZJ, Wu JC, Bai DS, Li JC, Liu KD, Fan J. Role of overexpression of CD151 and/or c-Met in predicting prognosis of hepatocellular carcinoma. Hepatology. 2009; 49:491-503.

59. Midorikawa Y, Tang W, Sugiyama Y. High-resolution mapping of copy number aberrations and identification of target genes in hepatocellular carcinoma. Biosci Trends. 2007; 1:26-32.

60. Wang ZL, Liang P, Dong BW, Yu XL, Yu de J. Prognostic factors and recurrence of small hepatocellular carcinoma after hepatic resection or microwave ablation: A retrospective study. J Gastrointest Surg. 2008; 12:327-337.

61. Kaposi-Novák P. Comparative genomic classification

of human hepatocellular carcinoma. Magy Onkol. 2009; 53:61-67.

62. Giordano S, Di Renzo MF, Narsimhan RP, Cooper CS, Rosa C, Comoglio PM. Biosynthesis of the protein encoded by the c-met proto-oncogene. Oncogene. 1989; 4:1383-1388.

63. Naldini L, Vigna E, Ferracini R, Longati P, Gandino L, Prat M, Comoglio PM. The tyrosine kinase encoded by the MET proto-oncogene is activated by autophosphorylation. Mol Cell Biol. 1991; 11:1793-1803.

64. Komada M, Kitamura N. Regulatory role of major tyrosine autophosphorylation site of kinase domain of c-Met receptor (scatter factor/hepatocyte growth factor receptor). J Biol Chem. 1994; 269:16131-16136.

65. Longati P, Bardelli A, Ponzetto C, Naldini L, Comoglio PM. Tyrosines 1234-1235 are critical for activation of the tyrosine kinase encoded by the MET proto-oncogene (HGF receptor). Oncogene. 1994; 9:49-57.

66. Pawson T. Protein modules and signalling networks. Nature. 1995; 373:573-580.

67. Christensen JG, Burrows J, Salgia R. c-Met as a target for human cancer and characterization of inhibitors for therapeutic intervention. Cancer Lett. 2005; 225:1-26.

68. Bardelli A, Longati P, Gramaglia D, Stella MC, Comoglio PM. Gab1 coupling to the HGF/Met receptor multifunctional docking site requires binding of Grb2 and correlates with the transforming potential. Oncogene. 1997; 15:3103-3111.

69. Lee HS, Huang AM, Huang GT, Yang PM, Chen PJ, Sheu JC, Lai MY, Lee SC, Chou CK, Chen DS. Hepatocyte growth factor stimulates the growth and activates mitogen-activated protein kinase in human hepatoma cells. J Biomed Sci. 1998; 5:180-184.

70. Tward AD, Jones KD, Yant S, Cheung ST, Fan ST, Chen X, Kay MA, Wang R, Bishop JM. Distinct pathways of genomic progression to benign and malignant tumors of the liver. Proc Natl Acad Sci U S A. 2007; 104:14771-14776.

71. Nakanishi K, Fujimoto J, Ueki T, Kishimoto K, Hashimoto-Tamaoki T, Furuyama J, Itoh T, Sasaki Y, Okamoto E. Hepatocyte growth factor promotes migration of human hepatocellular carcinoma *via* phosphatidylinositol 3-kinase. Clin Exp Metastasis. 1999; 17:507-514.

72. Neaud V, Faouzi S, Guirouilh J, Le Bail B, Balabaud C, Bioulac-Sage P, Rosenbaum J. Human hepatic myofibroblasts increase invasiveness of hepatocellular carcinoma cells: Evidence for a role of hepatocyte growth factor. Hepatology. 1997; 26:1458-1466.

73. Lee KH, Choi EY, Hyun MS, Jang BI, Kim TN, Lee HJ, Eun JY, Kim HG, Yoon SS, Lee DS, Kim JH, Kim JR. Role of hepatocyte growth factor/c-Met signaling in regulating urokinase plasminogen activator on invasiveness in human hepatocellular carcinoma: A potential therapeutic target. Clin Exp Metastasis. 2008; 25:89-96.

74. Horiguchi N, Takayama H, Toyoda M, Otsuka T, Fukusato T, Merlino G, Takagi H, Mori M. Hepatocyte growth factor promotes hepatocarcinogenesis through c-Met autocrine activation and enhanced angiogenesis in transgenic mice treated with diethylnitrosamine. Oncogene. 2002; 21:1791-1799.

75. Lasagna N, Fantappie O, Solazzo M, Morbidelli L, Marchetti S, Cipriani G, Ziche M, Mazzanti R. Hepatocyte growth factor and inducible nitric oxide synthase are involved in multidrug resistance-induced

angiogenesis in hepatocellular carcinoma cell lines. Cancer Res. 2006; 66:2673-2682.

76. Shiota G, Rhoads DB, Wang TC, Nakamura T, Schmidt EV. Hepatocyte growth factor inhibits growth of hepatocellular carcinoma cells. Proc Natl Acad Sci U S A. 1992; 89:373-377.

77. Liu ML, Mars WM, Michalopoulos GK. Hepatocyte growth factor inhibits cell proliferation *in vivo* of rat hepatocellular carcinomas induced by diethylnitrosamine. Carcinogenesis. 1995; 16:841-843.

78. Yaono M, Hasegawa R, Mizoguchi Y, Futakuchi M, Nakamura T, Ito N, Shirai T. Hepatocyte growth factor enhancement of preneoplastic hepatic foci development in rats treated with diethylnitrosamine and N-ethyl-N-hydroxyethylnitrosamine. Jpn J Cancer Res. 1995; 86:718-723.

79. Ogasawara H, Hiramoto J, Takahashi M, Shirahama K, Furusaka A, Hiyane S, Nakada T, Nagayama K, Tanaka T. Hepatocyte growth factor stimulates DNA synthesis in rat preneoplastic hepatocytes but not in liver carcinoma cells. Gastroenterology. 1998; 114:775-781.

80. Sakata H, Takayama H, Sharp R, Rubin JS, Merlino G, LaRochelle WJ. Hepatocyte growth factor/scatter factor overexpression induces growth, abnormal development, and tumor formation in transgenic mouse livers. Cell Growth Differ. 1996; 7:1513-1523.

81. Shiota G, Wang TC, Nakamura T, Schmidt EV. Hepatocyte growth factor in transgenic mice: Effects on hepatocyte growth, liver regeneration and gene expression. Hepatology. 1994; 19:962-972.

82. Santoni-Rugiu E, Preisegger KH, Kiss A, Audolfsson T, Shiota G, Schmidt EV, Thorgeirsson SS. Inhibition of neoplastic development in the liver by hepatocyte growth factor in a transgenic mouse model. Proc Natl Acad Sci U S A. 1996; 93:9577-9582.

83. Chen BH, Xie Q, Liu KD. Influence of the inhibitor of c-Met on the growth and motility of hepatocellular carcinoma cells. Zhonghua Gan Zang Bing Za Zhi. 2003; 11:487-489. (in Chinese)

84. Xie B, Xing R, Chen P, Gou Y, Li S, Xiao J, Dong J. Down-regulation of c-Met expression inhibits human HCC cells growth and invasion by RNA interference. J Surg Res. 2010; 162:231-238.

85. Bagai R, Fan W, Ma PC. ARQ-197, an oral small-molecule inhibitor of c-Met for the treatment of solid tumors. IDrugs. 2010; 13:404-414.

86. Zhang YW, Staal B, Essenburg C, Su Y, Kang L, West R, Kaufman D, Dekoning T, Eagleson B, Buchanan SG, Vande Woude GF. MET kinase inhibitor SGX523 synergizes with epidermal growth factor receptor inhibitor erlotinib in a hepatocyte growth factor-dependent fashion to suppress carcinoma growth. Cancer Res. 2010; 70:6880-6890.

87. Sampson ER, Martin BA, Morris AE, Xie C, Schwarz EM, O'Keefe RJ, Rosier RN. The orally bioavailable met inhibitor PF-2341066 inhibits osteosarcoma growth and osteolysis/matrix production in a xenograft model. J Bone Miner Res. 2011.

88. Takami T, Kaposi-Novak P, Uchida K, Gomez-Quiroz LE, Conner EA, Factor VM, Thorgeirsson SS. Loss of hepatocyte growth factor/c-Met signaling pathway accelerates early stages of N-nitrosodiethylamine induced hepatocarcinogenesis. Cancer Res. 2007; 67:9844-9851.

Brief Report

Antibacterial activities of *Sesbania grandiflora* extracts

Pimporn Anantaworasakul[1], Srikanjana Klayraung[2], Siriporn Okonogi[1,*]

[1] *Faculty of Pharmacy, Chiang Mai University, Chiang Mai, Thailand;*
[2] *Faculty of Science, Maejo University, Chiang Mai, Thailand.*

ABSTRACT: In this study, *Sesbania grandiflora*, a plant in the Leguminosae family, was investigated for its antibacterial activities. The agar well diffusion assay as well as the agar and broth dilution assays were used for determination of antibacterial activities. The crude ethanolic extracts obtained from different parts of this plant exhibited different potent activities. The stem bark has the most potential to yield an extract with the highest antibacterial action. The fractionation of the stem bark with different solvents indicated that the fractionated extracts obtained from ethyl acetate or butanol possessed the most pronounced antibacterial activity. The kinetic study of bactericidal activities revealed that the butanol fractionated extract of the stem bark was effective against Gram negative bacteria. This study suggests that the stem bark of *S. grandiflora* contains promising antibacterial substances for clinical purposes.

Keywords: *Sesbania grandiflora*, antibacterial activity, crude extract, pathogenic bacteria, killing kinetics

1. Introduction

In Thailand and other Asian countries like China, Japan, and India, medicinal plants are widely used by all sections of the population either directly as folk remedies or in different indigenous systems of medicine or indirectly in the pharmaceutical preparations of modern medicines. The world health organization recently accepted an inventory of more than 20,000 species of medicinal plants. Thai medicinal plants and their products are used to control diverse diseases and disorder symptoms such as cough, fever, bronchitis, itching, pneumonia, ulcers, and diarrhea. Researchers are hence increasingly turning their attention to medicinal plants looking for new bioactive or lead

compounds to develop better drugs against several degenerative diseases like cancer, diabetes, Alzheimer's, arteriosclerosis as well as diseases caused by pathogenic microorganisms (*1,2*).

From previous studies reported by different research groups, it was demonstrated that many naturally occurring compounds found in plants have been shown to possess biological activities such as antibacterial (*3-5*), antifungal (*3,6,7*), antiviral (*3,8*), anti-allergic (*4*), anti-cholinesterase (*5*), antioxidant (*9-11*), anti-inflammatory (*4,5,10*), antitumor (*12,13*), anti-tyrosinase (*14*), anti-plasmodial (*15*), and cytotoxic effects (*10,15*).

The plant genus *Sesbania*, family Leguminosae, is comprised of about 60 species which are widely distributed throughout tropical and subtropical regions. Most species are annual herbs or shrubs, but a few are small trees (*16*). Many species of *Sesbania* are used for soil improvement as green manners or agroforestry trees (*17*). *Sesbania grandiflora*, syn. *Aeschynomene grandiflora*, is a small erect tree that grows rapidly, is a sparsely branched tree that provides light shade, and is often grown as an ornamental (*18*). *S. grandiflora* is widely used in Thailand both for food and medicine. Its leaves and flowers are utilized as food whereas its stem has been long used as a traditional medicine for treatment of ulcers in the oral cavity. It was reported that all parts of *S. grandiflora* are utilized for medicine in Southeastern Asia and India including preparations derived from the roots, bark, gum, leaves, flowers and fruits. In the Philippines, the stem bark of this plant has been used for the treatment of thrush and infantile disorders of the stomach. In Cambodia, the pounded bark is applied to scabies. The juice of the leaves is considered anthelmintic and tonic and is used to treat worms, biliousness, fever, gout, itchiness, and leprosy (*19*). It was also reported that the root of this plant could be applied externally as a poultice against inflammation. The semisolid mass containing powdered roots of *S. grandiflora* in an appropriate amount of water demonstrated a decrease of rheumatic swelling when applied externally with moderate rubbing to the lesion (*20*). Although *S. grandiflora* has been used for treatment in many diseases, most of the biological activities have not yet been adequately evaluated.

---

*Address correspondence to:
Dr. Siriporn Okonogi, Faculty of Pharmacy, Chiang Mai University, Chiang Mai 50200, Thailand.
e-mail: sirioko@chiangmai.ac.th

The present study deals with the investigation of antibacterial activity of *S. grandiflora*. Several parts of the whole plant such as leaves, branches, stem barks, and stem cores were screened for their potency on growth inhibition of bacteria. The pathogenic organisms were selected for the study on the basis of their clinical and pharmaceutical importance as well as their potential to cause contamination of food and drugs. The high potent activity extracts of the most potential parts of the plant were further investigated deeply on bacterial killing kinetics.

2. Materials and Methods

2.1. *Plant materials*

S. grandiflora samples were collected in fresh condition from local areas of Northern Thailand. The plant was identified and deposited in the Herbarium of the Faculty of Pharmacy, Chiang Mai, Thailand.

2.2. *Preparation of plant extracts*

2.2.1. *The crude extracts*

Fresh material leaves, branches, stem bark, and stem core were collected and washed with distilled water. Samples were cut into small pieces and dried at 50°C for 24 h. The dried samples were pulverized into powder, and then macerated with 95% ethanol for 48 h × 3 at room temperature. The filtrates from the same part were pooled together and subjected to the rotary evaporator at 45°C and under vacuum for solvent removal. The crude extracts obtained were investigated further for antibacterial activity.

2.2.2. *Fractionation of the extracts*

The dried powder of stem bark was used in this study because its crude ethanolic extract showed the highest antibacterial activity. The plant powder was first macerated in hexane for 48 h × 3 at room temperature. The residue after the third filtration was dried at room temperature to ensure hexane was completely removed. The dried residue was further macerated respectively in three solvents as follows; ethyl acetate, butanol and methanol, in the same manner as hexane. The filtrates of the same solvent were pooled together. The solvent was removed using a rotary evaporator at 45°C under vacuum. The fractionated extracts obtained were subjected to antibacterial activity tests.

2.3. *Bacterial strains*

Standard strains of *Escherichia coli* ATCC 25922, *Staphylococcus aureus* ATCC 25923, *Salmonella typhi* DMST 5784, *Shigella sonnei* DMST 561 and clinical pathogenic bacterial strains of *Bacillus cereus*, *Enterobacter cloacae*, *Enterococcus faecalis*, *Pseudomonas aeruginosa*, *Serratia marcescens*, and *Staphylococcus epidermidis* obtained from the Faculty of Medicine, Chiang Mai University, Thailand were used throughout the study. The bacteria were sub-cultured individually on fresh Tryptic Soy Agar (TSA) and incubated overnight at 37°C. Each bacterial strain was then suspended in 0.9% NaCl, and diluted to a McFarland turbidity standard No. 0.5 (*21*). This bacterial suspension was used for testing antibacterial activity.

2.4. *Determination of antibacterial activities by agar diffusion*

The bacterial inhibitory effect of *S. grandiflora* extracts was carried out by standard agar well diffusion method (*21*). The TSA plate was seeded with the NS suspension of different bacteria. In each plate, a 6 mm diameter well was cut out using a sterile cork borer. Using a sterile autopipette, 50 µL of the proper diluted extract was carefully added into the wells. The same volume of 50% ethanol was used as a negative control. The plates were incubated overnight at 37°C. The antibacterial activity was evaluated by measuring the diameter of inhibition zone (DIZ). The experiment was carried out in triplicate and the means of diameter of the inhibition zone were calculated.

2.5. *Determination of minimum inhibitory concentration (MIC)*

2.5.1. *Agar dilution method*

The MIC of fractionated extract of the stem bark was determined against the test pathogenic bacteria by a standard agar dilution method (*22*). Briefly, to the tubes containing 9 mL melted Mueller-Hinton Agar (MHA) media, serial dilutions of the extract were added to 10 mL and poured into a sterile plate. Sample concentrations in the agar plates were in the range of 0.63-20.00 mg/mL. Equivalent amounts of sterile distilled water and sterile 50% ethanol were used as controls. Ten µL of each bacteria suspension with turbidity equivalent to McFarland No. 0.5 was inoculated into each agar dilution plate. The inoculated plates were incubated overnight at 37°C. The MIC was defined as the lowest concentration of the samples which prevented this change and exhibited complete inhibition of bacterial growth (*23*).

2.5.2. *Broth dilution method*

The MIC was also determined by using a broth dilution method (*24*). Briefly, the extract was first dissolved in sterile 50% ethanol. The sample obtained was added

to Mueller-Hinton Broth (MHB). This extract solution was serially diluted two-fold with MHB to obtain the extract concentration in a range of 0.63-10.00 mg/mL. Each bacterial suspension obtained from a McFarland turbidity standard No. 0.5 was inoculated into the broth dilution tube. The tubes were incubated overnight at 37°C. Negative controls were prepared with un-inoculated bacterial suspension and the positive controls contained inoculated bacterial suspension without the test samples. After incubation overnight at 37°C, the micro-dilution tubes were checked visually to detect growth inhibition of the bacteria. The growth end points were determined by comparing the amount of growth in the tubes containing the test samples with that in the negative control. Acceptable growth must occur in the positive control. The MIC was defined as the lowest concentration of the samples which is able to inhibit any visible bacterial growth (*25*).

2.6. *Determination of minimum bactericidal concentration (MBC)*

To determine MBC, a method of MIC determination was slightly modified. Briefly, the samples were taken from the tube of the MIC assays, where no visible turbidity (growth) was observed, and streaked on freshly prepared TSA plates. The plates were incubated overnight at 37°C so as to determine the MBC (*26*). The MBC was defined as the lowest concentration of the samples with no bacteria growth on the surface of the medium in the plates (*27,28*).

2.7. *Kinetics of bacteria killing*

Kinetics of bacteria killing was investigated by a broth dilution method (*29*). Briefly, an overnight culture in TSA was adjusted with normal saline (0.9% NaCl) to a McFarland Standard No. 0.5. The adjusted culture was added to MHB with the test extract at the same concentration of MBC and incubated for an appropriate time of 1.5, 3, 4.5, and 6 h, at 37°C, to achieve a logarithmic growth phase. All cultures contained approximately 1.5×10^6 CFU/mL at the initiation of the time course and were maintained at 37°C. The actual initial concentrations were determined by ten-fold serial dilution with a normal saline solution of the inoculums and plating the serial dilutions on TSA to calculate the logarithm of colony forming units per milliliter extract (log CFU/mL). At 0, 1.5, 3, 4.5, 6, and 24 h, samples were removed and serially diluted with normal saline. The log CFU/mL in the culture at each time point was determined by spreading on freshly prepared TSA plates and incubating overnight at 37°C. As a general rule, plates containing greater than 30, but less than 300 colonies were used to quantify viable CFU/mL. In some instances, the resulting number of colonies was less than 30 and considered below the

limit of quantification. In these few cases, the colonies were counted and the resulting CFU/mL was used to provide an estimate of the number of viable cells. It is noted in the appropriate figure legends when these estimates were used. Results of killing kinetic studies are expressed as the difference between the log CFU/mL at the indicated time point and the log CFU/mL of the inoculums at time zero. Bactericidal activity was defined as decreasing the original inoculums after 24 h of incubation (*30*).

3. Results and Discussion

The crude extracts of 4 parts of *S. grandiflora* showed different yields. The leaf extract gave the highest yield of 23.3% (w/w) followed by the stem bark with a yield of 13.3% (w/w). All of them were first screened for their antibacterial activity against *E. coli* and *S. aureus* as representations for Gram negative and Gram positive bacteria, respectively. Gentamicin at a concentration of 75 µg/mL was used as a positive control. It was found as shown in Table 1 that the stem bark extract showed the strongest inhibition against both pathogens with a DIZ of 9.4 and 13.7 mm for *E. coli* and *S. aureus* respectively whereas the leaf extracts gave no inhibition zone.

MIC of the fractionated extracts of the stem bark was further examined against ten strains of pathogenic bacteria. The results in Table 2 indicated that the extract with ethyl acetate possessed the strongest antibacterial activity followed by the butanol extract. The MIC of ethyl acetate extract against all tested pathogens was lower than other solvents. It was found that the yield of ethyl acetate extract was 1.75% which was a little lower than that of the methanol extract but higher than that of the butanol and hexane extracts. Considering the antibacterial activity, the ethyl acetate and butanol extracts were selected for further investigation.

The antibacterial activity in the ethyl acetate and the butanol extracts determined by agar dilution method were confirmed by using the broth dilution

Table 1. Diameter of inhibition zone of growth inhibition of crude extract (100 mg/mL) from each part of *S. grandiflora* and gentamicin (75 µg/mL) against different bacterial strains using the agar well diffusion method[a]

Samples	Diameter of inhibition zone (mm)[b]	
	E. coli	*S. aureus*
Leaves extract	NZ[c]	NZ
Branches extract	7.8 ± 0.3	10.7 ± 1.0
Stem bark extract	9.4 ± 0.1	13.7 ± 0.6
Stem core extract	NZ	8.9 ± 0.2
Gentamicin	16.3 ± 0.9	23.1 ± 2.5

[a] No bacterial growth in the negative control plate.
[b] Data are presented as means ± S.D. (*n* = 3).
[c] NZ represents no inhibition zone.

method. In this experiment, *B. cereus*, *E. faecalis*, *S. aureus*, and *S. epidermidis*, as representatives for Gram positive bacteria and *S. typhi* and *S. sonnei*, as representatives for Gram negative bacteria were used as test microorganisms. The results shown in Table 3 demonstrate that the MIC values determined by broth dilution method were equal or less than those obtained by the agar dilution method. Moreover the results indicated that the MBC values of extracts against the Gram positive bacteria were equal to the MIC values on corresponding bacteria. Regarding the Gram negative bacteria, it was found that the MBC values were higher than the MIC values on corresponding bacteria.

To study the killing kinetics effect of the highest potential antibacterial activities, the ethyl acetate and the butanol extracts with a concentration at MBC, were subjected to test four pathogens including *E. faecalis*, *S. aureus*, *S. typhi*, and *S. sonnei*. In this experiment *E. faecalis* and *S. aureus* were used as the model of Gram positive bacteria whereas *S. typhi* and *S. sonnei* were used as the model of Gram negative microorganisms. The bactericidal kinetics was examined using time course experiments measuring the number of surviving bacteria, Log CFU/mL. It was seen that both extracts

possessed a similar killing rate against the tested Gram positive bacteria. Both extracts showed killing activity against *E. faecalis* within 30 min (Figure 1A). For *S. aureus*, more than 90% of cells were killed within 1.5 h (Figure 1B). It was found that the butanol extract had a high ability to kill *S. typhi* and *S. sonnei*, the tested Gram negative bacteria, faster than the ethyl acetate extract. The results demonstrated that both extracts could kill *S. typhi* and *S. sonnei* within 1.5 h. However, the butanol extract showed complete inhibiton against both strains at 6 h whereas the complete killing time

Figure 1. Killing kinetic curves of Gram positive bacteria, *E. faecalis* (A) and *S. aureus* (B), with ethyl acetate (EtOAc) and butanol (BuOH) extracts, from stem bark of *S. grandiflora*.

Table 2. The agar dilution method was used to determine MIC of the extract with different organic solvents from stem bark of *S. grandiflora* against different bacterial strains[a]

Microorganisms	MIC for test samples (mg/mL)			
	Hexane	Ethyl acetate	Butanol	Methanol
Bacillus cereus	> 20	2.5	2.5	2.5
Enterobacter cloacae	> 20	5	20	> 20
Enterococcus faecalis	20	5	5	10
Escherichia coli	> 20	5	20	> 20
Pseudomonas aeruginosa	> 20	10	20	20
Salmonella typhi	> 20	5	2.5	10
Serratia marcescens	> 20	10	20	> 20
Shigella sonnei	> 20	5	5	20
Staphylococcus aureus	10	2.5	2.5	5
Staphylococcus epidermidis	20	2.5	2.5	10

[a] No bacterial growth in the negative control plate.

Table 3. The broth dilution method was used to determine MIC and MBC of the ethyl acetate and the butanol extracts from stem bark of *S. grandiflora* against some different bacterial strains[a]

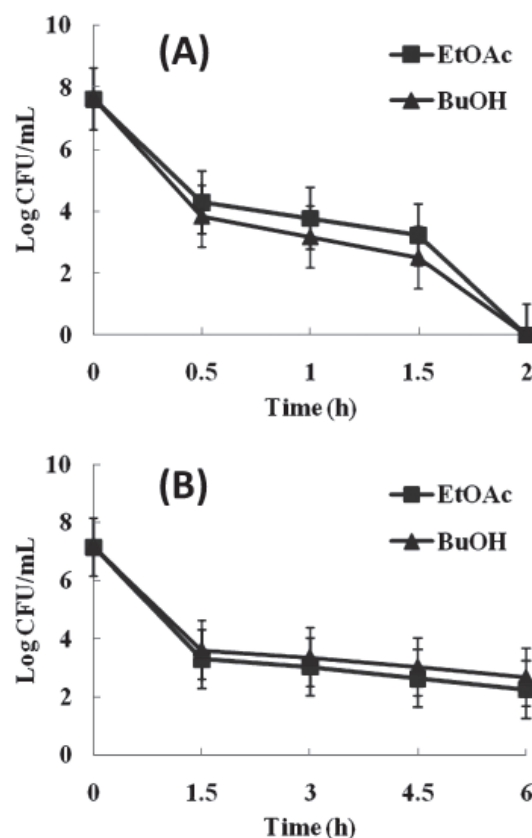| Microorganisms	MIC for test samples (mg/mL)		MBC for test samples (mg/mL)	
	Ethyl acetate	Butanol	Ethyl acetate	Butanol
Bacillus cereus	1.25	1.25	1.25	1.25
Enterococcus faecalis	5	5	5	5
Salmonella typhi	1.25	1.25	2.5	2.5
Shigella sonnei	2.5	2.5	5	5
Staphylococcus aureus	2.5	2.5	2.5	2.5
Staphylococcus epidermidis	2.5	2.5	2.5	2.5

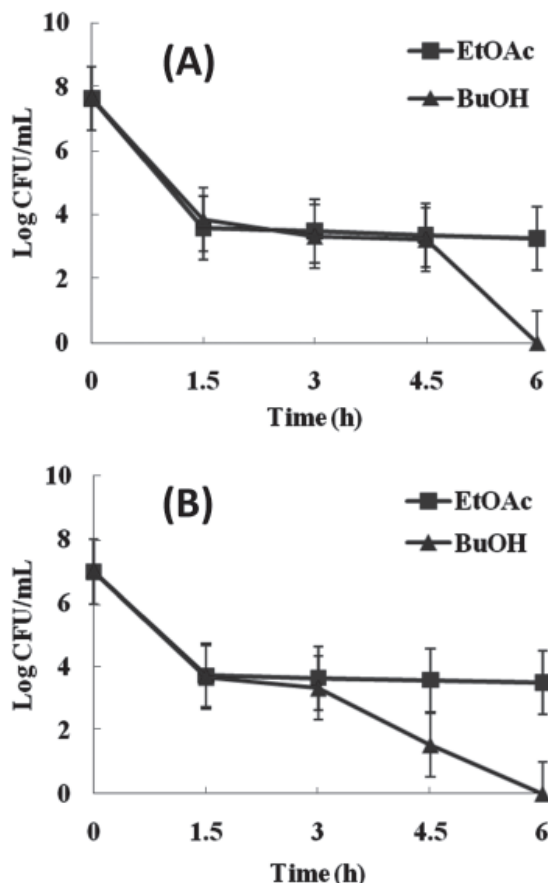[a] No bacterial growth in the negative control plate.

Figure 2. Killing kinetic curves of Gram negative bacteria, *S. typhi* (A) and *S. sonnei* (B), with ethyl acetate (EtOAc) and butanol (BuOH) extracts, from stem bark of *S. grandiflora*.

of ethyl acetate extract for Gram negative bacteria was more than 6 h (Figure 2). From these results, it could be clearly seen that the butanol extract had a more pronounced killing rate on Gram negative bacteria than the ethyl acetate extract. The killing kinetics of both extracts on Gram positive bacteria was not distinguishable.

Acknowledgements

References

1. Galal M, Bashir AK, Salih AM, Adam SE. Activity of water extracts of *Albizzia anthelmintica* and *A. lebbek* barks against experimental *Hymenolepis diminuta* infection in rats. J Ethnopharmacol. 1991; 31:333-337.
2. Chaiyana W, Saeio K, Hennink WE, Okonogi S. Characterization of potent anticholinesterase plant oil based microemulsion. Int J Pharm. 2010; 401:32-40.
3. Ozçelik B, Aslan M, Orhan I, Karaoglu T. Antibacterial, antifungal, and antiviral activities of the lipophylic extracts of *Pistacia vera*. Microbiol Res. 2005; 160:159-164.
4. Panichayupakaranant P, Tewtrakul S, Yuenyongsawad S. Antibacterial, anti-inflammatory and anti-allergic activities of standardized pomegranate rind extract. Food Chem. 2010; 123:400-403.
5. Eldeen IM, Elgorashi EE, van Staden J. Antibacterial, anti-inflammatory, anti-cholinesterase and mutagenic effects of extracts obtained from some trees used in South African traditional medicine. J Ethnopharmacol. 2005; 102:457-464.
6. Kuete V, Poumale Poumale HM, Guedem AN, Shiono Y, Randrianasolo R, Ngadjui BT. Antimycobacterial, antibacterial and antifungal activities of the methanol extract and compounds from *Thecacoris annobonae* (Euphorbiaceae). S Afr J Bot. 2010; 76:536-542.
7. Mativandlela SPN, Lall N, Meyer JJM. Antibacterial, antifungal and antitubercular activity of (the roots of) *Pelargonium reniforme* (CURT) and *Pelargonium sidoides* (DC) (Geraniaceae) root extracts. S Afr J Bot. 2006; 72:232-237.
8. Glatthaar-Saalmüller B, Sacher F, Esperester A. Antiviral activity of an extract derived from roots of *Eleutherococcus senticosus*. Antiviral Res. 2001; 50:223-228.
9. Ahmad R, Ali AM, Israf DA, Ismail NH, Shaari K, Lajis NH. Antioxidant, radical-scavenging, anti-inflammatory, cytotoxic and antibacterial activities of methanolic extracts of some *Hedyotis* species. Life Sci. 2005; 76:1953-1964.
10. Boonkaew T, Camper ND. Biological activities of Ginkgo extracts. Phytomedicine. 2005; 12:318-323.
11. Okonogi S, Duangrat C, Anuchpreeda S, Tachakittirungrod S, Chowwanapoonpohn S. Comparison of antioxidant capacities and cytotoxicities of certain fruit peels. Food Chem. 2007; 103:839-846.
12. Lampronti I, Khan MTH, Bianchi N, Lambertini E, Piva R, Borgatti M, Gambari R. Plants with antitumor properties: From biologically active molecules to drugs. Advances in Phytomedicine. 2006; 2:45-63.
13. Haque N, Chowdhury SA, Nutan MT, Rahman GM, Rahman KM, Rashid MA. Evaluation of antitumor activity of some medicinal plants of Bangladesh by potato disk bioassay. Fitoterapia. 2000; 71:547-552.
14. Lee SS, Lee EM, An BC, Kim T-H, Lee KS, Cho J-Y, Yoo S-H, Bae J-S, Chung BY. Effects of irradiation on decolourisation and biological activity in *Schizandra chinensis* extracts. Food Chem. 2011; 125:214-220.
15. Kamatou GPP, Van Zyl RL, Van Vuuren SF, Figueiredo AC, Barroso JG, Pedro LG, Viljoen AM. Seasonal variation in essential oil composition, oil toxicity and the biological activity of solvent extracts of three South African *Salvia* species. S Afr J Bot. 2008; 74:230-237.
16. Burgess ND, Evans CE, Thomas GJ. Vegetation change on the Ouse Washes Wetland, England, 1972-88 and effects on their conservation importance. Biol Conserv. 1990; 53:173-189.
17. Palm CA, Gachengo CN, Delve RJ, Cadisch G, Giller KE. Organic inputs for soil fertility management in tropical agroecosystems: Application of an organic resource database. Agric Ecosyst Environ. 2001; 83:27-42.
18. Staples GW, Herbst DR. A Tropical Garden Flora: Plants

Cultivated In The Hawaiian Islands And Other Tropical Places. Mutual Pub Co, Honolulu, Hawaii, USA, 2005.

19. Duke JA. Handbook of Energy Crops (Unpublished). Purdue University. 1983.

20. Kasture VS, Deshmukh VK, Chopde CT. Anxiolytic and anticonvulsive activity of *Sesbania grandiflora* leaves in experimental animals. Phytother Res. 2002; 16:455-460.

21. National Committee for Clinical Laboratory Standards (NCCLS). Performance standards for antimicrobial susceptibility testing; Ninth informational supplement, NCCLS document M100-S9. Wayne, PA, USA, 2008.

22. Negi PS, Jayaprakasha GK, Jagan Mohan Rao L, Sakariah KK. Antibacterial activity of turmeric oil: A byproduct from curcumin manufacture. J Agric Food Chem. 1999; 47:4297-4300.

23. Ngameni B, Kuete V, Simo IK, Mbaveng AT, Awoussong PK, Patnam R, Roy R, Ngadjui BT. Antibacterial and antifungal activities of the crude extract and compounds from *Dorstenia turbinata* (Moraceae). S Afr J Bot. 2009; 75:256-261.

24. National Committee for Clinical Laboratory Standards (NCCLS). Method for dilution antimicrobial susceptibility tests for bacteria that growth aerobically; Approved standard, NCCLS Document M7-A6. Wayne, PA, USA, 2003.

25. Vuotto ML, Basile A, Moscatiello V, De Sole P, Castaldo-Cobianchi R, Laghi E, Ielpo MT. Antimicrobial and antioxidant activities of *Feijoa sellowiana* fruit. Int J Antimicrob Agents. 2000; 13:197-201.

26. Patrick R. Antimicrobial Agents and Susceptibility Testing. Murray, Washington, DC, USA, 1996.

27. Lenette TH, Barilows A, Hausler WJ, Shadony HJ. Manual of Clinical Microbiology. 5th ed., American Society for Microbiology, Washington, DC, USA, 1991.

28. Lorain V. Antibiotics in laboratory medicine. In: Disk Susceptibility Test (Acar JF, Goldstein FW, eds.). 4th ed., Williams & Walkins Awaverly, London, UK, 1995; p. 1.

29. National Committee for Clinical Laboratory Standards (NCCLS). Methods for determining bactericidal activity of antimicrobial agents, Tentative guideline M26-T. Villanova, PA, USA, 1992.

30. Smith CE, Foleno BE, Barrett JF, Frosco MB. Assessment of the synergistic interactions of levofloxacin and ampicillin against *Enterococcus faecium* by the checkerboard agar dilution and time-kill methods. Diagn Microbiol Infect Dis. 1997; 27:85-92.

Purification of innate immunostimulant from green tea using a silkworm muscle contraction assay

Saphala Dhital, Hiroshi Hamamoto, Makoto Urai, Kenichi Ishii, Kazuhisa Sekimizu*

Laboratory of Microbiology, Graduate School of Pharmaceutical Sciences, The University of Tokyo, Tokyo, Japan.

ABSTRACT: A polysaccharide was purified from a hot water extract of green tea leaves by measuring the immunostimulatory activity in silkworm larvae. Nuclear magnetic resonance and chemical analysis of acid hydrolysates revealed that the purified substance possessed a backbone containing polygalacturonic acids with methyl ester residues. Treatment with β-glucanase attenuated the muscle contraction activity of the purified sample, suggesting that the β-glucan structure, probably as a branched form, was required for its activity. The purified fraction stimulated the production of interleukin-6 by mouse peritoneal macrophages. These results suggest that measuring immunostimulation in silkworm larvae is useful for evaluating innate immunostimulants from various sources.

Keywords: Polysaccharides, pectin, green tea, innate immunity, mice, macrophages, IL-6, insect

1. Introduction

In addition to its use as a popular beverage, tea (*Camellia sinensis*) is also used as medicine to maintain health in humans. The therapeutic effects of green tea components have been studied in several disease models. For example, feeding green tea to mice with lupus-like syndrome improved survival and delayed disease progression (*1*). Laurie *et al*. studied the effect of a green tea extract in human patients with advanced lung cancer (*2*). Several compounds of green tea leaves such as polyphenols are reported to possess antitumor (*3*), antioxidant, and anti-diabetic properties (*4*). Thus we focused on green tea as a source of bioactive substances that stimulate innate immunity.

The immune system is divided into two categories; adaptive and innate immunity. Innate immunity is the first barrier of host animals against invading pathogens and the system is well conserved among species. In insects, microbial components trigger defensive reactions such as melanization of the blood (*5,6*) and the production of antimicrobial factors (*7,8*). We previously reported that the injection of peptidoglycans and β-glucans, cell wall components of bacteria and fungi, respectively, induces slow paralysis in silkworms (*9*). Peptidoglycans and β-glucans are thought to be recognized by immune cells in silkworms followed by the activation of an insect cytokine, paralytic peptide, which induces muscle contraction and several self-defense reactions (*9-11*). Because peptidoglycan and β-glucan are well-known stimulants of innate immunity in various organisms, we hypothesized that quantitative measurement of silkworm muscle contraction would be useful for assessing the immunostimulatory activities of natural products or compounds. Here, we purified an immunostimulant from a hot water extract of green tea leaves using a silkworm muscle contraction assay. We further observed the stimulatory effect of the extract on murine macrophages. Structural analysis revealed that polygalacturonic acid was responsible for the activity.

2. Materials and Methods

2.1. Reagents

Green tea leaves were purchased from a local market. Tea polyphenols [catechin (±), catechin (+), and polyphenon 60], lipopolysaccharides (LPS) from *Escherichia coli*, and thioglycollate medium were purchased from Sigma-Aldrich. RPMI 1640, antibiotics (penicillin and streptomycin), and fetal bovine serum were purchased from Invitrogen. Enzyme-linked immunosorbent assay (ELISA) kits (Ready-Set-go) and interleukin (IL)-6 were purchased from eBioscience.

2.2. Silkworms

Eggs of silkworms (*Bombyx mori*, HuYo Tukuba Ne) were purchased from Ehime Sanshu (Ehime, Japan). Silkworm

---

Address correspondence to:
Dr. Kazuhisa Sekimizu, Laboratory of Microbiology, Graduate School of Pharmaceutical Sciences, The University of Tokyo, 7-3-1 Hongo, Bunkyo-ku, Tokyo 113-0033, Japan.
e-mail: sekimizu@mol.f.u-tokyo.ac.jp

larvae were reared on an artificial diet (Silkmate 2S, Nihon Nosan, Yokohama, Japan) at 27°C (*12*).

2.3. *Silkworm muscle contraction assay*

Quantitative measurement of silkworm muscle contraction to evaluate innate immunity activation was described previously (*9*). Briefly, heads of fifth instar silkworm larvae (3-5 g) were cut off and the peritrophic membranes were removed. Each specimen was immobilized and attached with a 27-g load. Samples were dissolved or suspended in sterile saline, and 50 μL of each sample was injected into the body fluid of a specimen with a 1-mL syringe attached to a 27-gauge needle (Terumo, Tokyo, Japan). The muscle contraction value was calculated by measuring the maximum length of each specimen before (x cm) and after (y cm) the injection using the formula $(x - y)/x$. One unit of activity was defined as that which caused muscle contraction with the value of 0.15. The muscle contraction activity was measured by injecting 50 μL of sample dissolved in saline. The specific activity of the fraction was determined by creating a titration curve with diluted samples.

2.4. *Measurement of total sugar*

The amount of total sugar in the fractions was determined using the phenol-sulfuric acid method, a colorimetric test with D-glucose (Nacalai Tesque, Kyoto, Japan) as a standard (*13*). One hundred microliters of the sample was added to an equal volume of 5% phenol solution, and the mixture was vigorously mixed for 1 min. Concentrated sulfuric acid (98%; 500 μL; Nacalai Tesque) was added and the solution was immediately mixed vigorously. The samples were incubated at room temperature for 30 min and the OD_{490} values were measured using an MTP-300 Microplate reader (Corona Electric, Ibaraki, Japan).

2.5. *Preparation and purification of a hot water extract of green tea leave*

Green tea leaves (100 g) were autoclaved at 121°C for 15 min in 1 L of water. The sample was cooled and then centrifuged at 8,000 × g in a Hitachi centrifugation rotor [Himac CR 21E (rotor R10A)] for 10 min at 4°C. The supernatant was filtered through a paper filter (Advantec, pore size 0.45 μm), and the filtrate was freeze-dried for 48 h (Fraction I). The extracted fraction was added to two volumes of ethanol (99.5%; Nacalai, Japan) followed by centrifugation to collect the precipitated active substance (Fraction II).

1st DEAE-cellulose chromatography (pH 7.9) The ethanol precipitate (Fraction II, 610 mg in 8 mL buffer) was slowly applied onto a 20-mL DEAE-cellulose (DE-52, Whatman) column equilibrated with 10 mM Tris-HCl buffer (pH 7.9). After washing with 120 mL

Tris buffer, the column was developed with a 0-0.4 M NaCl gradient (250 mL × 2). The eluted fractions (6 mL each) were collected using a CHF fraction collector (Advantec, Japan). The sugar concentrations in the eluted fractions were determined using the phenol-sulfuric acid method as described above.

2nd DEAE-cellulose chromatography (pH 5.6) Active fractions of the 1st DEAE-cellulose chromatography (pH 7.9) were pooled and loaded onto a 20-mL DEAE-cellulose (DE-52, Whatman) column equilibrated with 10 mM MES buffer (pH 5.6). The column was developed with a linear gradient of 0-0.4 M NaCl (250 mL × 2), and 6-mL fractions were collected. Active fractions were pooled and named Fraction III.

1st Mono Q chromatography (pH 7.9) Fraction III (pH 5.6) was loaded onto a Mono Q column equilibrated with 10 mM Tris-HCl, pH 7.9, and fractionated at a flow rate of 0.4 mL/min (2 mL/fraction). After loading the sample, the column was washed with 14 mL of buffer. Two steps of gradient elution, 16 mL of 0-20 mM and 40 mL of 20 mM-1 M NaCl, were performed.

2nd Mono Q chromatography (pH 5.6) The pooled fraction of the 1st Mono Q chromatography (pH 7.9) was loaded onto a Mono Q column (GE Healthcare, Buckinghamshire, UK) equilibrated with 10 mM MES buffer (pH 5.6). Elution by NaCl gradient to elute the bound materials was performed as described above for the 1st Mono Q chromatography (pH 7.9). The fractions were concentrated 6.5-fold by ethanol precipitation, and 50 μL of each sample was subjected to the muscle contraction assay. Active fractions were pooled and named Fraction IV.

Gel filtration with Superdex 200 Five hundred microliters of Fraction IV (14 mg/mL) was loaded on a 24-mL Superdex 200 (GE Healthcare) column equilibrated with 10 mM Tris-HCl (pH 7.9) and 150 mM NaCl. The column was calibrated with compounds of known molecular mass; sodium dextran sulfate (500 kDa), dextran 40 (40 kDa), and D-galacturonic acid monohydrate (0.2 kDa). Fractionation was performed with fast protein liquid chromatography equipment (GE Healthcare) at a flow rate of 0.5 mL/min.

2.6. *Monosaccharide analysis*

Purified fractions from green tea and the standard (D-glucose) were treated with 4 M trifluoroacetic acid at 100°C for 3 h. After acid hydrolysis, *N*-acetylation was performed to change amino sugars to their *N*-acetylated forms, by mixing the sample with pyridine methanol (1:9, v/v) and then treating with pyridine/acetic anhydride (4:1, v/v) for 30 min at room temperature. The samples were labeled with aminobenzoic acid ethyl ester (ABEE) by incubating at 80°C for 1 h, and analyzed by reversed phase-high performance liquid chromatography [RP-HPLC; Honenpak C18 (75 mm × 4.6 ID)] with 0.2 M potassium borate: acetonitrile (93:7)

at a flow rate of 1 mL/min. Peaks were detected by UV 305 nm according to retention time.

The standard comprised a mixture of 13 mono-saccharides (2 nmol each; L-arabinose, L-fucose, D-galactose, D-glucose, D-mannose, L-rhamnose, D-ribose, D-xylose, D-galacturonic acid, D-glucuronic acid, *N*-acetyl-D-galactosamine, *N*-acetyl-D-glucosamine, and *N*-acetyl-D-mannosamine).

2.7. *Nuclear magnetic resonance (NMR) analysis*

Fraction V (11 mg) was dissolved in deuterium oxide (D_2O), and ^1H and ^{13}C NMR (ECA-500, JEOL) analyses were performed at 40°C.

2.8. *β-glucanase sensitivity test*

Five milligrams of Fraction V was incubated with or without 11 mg of endo-1,3(4)-β-glucanase from *Apergillus niger* (Sigma) in 0.1 M sodium citrate buffer (pH 5.0) at 25°C for 6 h. After incubation, the enzyme was inactivated by boiling at 100°C for 5 min. Immunostimulation activity of the sample was measured by the silkworm muscle contraction assay as described above.

2.9. *IL-6 production by mouse peritoneal macrophages*

Peritoneal mouse macrophages were collected from C57BL/6 male mice 3 days after the injection of 1 mL of 4% thioglycollate medium. Twenty microliters of each sample was added to tissue culture plates (96 well, flat bottom, Iwaki Science Department, Asahi Glass Corporation, Japan) containing 10^5 cells/well in 200 μL of RPMI 1640 medium. The medium was supplemented with L-glutamine, 25 mM HEPES, 10% fetal bovine serum, and 100 μg/mL each of penicillin/streptomycin. The cells were incubated at 37°C for 24 h. The IL-6 concentration of 100 μL of each culture supernatant was measured using an ELISA kit (eBioscience). The standard curve was drawn using recombinant IL-6 (eBioscience) as the standard.

2.10. *Statistical analysis*

The significance of differences was calculated using the Student's *t*-test. Differences with a *p* value of less than 0.05 were considered statistically significant.

3. Results

3.1. *Induction of silkworm muscle contraction by a hot water extract of green tea leaves*

Screening of hot water extracts of food samples using the silkworm muscle contraction assay indicated that a hot water extract of green tea leaves had high innate immunostimulation activity. A freeze-dried fraction of the hot water extract of green tea had 6 units/mg of specific activity (Table 1). Activity per weight of dried green tea leaves was 1,300 units/g dry weight. Tea polyphenols [catechin (±), catechin (+), and polyphenon 60] and cellulose, components in green tea leaves, did not induce muscle contraction. Therefore, we concluded that substances other than polyphenols and cellulose were responsible for the innate immunostimulation in the hot water extract of green tea leaves. The fraction was further purified by ethanol precipitation followed by chromatographies with DEAE-cellulose and Mono Q.

3.2. *DEAE-cellulose chromatography*

Acid polysaccharides were reported from plant, such as pectin (*14*). To elucidate whether the substance in tea extract have acid moieties, we performed the DEAE-cellulose chromatography. The elution profile of chromatography (pH 7.9) is shown in Figure 1. A major part of the activity was adsorbed on the column, suggesting the presence of acidic moieties in the active substance. The specific activity of the active fraction recovered from the column was 28 units/mg, which was equivalent to that of the loaded sample. Rechromatography of the fraction with a DEAE-cellulose column at pH 5.6 showed absorbance of the active substance to the column, and there was no increase in specific activity in the salt-eluted fractions (Fraction III).

3.3. *Mono Q chromatography*

To further purify the immunostimulant from green tea leaves, we performed two rounds of Mono Q column chromatography. The active substance was adsorbed to the column (Figure 2). A major part of the activity was eluted by the salt gradient. Quantification of total sugar by the phenol-sulfuric acid method revealed that the activity peak coincided with the presence of polysaccharide. The specific activity of the active fraction was 40 units/mg. There was

Table 1. Summary of purification of innate immunity stimulating fraction from 100 g of green tea leaves

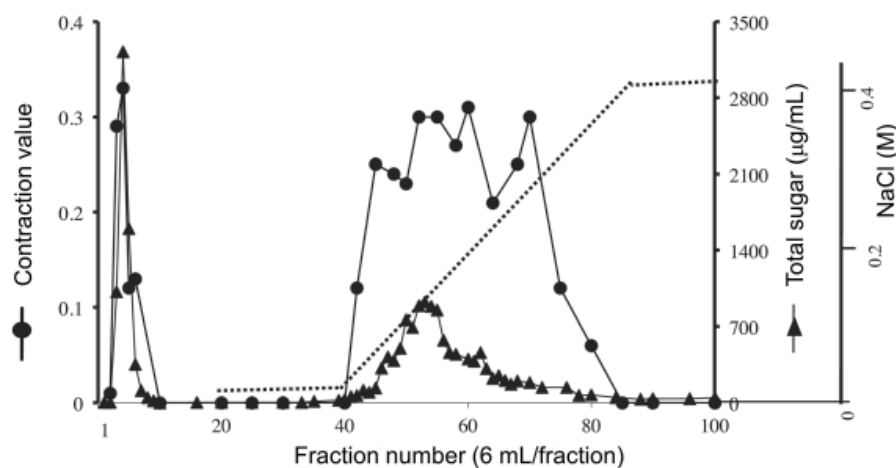| Fraction	Total activity (units)	Yield (%)	Amount (mg)	Specific activity (units/mg)
I Hot water extract	132,000	100	22,000	6
II Ethanol extract	75,600	57	2,700	28
III DEAE-cellulose chromatographies (pH 7.9 and 5.6)	16,200	12	810	20
IV Mono Q chromatographies (pH 7.9 and 5.6)	7,400	6	185	40
V Superdex 200 chromatography	4,000	3	100	40

Figure 1. Elution profile of 1st DEAE-cellulose chromatography (pH 7.9). Silkworm muscle contraction assay was performed by injecting 50 μL of each sample (concentrated 6.5-fold). Total sugar concentration was measured by the phenol-sulfuric acid method. Active fractions (43-80) were pooled for further procedures.
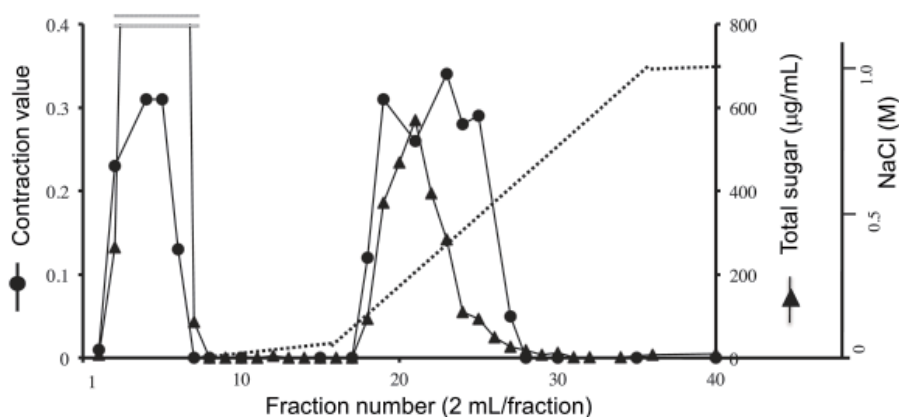

Figure 2. Elution profile of Mono Q chromatography (pH 7.9). Silkworm muscle contraction assay was performed by injecting 50 μL of each sample (concentrated 6.5-fold). Active fractions (18-27) were pooled and used for further purification.

no increase in the specific activity by rechromatography with Mono Q at pH 5.6 (Fraction IV).

3.4. *Gel filtration with Superdex 200*

To further evaluate the purity of the fraction obtained by rechromatography with the Mono Q column (Fraction IV), gel filtration was performed using Superdex 200 (GE Healthcare). The activity co-migrated with the polysaccharide peak (Figure 3). The specific activity of the pooled fraction (Fraction V) was 40 units/mg, equivalent to that of the loaded fraction. The active substance was eluted in fractions between those of sodium dextran sulfate (500 kDa) and dextran 40 (40 kDa), suggesting that the innate immunostimulants in green tea leaves possessed heterogeneous molecular masses.

3.5. *Monosaccharide analysis of acid hydrolysate*

Purified fraction (Fraction V) was hydrolyzed by acid treatment, and the monosaccharide composition was determined. RP-HPLC analysis of the ABEE-labeled

sample revealed the presence of galacturonic acid, galactose, glucose, and rhamnose (Figure 4). The molar ratio of each monosaccharide was determined by measuring the peak area. The ratio of galacturonic acid: galactose:glucose:rhamnose was 22:4:5:1, respectively. These findings suggested that a major component in the fraction was D-galacturonic acid.

3.6. *NMR analysis*

Four kinds of anomeric proton signals were detected by ^{1}H NMR at 5.12, 5.15, 5.16, and 5.19 parts per million (ppm). The relative intensity of the signal detected at 5.12 ppm was two times higher than that of the other anomeric signals. Based on the observed chemical shifts of anomeric protons, these saccharide residues might have an alpha anomeric configuration. A methyl proton signal characteristic to galacturonic acid methyl ester was also detected at 3.87 ppm. Based on comparisons with the relative intensity of the methyl proton signal to that of the anomeric proton signals, approximately half of the galacturonic acid was the methyl ester (Figure 5).

The chemical shifts obtained by ^{13}C NMR analysis of Fraction V were similar to that of polygalacturonic acid (*15,16*). Four kinds of anomeric carbon signals were detected at 99.2, 99.6, 100.3, and 100.6 ppm. The intensity of the signal detected at 99.2 ppm was higher than that of the other anomeric signals. Based on the observed chemical shifts of anomeric carbons, saccharide residues were assigned an alpha anomeric configuration. Three kinds of methyl carbon signals characteristic of galacturonic acid methyl ester were detected at 52.5, 52.8, and 53.1 ppm. Signals of carbons thought to be of

carboxylic acid (around 175 ppm) and methyl esterified carboxylic acid (around 171 ppm) were also detected (Figure 5).

3.7. *Effect of β-glucanase on the activity of green tea*

β-glucans are major cell wall components of plants and fungi. We previously reported that yeast β-glucans induce muscle contraction in silkworms (*9*). To test whether the purified fraction from green tea leaves contained a β-glucan structure that contributes to its activity, we
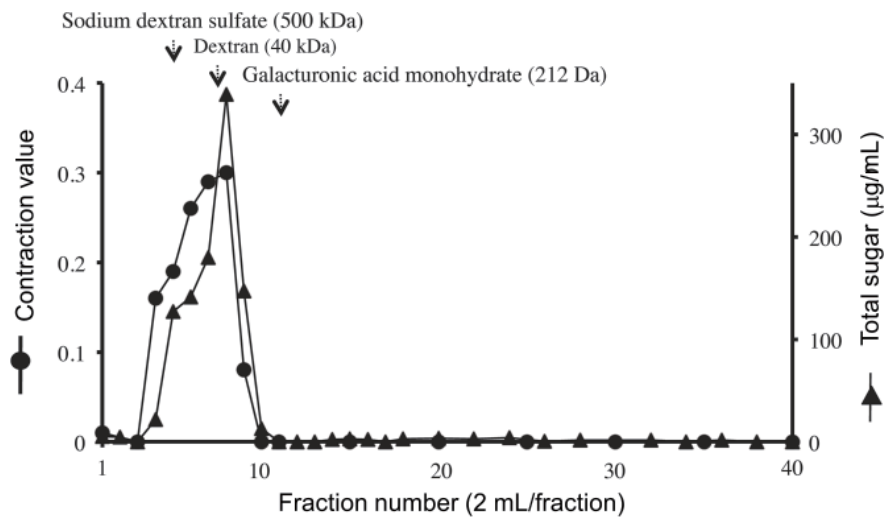

Figure 3. Elution profile of gel filtration with Superdex 200. Silkworm muscle contraction assay was performed by injecting 50 µL of each sample (concentrated 6.5-fold).
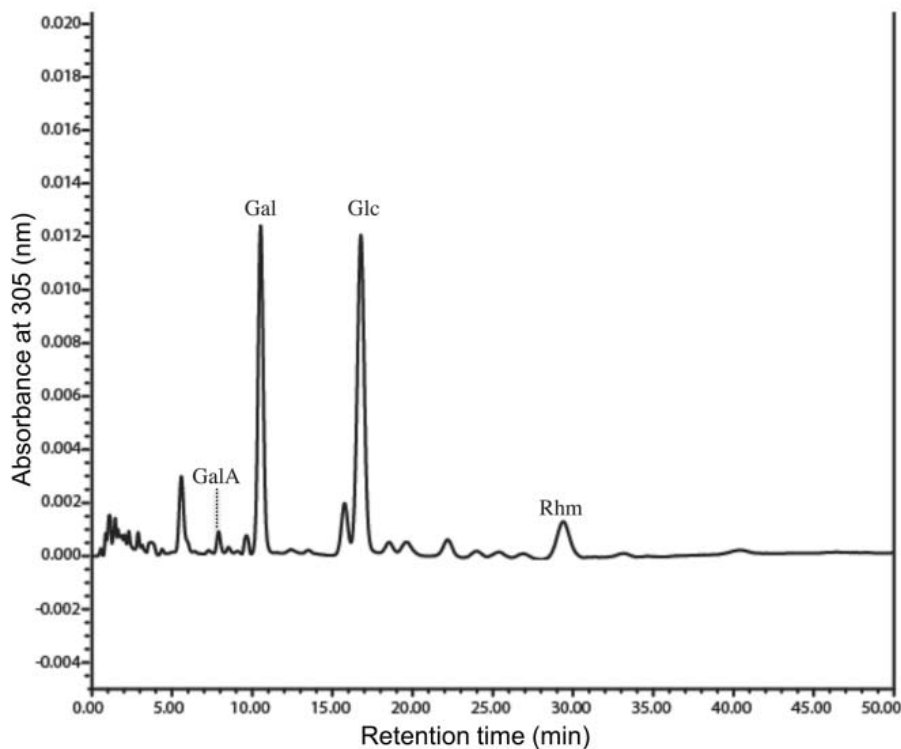

Figure 4. HPLC analysis of acid hydrolyzed monosaccharides from green tea. Acid hydrolyzed monosaccharides labeled with aminobenzoic acid ethyl ester were analyzed by RP-HPLC.
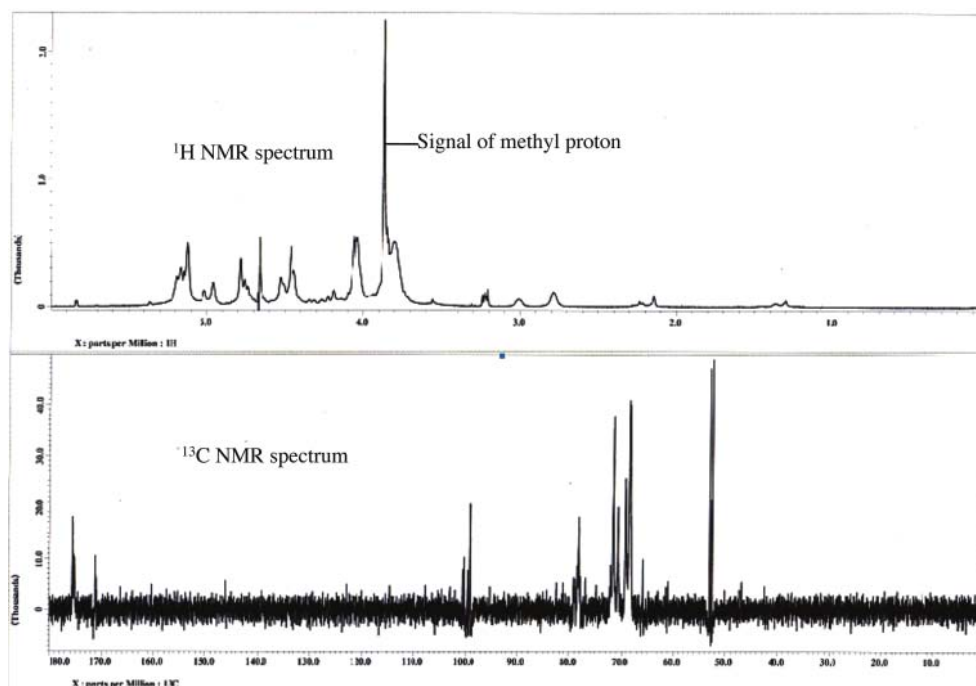
Figure 5. ¹H NMR and ¹³C NMR spectrum of the purified substance from green tea. Fraction V (11 mg) dissolved in deuterium oxide (D_2O), was analyzed by ¹H and ¹³C NMR (ECA-500, JEOL).
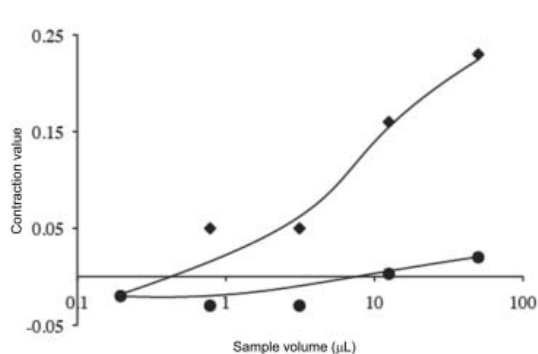
Figure 6. Effect of 1,3(4)β-glucanase on green tea Fraction IV. Fraction IV (5 mg) was incubated with (closed circles) or without (closed diamonds) 11 mg of 1,3(4)β-glucanase from *A. niger* in a sodium citrate buffer (pH 5.0) at 25°C for 6 h. After the incubation, the enzyme was inactivated by boiling at 100°C for 5 min. Immunostimulation activity was measured using the silkworm muscle contraction assay.

examined the sensitivity of the fraction to β-glucanase. The result of the muscle contraction assay indicated that β-glucanase treatment of the purified fraction (Fraction IV) of green tea abolished the innate immunostimulation activity in silkworm. In contrast, the sample treated under the same condition without β-glucanase induced muscle contraction of the larval specimen (Figure 6). These findings demonstrated that the immunostimulation activity of the purified material was sensitive to β-glucanase from *A. niger*.

3.8. *IL-6 production by mouse macrophages stimulated by polysaccharide purified from green tea*

Silkworm larvae muscle contraction was used to evaluate the innate immunostimulating activity of the samples
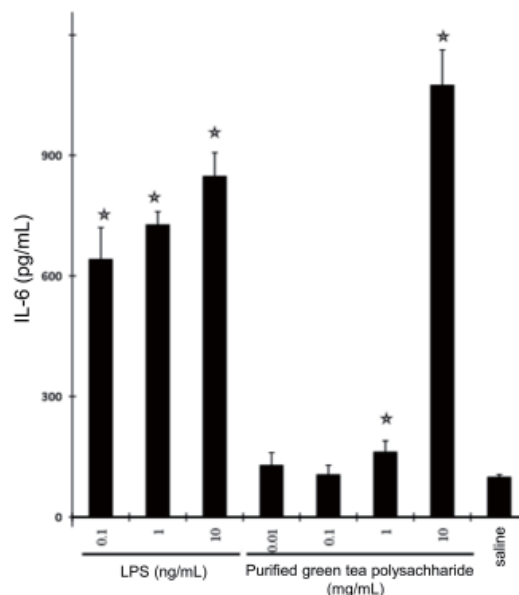
Figure 7. Induction of IL-6 production by mouse peritoneal macrophages incubated with purified compounds from green tea. Mouse peritoneal macrophages stimulated with thioglycollate (4%) from C57BL/6 male mice were incubated with different concentrations of samples for 24 h. The amount of IL-6 in the supernatant of culture medium was measured by ELISA. Data represent mean ± S.D. of 3 experiments (★, $p < 0.05$ compared with saline).

during the purification process. Whether the purified fraction stimulates innate immunity in the mammalian system remained to be clarified. To address this question, we examined the effect of the purified fraction (Fraction V) on mouse macrophages. The amount of IL-6 produced by mouse peritoneal macrophages was significantly increased by incubation with Fraction V (Figure 7). These results suggest that the innate immunostimulants purified

using the silkworm system also stimulate innate immunity in mammalian systems. The specific activity of Fraction V in terms of IL-6 production by mouse macrophages, however, was much less than that of LPS.

4. Discussion

The innate immune system has a vital role in eliminating microbial invaders in insects that lack an adaptive immune system. Based on our previous report demonstrating that an insect cytokine paralytic peptide induced both muscle contraction and defensive reactions in immune cells (*9*), we hypothesized that the immunostimulatory activities of foreign compounds could be assessed using a silkworm muscle contraction assay. Here, using green tea (*C. sinensis*) leaves as a starting material, we demonstrated that this silkworm muscle contraction assay system could be utilized for the purification of immunostimulants.

The active immunostimulating substance was fractionated by successive chromatographies of DEAE-cellulose, Mono Q, and gel filtration. The results indicated that these procedures produced little increase in the specific activities of the substances, suggesting that the active materials were almost pure. Since DEAE-cellulose column chromatography did not increase the specific activity, this step could omit for the purification of innate immunity stimulant of green tea. The results further indicated that the innate immunostimulating factor in green tea had an acidic nature, since the substance was absorbed on DEAE-cellulose column. Previous studies demonstrated that acidic polysaccharides derived from plants activate innate immunity in mice. Yang *et al*. reported that an acidic polysaccharide isolated from the roots of *Angelica sinensis* activated macrophages, resulting in the increased production of nitric oxide (*14*). Further comparative analysis is required to identify the relevance of the acidic nature to immunostimulatory activities of the acidic polysaccharides from different plant sources.

Structural analysis of the innate immunostimulant purified from green tea extract was performed by monosaccharide composition analysis and NMR. The ^{1}H and ^{13}C NMR results allowed us to identify the chemical-shift of each atom. The main structures of the purified green tea fraction were polygalacturonic acid and methyl ester residues. The sensitivity of this fraction to β-glucanase (*A. niger*) is likely due to the presence of an endo-1,3(4)β-glucanase-sensitive structure with the main polygalacturonic acid backbone, which is responsible for the biologic activity to stimulate silkworm innate immunity. Apple pectin, another acidic polysaccharide with a polygalacturonic acid backbone, had a low stimulatory effect in the silkworm muscle contraction assay (unpublished data). Based on these findings, we propose for the first time that modification of polygalaturonic acid backbones with a β-glucan structure is critical for the immunostimulatory activity.

Purified substances from green tea stimulated mouse macrophages to produce IL-6, suggesting that the purification method using silkworms could be applied to search for immunostimulants that act on mammalian cells. Because LPS do not cause silkworm muscle contraction even at high doses (unpublished data), we assumed that the activity of the purified sample observed in the silkworm system was not due to LPS contamination. On the other hand, because of the high sensitivity of mouse macrophages, we could not exclude the possibility that a trace amount of LPS contamination stimulated the IL-6 production.

β-glucans are recognized by several immune receptors such as Toll-like receptor 4, Toll-like receptor 2/6, Dectin-1, specific intercellular adhesion molecule-3-grabbing non-integrin 1, complement receptor 3, lactosylceramide, and β-glucan recognizing proteins. β-glucans trigger the activation of a group of immune cells, including macrophages, neutrophils, monocytes, natural killer cells, and dendritic cells, in mammals (*17*). Because some of the microbial recognition mechanisms are conserved among species, we propose that the purified fraction from green tea leaves might stimulate innate immunity in both insects and mammals *via* common mechanisms. Future studies to identify the receptors and signaling molecules involved in stimulating innate immunity will help to clarify this point.

References

1. Sayama K, Oguni I, Tsubura A, Tanaka S, Matsuzawa A. Inhibitory effects of autoimmune disease by green tea in MRL-Faslprcg/Faslprcg mice. In Vivo. 2003; 17:545-552.
2. Laurie SA, Miller VA, Grant SC, Kris MG, Ng KK. Phase I study of green tea extract in patients with advanced lung cancer. Cancer Chemother Pharmacol. 2005; 55:33-38.
3. Shimizu M, Shirakami Y, Moriwaki H. Targeting receptor tyrosine kinases for chemoprevention by green tea catechin, EGCG. Int J Mol Sci. 2008; 9:1034-1049.
4. Cabrera C, Artacho R, Giménez R. Beneficial effects of green tea – a review. J Am Coll Nutr. 2006; 25:79-99.
5. Ishii K, Hamamoto H, Imamura K, Adachi T, Shoji M, Nakayama K, Sekimizu K. Porphyromonas gingivalis peptidoglycans induce excessive activation of the innate immune system in silkworm larvae. J Biol Chem. 2010; 285:33338-33347.
6. Kanost MR, Jiang H, Yu XQ. Innate immune responses of a lepidopteran insect, Manduca sexta. Immunol Rev. 2004; 198:97-105.
7. Hoffmann JA, Kafatos FC, Janeway CA, Ezekowitz RA. Phylogenetic perspectives in innate immunity. Science. 1999; 284:1313-1318.
8. Natori S. Bactericidal substance induced in the haemolymph of *Sarcophaga peregrina* larvae. J Insect Physiol. 1977; 23:1169-1173.

9. Ishii K, Hamamoto H, Kamimura M, Sekimizu K. Activation of the silkworm cytokine by bacterial and fungal cell wall components *via* a reactive oxygen species-triggered mechanism. J Biol Chem. 2008; 283:2185-2191.

10. Nakahara Y, Kanamori Y, Kiuchi M, Kamimura M. Effects of silkworm paralytic peptide on *in vitro* hematopoiesis and plasmatocyte spreading. Arch Insect Biochem Physiol. 2003; 52:163-174.

11. Ishii K, Hamamoto H, Kamimura M, Nakamura Y, Noda H, Imamura K, Mita K, Sekimizu K. Insect cytokine paralytic peptide (PP) induces cellular and humoral immune responses in the silkworm *Bombyx mori*. J Biol Chem. 2010; 285:28635-28642.

12. Sekimizu K, Larranaga J, Hamamoto H, Sekine M, Furuchi T, Katane M, Homma H, Matsuki N. D-Glutamic acid-induced muscle contraction in the silkworm, *Bombyx mori*. J Biochem. 2005; 137:199-203.

13. Handa N. Examination of the applicability of the phenol-sulfuric acid method to the determination of dissolved carbohydrate in sea water. J Oceanogr Soc Japan. 1966; 22:79-86.

14. Yang X, Zhao Y, Wang H, Mei Q. Macrophage activation by an acidic polysaccharide isolated from *Angelica sinensis* (Oliv.) Diels. J Biochem Mol Biol. 2007; 40:636-643.

15. Petersen BO, Meier S, Duus JO, Clausen MH. Structural characterization of homogalacturonan by NMR spectroscopy-assignment of reference compounds. Carbohydr Res. 2008; 343:2830-2833.

16. Monge ME, Negri RM, Kolender AA, Erra-Balsells R. Structural characterization of native high-methoxylated pectin using nuclear magnetic resonance spectroscopy and ultraviolet matrix-assisted laser desorption/ionization time-of-flight mass spectrometry. Comparative use of 2,5-dihydroxybenzoic acid and nor-harmane as UV-MALDI matrices. Rapid Commun Mass Spectrom. 2007; 21:2638-2646.

17. Chan GC, Chan WK, Sze DM. The effects of beta-glucan on human immune and cancer cells. J Hematol Oncol. 2009; 2:25.

Anti-influenza viral effects of novel nuclear export inhibitors from Valerianae Radix and *Alpinia galanga*

Ken Watanabe[1], Hanae Takatsuki[1], Megumi Sonoda[1], Satoru Tamura[2], Nobutoshi Murakami[2], Nobuyuki Kobayashi[1,3,*]

[1] *Laboratory of Molecular Biology of Infectious Agents, Graduate School of Biomedical Sciences, Nagasaki University, Nagasaki, Japan;*

[2] *Laboratory of Exploration of Medicinal Plant Resources, Graduate School of Pharmaceutical Sciences, Osaka University, Osaka, Japan;*

[3] *Central Research Center, AVSS Corporation, Nagasaki, Japan.*

ABSTRACT: Many pathogenic viruses, such as the influenza virus and the Human Immunodeficiency Virus (HIV)-1, are a threat to humans, thus leading to thousands of deaths annually. The development of antiviral drugs is urgent, and it is an essential strategy for the suppression of these infectious diseases. However, regardless of the rapid emergence of many infectious diseases, the development of novel anti-viral drugs has been slow, except for the case of the AIDS. In addition, several viruses can easily mutate and escape the inhibitory activity of anti-viral drugs. It was already well-established that HIV escapes from anti-viral drug effects because of the lack of proofreading activity in its reverse transcriptase. It is known that the influenza virus, which is resistant to Tamiflu, is already spread all over the world. Viruses utilize the host cell environment and cellular factors to propagate. Therefore, the development of novel drugs which inhibit viral protein-host protein interactions or cellular functions appear to be good candidates. The influenza virus is unique in replicating in host nuclei, and we therefore focused on the nuclear export processes for the development of anti-influenza viral drugs. We previously reported that leptomycin B (LMB), which inhibited the nuclear export processes *via* the nuclear export signal (NES) inhibited the nuclear export of influenza viral RNP (vRNP), and resulted in the inhibition of influenza viral propagation. We herein examined novel CRM1 inhibitors, valtrate from Valerianae Radix, and 1'-acetoxychavicol acetate (ACA) from *Alpinia galanga* as potent inhibitors for the influenza virus replication.

1. Introduction

Nuclear pore complexes (NPCs) mediate the bi-directional transport of molecules between the cytoplasm and the nucleus. The NPC forms a channel that is approximately 9 nm in diameter. Small molecules with a molecular mass of less than 40 kDa can diffuse through this channel. However, larger molecules are transported through this channel by energy-dependent mechanisms. In the nuclear import processes, the proteins that are selectively transported to the nucleus have a sequence called the nuclear localization signal (NLS). The cellular factor importin-alpha, which complexes with importin-beta, binds to the NLS and passes through the NPC into the nucleus (*1*). In the nuclear export processes, proteins are selectively exported from the nucleus to the cytoplasm when they contain a leucine-rich consensus sequence called the nuclear export signal (NES) (*2*). The NES binds to the nuclear export factor CRM1, and nuclear export occurs under the regulation of the Ran protein (*3*); for a review, see (*4*). The NES was identified in various proteins such as HIV-1 Rev (*5*), protein kinase A inhibitor (*2*), MKK6 (an activator of p38 MAPK) (*6*), p53 (*7*).

The influenza virus binds to sialic acids on the cell surface through hemagglutinin (HA) and it is incorporated into the cell *via* endocytosis. The viral ribonucleoprotein complex (vRNP) is released into the cytoplasm by M2 protein ion channel activity. In contrast to many other RNA viruses, replication of the influenza virus occurs in the nucleus (*8*). The vRNP consists of viral RNA, NP and the viral RNA polymerases PA, PB1, and PB2, and each vRNP protein contains an NLS. Therefore, the viral RNP is transported into the nucleus by the NLS-mediated nuclear import pathway. In the

Address correspondence to:
Dr. Nobuyuki Kobayashi, Laboratory of Molecular Biology of Infectious Agents, Graduate School of Biomedical Sciences, Nagasaki University, 1-14 Bunkyo-machi, Nagasaki 852-8521, Japan.
e-mail: nobnob@nagasaki-u.ac.jp

nucleus, early transcription from vRNP occurs and viral mRNAs are exported from the nucleus. Newly-synthesized viral early proteins NP, PB1, PB2, and PA are imported into the nucleus *via* their NLS, and complex with newly-synthesized viral RNA. The late transcription occurs from progeny vRNP, and the viral late proteins M1, M2, HA, NA, and NS2 are synthesized thereafter. It has been reported that M1 and NS2 are important for the nuclear export of the progeny vRNP. M1 binds to both vRNP and NS2, but only NS2 have an NES. However the function of M1 for the nuclear export of vRNP is not yet completely understood, since M1 does not contain an NES. The nuclear export of vRNP is hypothesized to be mediated as the vRNP-M1-NS2-CRM1 complex (*9,10*). However, other reports have suggested that NS2 is not essential for the nuclear export of vRNP, since NS2 does not colocalize with RNP (*11*). Recently, we have identified that the host heat shock protein Hsc70 can bind to M1 and mediates the nuclear export of vRNP (*12,13*). Hsc70 has an NES signal (*14*) and processes the nuclear export of importin and transportin (*15*). Therefore, either NS2, Hsc70, or both may mediate the nuclear export of vRNP. These findings suggest that the inhibition of the influenza viral RNP nuclear export by a specific nuclear export inhibitor is effective for reducing the influenza virus production (*13*).

Antiviral drugs are one of the most important strategies for the treatment of infected patients, but some viruses, especially RNA viruses, easily mutate and become resistant to drugs designed for viral gene products. It is well known that the influenza virus, which is resistant to amantadine (the inhibition of viral M2 protein) or Tamiflu (a viral neuraminidase inhibitor), is already spreading throughout the world. The same problems are prevalent in HIV treatment, and a recent multi-drug combination therapy protocol, termed HAART therapy, is essential to treat patients with HIV. Novel drugs that target cellular proteins may avoid such problems. Inhibitors that regulate the nuclear export system appear to be a good candidate for HIV therapy. We recently demonstrated that leptomycin B (LMB) treatment inhibits the nuclear export of influenza viral vRNP and results in reduced viral production (*13*). However, LMB and its derivatives are highly hydrophobic, and are therefore unsuitable for clinical treatment purposes. Previously we reported a new class of nuclear export inhibitors, valtrate and 1'-acetoxychavicol acetate (ACA) (Figure 1) which were isolated from Valerianae Radix, the roots of *Valeriana fauriei* (*16*) and the roots of *Alpinia galanga* (*17*), respectively. These compounds covalently bind to the CRM1, and inhibit the nuclear export of HIV-1 Rev containing NES (*16,17*). Since valtrate and ACA possess moderate hydrophobicity which is suitable for chemotherapeutic application, we herein examined whether valtrate and ACA can inhibit the nuclear export of influenza viral RNP complex and reduce viral production.

2. Materials and Methods

2.1. *Cells, virus, chemicals and antibody*

Madin-Darby canine kidney (MDCK) cells were grown in Eagle's Minimum Essential Medium (MEM) supplemented with 5% fetal bovine serum (FBS) at 37°C in 5% CO_2. HeLa cells were grown in MEM supplemented with 10% FBS at 37°C in 5% CO_2. Influenza virus A/WSN/33(H1N1) was propagated in 10-day-old embryonated eggs as described previously (*12*) and titrated by the plaque assay as described below. LMB was purchased from Enzo Life Sciences International, Inc. (PA, USA) and was dissolved in EtOH at a concentration of 10 μg/mL. The solution was stored at –20°C. ClogPs of valtrate, ACA, and LMB were calculated using the computer software program (version 4.0, Bio Byte Corporation, CA, USA). An anti-NP mouse mAb that specifically binds to vRNP was kindly supplied by Dr. Fumitaka Momose (Kitazato University) (*18*).

2.2. *Isolation of valtrate and ACA*

Isolation of valtrate: The crushed Valerianae Radix (100 g, Tochimoto Tenkaido, Osaka, Japan) was extracted with MeOH at room temperature for 6 h. After filtration, the residue was further extracted with MeOH under reflux for 3 h twice. The combined filtrates were concentrated under reduced pressure to give MeOH extract (13.2 g). The extract was partitioned between EtOAc and H_2O, and the EtOAc layer was evaporated in vacuo to yield the EtOAc extract (3.6 g). The extract was separated by SiO_2 column chromatography (80 g) using *n*-hexane-EtOAc (20:1 → 5:1 → 1:1) as eluents to provide the fraction (97.2 mg) containing valtrate. The fraction was further separated by normal-phase HPLC [column: Cosmosil 5SL 10 × 250 mm (Nacalai Tesque, Kyoto, Japan), flow rate: 4.0 mL, mobile phase: *n*-hexane:EtOAc = 10:1, detection: 220 nm] to give a crude mixture of valtrate. The mixture was finally purified by reverse-phase HPLC [column: Cosmosil 5C18-AR-II 10 × 250 mm (Nacalai Tesque, Kyoto, Japan), flow rate: 3.0 mL, mobile phase: MeOH:H_2O = 4:1, detection: 220 nm] to furnish valtrate (6.3 mg) (*16*). After the purified valtrate was dissolved in DMSO at a concentration of 5 mg/mL, the solution was stored at −20°C.

Isolation of ACA: The dried and powdered roots of *A. galanga* (22 g, Shinwa Bussan, Osaka, Japan) were extracted with MeOH in the same manner in the extraction of the crushed Valerianae Radix. The combined filtrates were concentrated under reduced pressure to give MeOH extract (2.1 g). The extract (210 mg) was separated by SiO_2 (Fuji Silysia Chemical, Kasugai, Japan) column chromatography (6 g) using *n*-hexane-EtOAc (20:1 → 10:1 → 1:1) as eluents to

furnish 1'-acetoxychavicol acetate (31.7 mg, ACA) (*17*). After the purified ACA was dissolved in DMSO at a concentration of 10 mg/mL, the solution was stored at –20°C.

2.3. *Preparation of inhibitor solutions and virus suspensions*

The inhibitor solutions were prepared from the stock solutions of valtrate, ACA, and LMB by dilution to the indicated concentrations with the culture media just prior to use. In the experiment of nuclear translocation assay, the solutions were diluted with the culture medium. The concentrations of DMSO and EtOH in the culture media were 0.5% and 0.1%, respectively. The virus suspensions were prepared from the titrated virus sample by dilution to the indicated multiplicity of infection (MOI) with 1% BSA in MEM just prior to use.

2.4. *Indirect immunofluorescence*

HeLa cells were seeded onto a 12-well plate at a concentration of 5×10^4 cells per well with 1 mL of MEM containing 10% FBS and were incubated for 15 h. After washing with MEM twice, the cells were infected with 200 μL of the influenza virus suspension at a MOI of 3 at 37°C in 5% CO$_2$ for 1 h. After the medium was removed, the cells were further incubated with 0.5 mL of the inhibitor solutions for 9 h. The cells were fixed with 4% paraformaldehyde in PBS for 10 min and were treated with a wash buffer (0.1% NP-40 in PBS) for 20 min. The cells were immersed in a blocking solution (1% skim milk in PBS) for 1 h, and then were treated with anti-NP mouse mAb in the blocking solution for 1 h. After rinsing with the wash buffer for three times, the cells were further treated with Alexa 546-conjugated anti-mouse immunoglobulin (Ig) in the blocking solution for 1 h. The cells were washed with the wash buffer, and then location of NP was observed with a fluorescence microscopy (Axiophot, Carl Zeiss, Germany).

2.5. *Evaluation of anti-influenza viral effects*

MDCK cells were seeded onto a 96-well plate at a concentration of 3×10^4 cells per well with 0.1 mL of MEM containing 5% FBS and were incubated for 15 h. After washing with MEM twice, the cells were infected with 100 μL of the influenza virus suspension at a MOI of 0.01 at 37°C in 5% CO$_2$ for 1 h. The medium was removed, and then the cells were incubated with 200 μL of the inhibitor solutions. After 12 h or 24 h, an aliquot (5 μL) of each supernatant was appropriately diluted and the resulting samples were subjected to the plaque assay to evaluate anti-influenza viral effects.

2.6. *Plaque assay*

MDCK cells were seeded onto a 6-well plate at a concentration of 2×10^6 cells per well with 2 mL of MEM containing 5% FBS and were incubated for 15 h. The medium was removed, and then the cells were infected with 400 μL of virus suspension at 37°C in 5% CO$_2$ for 1 h. After the medium was removed, the cells were overlaid with 4 mL of agarose solution [MEM containing 0.8% agarose, 0.1% BSA and 1% 100 × Vitamin solution (Lifetechnologies Japan, Tokyo, Japan)] and were incubated for 3 days. To visualize the plaques, the cells were fixed in AcOH:EtOH (1:1) for 1 h, and then were stained with 0.5% Amido black 10B solution (Nacalai Tesque) for 3 h. After washing with water and air-drying, the number of plaques was visibly counted. The viral titer was determined as PFU (plaque forming unit)/mL.

2.7. *Determination of CC$_{50}$ and IC$_{50}$ values of vRNP-export inhibitors*

MDCK cells were seeded onto a 96-well plate at a concentration of 3×10^4 cells per well with 0.1 mL of MEM containing 5% FBS and were incubated for 15 h. In the case of the determination of CC$_{50}$ values (50% cell toxicity concentrations of samples), the medium was removed, and then the cells were incubated with 200 μL of the inhibitor solutions for 12 h. After the medium was removed, the cells were treated with 0.5% crystal violet in 70% EtOH for 5 min. After washing with water and air-drying, the absorbance was measured at 560 nm with an Infinite M200 Tecan plate reader (Wako Pure Chemical Industries, Osaka, Japan) to evaluate cell toxicity. In the case of the determination of IC$_{50}$ values, (50% virus inhibitory concentrations of samples), successive viral infection and inhibitor treatment for 12 h were conducted in the same manner in the experiment of evaluation of anti-influenza viral effects. After an aliquot (5 μL) of each supernatant was appropriately diluted, the resulting samples were subjected to the plaque assay to evaluate anti-influenza viral effects. The CC$_{50}$ and the IC$_{50}$ values were calculated from the dose-response curves using the Graph Pad Prism software program (Prism version 5.01, Graph Pad Software, Inc., CA, USA).

3. Results

3.1. *Valtrate and ACA inhibit the nuclear export of vRNP*

We established a cell line that stably expressed the GFP protein conjugated with an NES signal (GES5 cells) (*19*). The GES5 cells were treated with a series of inhibitors (Figure 1) for 9 h, and the nuclear
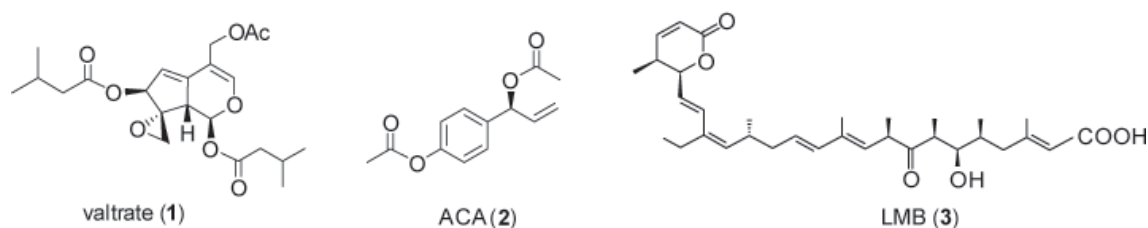
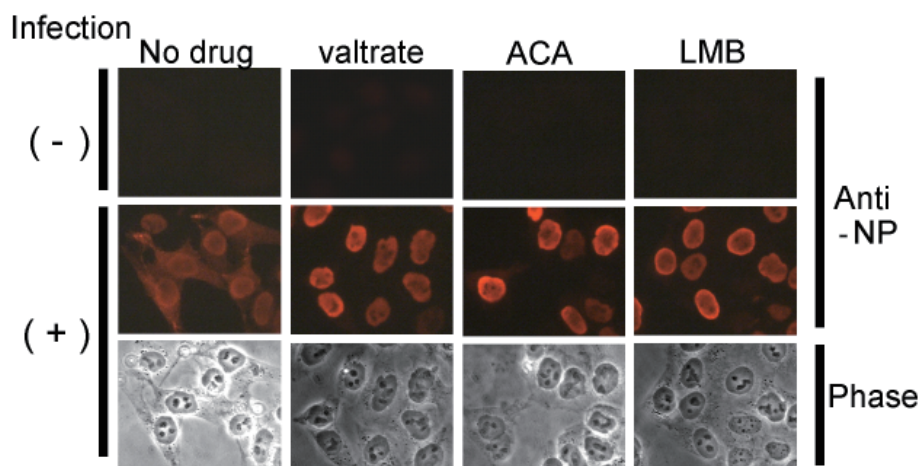**Figure 1. Chemical structures of valtrate (1), ACA (2), and LMB (3).**

Figure 2. Effect of vRNP-export inhibitors on the nuclear accumulation of influenza viral NP. HeLa cells infected with the influenza virus A/WSN/33 strain were incubated with valtrate (1.5 μg/mL, 3.6 μM), ACA (3 μg/mL, 12.8 μM), or LMB (10 ng/mL, 18.5 nM) for 9 h. The influenza viral NP was detected by an indirect immunofluorescence technique. The localization of NP and the location of cells was respectively observed as fluorescence (anti-NP) and phase contrast (phase) with the fluorescence microscopy.

localization of GFP-NES was observed with the fluorescence microscopy. The minimum inhibitory concentrations (MIC) of valtrate, ACA, and LMB were 1 μg/mL (2.4 μM), 3 μg/mL (12.8 μM), and 0.3 ng/mL (0.6 nM), respectively (data not shown). To monitor whether valtrate and ACA can inhibit the nuclear export of vRNP, indirect immunofluorescence experiment was performed (Figure 2). HeLa cells were infected with the influenza virus for 1 h. Nuclear export inhibitors were added into the culture plate then incubated for another 9 h. After fixation, the cells were incubated with an anti-NP mAb. NP is a viral protein and is one of the major components of the vRNP. The mAb used in the current study was developed by Momose *et al*. (*18*) and recognizes the conformational epitope of the NP; therefore, it preferentially interacts with the vRNP complex rather than the NP alone. In the influenza virus-infected cells, NP localized in the nucleus and in the cytoplasm, and its accumulation in the nucleus was not observed. However, in the presence of LMB, NP drastically accumulated in the nucleus, as has been previously reported (*20*), since viral NS2 or host factor Hsc70 which possesses an NES is known to associate with vRNP. When the cells were treated with valtrate or ACA, the nuclear accumulation of NP was also clearly observed. These results show that valtrate and ACA efficiently suppress the nuclear export of influenza viral vRNP.

3.2. *Valtrate and ACA suppress the influenza virus production*

To determine whether valtrate and ACA affect influenza virus production, MDCK cells were firstly infected with the influenza virus A/WSN/33 for 1 h, then valtrate or ACA were added into the plate (Figure 3). At 12 or 24 h after viral infection, the supernatants of the infected cells were recovered and subjected to a plaque assay. In the absence of vRNP-export inhibitors, the viral titer in the supernatant were not significantly differed at 12 and 24 h. However, we observed that the viral titer in the supernatant of cells treated with valtrate ($< 10^2$ PFU/mL), ACA (4×10^2 PFU/mL), and LMB ($< 10^2$ PFU/mL), was markedly reduced at 12 h. Twenty-four hours after infection, similar results with the 12-h samples were obtained, except the ACA treated cells.

The CC_{50} value of the vRNP-export inhibitors were calculated by crystal violet staining method (Table 1). The CC_{50} value of valtrate was 36 μM (15 μg/mL), and the CC_{50} of ACA was 5.5 μM (1.3 μg/mL). Cytotoxicity, as evaluated by the WST-1 assay, gave similar results (data not shown). The IC_{50} was calculated by titrating the viruses in the cell culture supernatant using the plaque assay (Table 1). The IC_{50} of valtrate was 0.19 μM (82 ng/mL), and the IC_{50} of ACA was 2.0 μM (460 ng/mL). The selective index of valtrate and ACA was found to be 180 and 2.8, respectively. The selective index of LMB was calculated to be greater than 16,000.
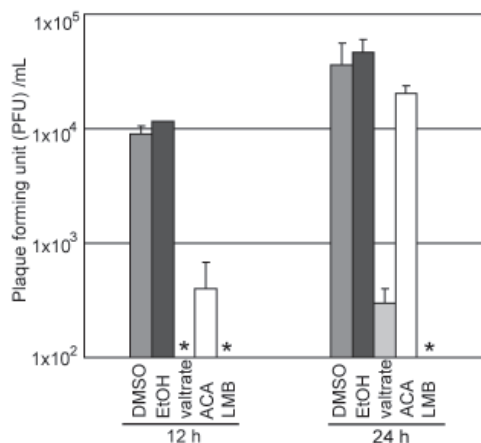
Figure 3. Nuclear vRNP-export inhibitors suppress the influenza viral production. MDCK cells infected with the influenza virus A/WSN/33 strain were treated with valtrate (1.5 μg/mL, 3.6 μM), ACA (1.5 μg/mL, 6.4 μM), or LMB (15 ng/mL, 27.8 nM). After 12 or 24 h, the anti-influenza viral effects were evaluated by the plaque assay. Samples treated with 0.5% DMSO and 0.1% EtOH were used as the vehicle controls. Asterisks indicate below the detection limit ($< 10^2$ PFU/mL). The results are represented by the mean ± S.D. obtained from the three independent experiments.

Table 1. Anti-influenza viral effects of nuclear export inhibitors of vRNP[a]

Compound	CC_{50} (μM)[b]	IC_{50} (μM)[c]	Selective index (SI)[d]
valtrate	36	0.19	180
ACA	5.5	2.0	2.8
leptomycin B	> 1.9	0.00012	> 16,000

[a] Evaluation after 12 h treatment.
[b] 50% Cytotoxic concentration.
[c] 50% Virus growth inhibitory concentration.
[d] Selective index = CC_{50}/IC_{50}.

4. Discussion

The present study demonstrated that a new class of nuclear export inhibitors, valtrate and ACA, regulates the nuclear export of influenza viral RNP (Figure 2) and effectively suppresses virus production (Figure 3). The transcription and replication of the influenza virus occurs in the nucleus, and the nuclear import and the export of vRNP are important steps in the viral life cycle. We previously reported that the nuclear export of vRNP occurs from 6 to 9 h after viral infection (20) and then viral production occurs approximately 12 h after infection (12). Accumulated vRNP in the nucleus was observed at 9 h after infection when valtrate or ACA was present in the culture medium (Figure 2). These results suggest that the vRNP-export inhibitors are effective during the influenza virus life cycle.

LMB has been reported to inhibit the CRM1-mediated nuclear export system by binding to the Cys529 residue of CRM1 (21). Using a biotinylated LMB as a probe, competition experiments using valtrate or ACA showed that the addition of valtrate and ACA competed with the binding of LMB to CRM1. Therefore, valtrate or ACA inhibition of nuclear export appeared to act

through a similar mechanism as LMB (16,17). We also reported that influenza virus production is significantly decreased in the presence of LMB (13). The selective index of LMB (12 h treatment) is good compared to that of valtrate and ACA (Table 1). However, our preliminary results show that longer time treatment of LMB show significant cytotoxicity to the cells [CC_{50}: 110 ng/mL (200 nM) at 48 h, 11 ng/mL (20 nM) at 72 h in MDCK cells]. It was previously reported that LMB treatment for 72 h resulted in the formation of polynuclear giant cells (22). Therefore, prolonged treatment with LMB is strongly toxic to cells. The cytotoxicity of valtrate and ACA (valtrate: 4,000 ng/mL (9.5 μM) at 48 h and 4,100 ng/mL (9.8 μM) at 72 h; ACA: 780 ng/mL (3.3 μM) at 48 h, 850 ng/mL (3.6 μM) and at 72 h, respectively) was not drastically altered. ClogP is a parameter correlated to the permeability of drugs, and is therefore believed to be an important index in predicting the biological activity in animal models. Generally, clogP values larger than +3 and less than −3 tend to significantly lose the *in vivo* pharmacological efficacy, regardless of a good *in vitro* biological score (23). The hydrophobicity of LMB is very high (clogP = +6.9), and therefore the application of LMB is not yet established. In contrast to LMB, valtrate (clogP = +1.92) and ACA (clogP = +1.86) have moderate hydrophobicity, and therefore may be clinically applicable. Valtrate and ACA are isolated from medicinal plants Valerianae Radix and *A. galanga*, respectively. The former has been orally administered as a traditional folk medicine in Japan and China, and the latter has been used as a spice or ginger substitute for flavoring foods in the Southeast Asia and as a traditional folk medicine by oral administration in China and Thailand. Considering the safety of these traditional uses, valtrate and ACA are suitable as lead compounds for further development of inhibitors for nuclear export of vRNP.

The anti-influenza drugs clinically available are directed against viral proteins. Amantadine blocks the ion-channel activity of the viral M2 protein, which is required for viral entry and is effective only for the type A influenza virus. Zanamivir and oseltamivir block the receptor-destroying activity of the viral NA protein, prevent viral budding form the cell surface and are effective against type A and type B influenza viruses. Currently, these drugs are approved and commercially available in many countries. However, the influenza virus easily changes its genomic sequence, and many mutated drug-resistant viruses have been already reported; for a review, see (24). It is essential to develop novel anti-influenza virus drugs, especially agents that are effective against resistant viruses. It has been reported that the nuclear export of vRNP is mediated by the viral proteins M1 and NS2 (9,25), and is inhibited by LMB treatment (11,26). The nuclear export of vRNP is also mediated by the cellular protein CRM1. Therefore, inhibitors that affect this nuclear export system could be used as anti-influenza agent. It has been reported that the replication

of other viruses, such as HIV-1 and HSV-1, are also inhibited by treatment with nuclear export inhibitors (*16,27*). Specific cellular proteins essential for viral propagation, such as CRM1, may therefore be a good target for the development of novel drugs which can suppress many viral diseases, including the influenza virus, without inducing viral resistance.

Acknowledgements

References

1. Adam SA, Gerace L. Cytosolic proteins that specifically bind nuclear location signals are receptors for nuclear import. Cell. 1991; 66:837-847.
2. Wen W, Meinkoth JL, Tsien RY, Taylor SS. Identification of a signal for rapid export of proteins from the nucleus. Cell. 1995; 82:463-473.
3. Fornerod M, Ohno M, Yoshida M, Mattaj IW. CRM1 is an export receptor for leucine-rich nuclear export signals. Cell. 1997; 90:1051-1060.
4. Nagata K, Takizawa N, Haruki H, Mibayashi M, Watanabe K. Nuclear import and export of influenza virus ribonucleoprotein complexes. In: Recent advances in influenza virus research (Hayase Y, ed.). Research Signpost, Kerala, India, 2002; pp. 14-43.
5. Fischer U, Huber J, Boelens WC, Mattaj IW, Luhrmann R. The HIV-1 Rev activation domain is a nuclear export signal that accesses an export pathway used by specific cellular RNAs. Cell. 1995; 82:475-483.
6. Hashimoto H, Fukuda M, Matsuo Y, Yokoyama Y, Nishida E, Toyohara H, Sakaguchi M. Identification of a nuclear export signal in MKK6, an activator of the carp p38 mitogen-activated protein kinases. Eur J Biochem. 2000; 267:4362-4371.
7. Stommel JM, Marchenko ND, Jimenez GS, Moll UM, Hope TJ, Wahl GM. A leucine-rich nuclear export signal in the p53 tetramerization domain: Regulation of subcellular localization and p53 activity by NES masking. Embo J. 1999; 18:1660-1672.
8. Herz C, Stavnezer E, Krug R, Gurney T Jr. Influenza virus, an RNA virus, synthesizes its messenger RNA in the nucleus of infected cells. Cell. 1981; 26:391-400.
9. O'Neill RE, Talon J, Palese P. The influenza virus NEP (NS2 protein) mediates the nuclear export of viral ribonucleoproteins. Embo J. 1998; 17:288-296.
10. Neumann G, Hughes MT, Kawaoka Y. Influenza A virus NS2 protein mediates vRNP nuclear export through NES-independent interaction with hCRM1. Embo J. 2000; 19:6751-6758.
11. Ma K, Roy AM, Whittaker GR. Nuclear export of influenza virus ribonucleoproteins: Identification of an export intermediate at the nuclear periphery. Virology. 2001; 282:215-220.
12. Watanabe K, Fuse T, Asano I, Tsukahara F, Maru Y, Nagata K, Kitazato K, Kobayashi N. Identification of Hsc70 as an influenza virus matrix protein (M1) binding factor involved in the virus life cycle. FEBS Lett. 2006; 580:5785-5790.
13. Watanabe K, Takizawa N, Noda S, Tsukahara F, Maru Y, Kobayashi N. Hsc70 regulates the nuclear export but not the import of influenza viral RNP: A possible target for the development of anti-influenza virus drugs. Drug Discov Ther. 2008; 2:77-84.
14. Tsukahara F, Maru Y. Identification of novel nuclear export and nuclear localization-related signals in human heat shock cognate protein 70. J Biol Chem. 2004; 279:8867-8872.
15. Kose S, Furuta M, Koike M, Yoneda Y, Imamoto N. The 70-kD heat shock cognate protein (hsc70) facilitates the nuclear export of the import receptors. J Cell Biol. 2005; 171:19-25.
16. Murakami N, Ye Y, Kawanishi M, Aoki S, Kudo N, Yoshida M, Nakayama EE, Shioda T, Kobayashi M. New Rev-transport inhibitor with anti-HIV activity from Valerianae Radix. Bioorg Med Chem Lett. 2002; 12:2807-2810.
17. Tamura S, Shiomi A, Kaneko M, Ye Y, Yoshida M, Yoshikawa M, Kimura T, Kobayashi M, Murakami N. New Rev-export inhibitor from *Alpinia galanga* and structure-activity relationship. Bioorg Med Chem Lett. 2009; 19:2555-2557.
18. Momose F, Kikuchi Y, Komase K, Morikawa Y. Visualization of microtubule-mediated transport of influenza viral progeny ribonucleoprotein. Microbes Infect. 2007; 9:1422-1433.
19. Watanabe K, Noda S, Kobayashi N. Establishment of a new cell line for performing sensitive screening of nuclear export inhibitors. Drug Discov Ther. 2008; 2:7-9.
20. Watanabe K, Takizawa N, Katoh M, Hoshida K, Kobayashi N, Nagata K. Inhibition of nuclear export of ribonucleoprotein complexes of influenza virus by leptomycin B. Virus Res. 2001; 77:31-42.
21. Kudo N, Matsumori N, Taoka H, Fujiwara D, Schreiner EP, Wolff B, Yoshida M, Horinouchi S. Leptomycin B inactivates CRM1/exportin 1 by covalent modification at a cysteine residue in the central conserved region. Proc Natl Acad Sci U S A. 1999; 96:9112-9117.
22. Komiyama K, Okada K, Tomisaka S, Umezawa I, Hamamoto T, Beppu T. Antitumor activity of leptomycin B. J Antibiot (Tokyo). 1985; 38:427-429.
23. Leo AJ. Calculating log Poct from structures. Chem Rev. 1993; 93:1281-1306.
24. De Clercq E. Antiviral agents active against influenza A viruses. Nat Rev Drug Discov. 2006; 5:1015-1025.
25. Martin K, Helenius A. Nuclear transport of influenza virus ribonucleoproteins: The viral matrix protein (M1) promotes export and inhibits import. Cell. 1991; 67:117-130.
26. Elton D, Simpson-Holley M, Archer K, Medcalf L, Hallam R, McCauley J, Digard P. Interaction of the influenza virus nucleoprotein with the cellular CRM1-mediated nuclear export pathway. J Virol. 2001; 75:408-419.
27. Lengyel J, Strain AK, Perkins KD, Rice SA. ICP27-dependent resistance of herpes simplex virus type 1 to leptomycin B is associated with enhanced nuclear localization of ICP4 and ICP0. Virology. 2006; 352:368-379.

A comparative study of protective mechanisms of glycine and L-arginine against cisplatin-induced nephrotoxicity in rat renal cortical slices

Yasmen YFK Mahran, Amani E Khalifa, Ebtehal El-Demerdash*

Pharmacology & Toxicology Department, Faculty of Pharmacy, Ain Shams University, Cairo, Egypt.

ABSTRACT: Amino acids exert nephroprotective effects in various forms of acute renal injury depending on their renal hemodynamic effects. The present study was designed to elucidate and compare the role of non hemodynamic mechanisms in protective actions afforded by glycine and L-arginine against cisplatin (CDDP)-induced nephrotoxicity using rat renal cortical slices (RCS). We have investigated the possible modulatory effect of glycine and L-arginine on oxidative stress and necrosis induced by CDDP as well as on CDDP uptake by kidney. After 4 h of incubation with 2 mM CDDP, nephrotoxicity was demonstrated by significant increased lactate dehydrogenase leakage, decreased ability of the slices to reduce 3-(4,5-dimethylthiazol-2-yl)-2,5-diphenyltetrazolium bromide, increased lipid peroxides and depleted reduced glutathione. Also, CDDP significantly inhibited pyruvate-stimulated gluconeogenesis. Histopathological examination of RCS confirmed the occurrence of tubular coagulative necrosis in cortex and corticomedullary regions. Preincubation of RCS with 1 mM glycine or L-arginine 1 h before CDDP addition significantly attenuated the oxidative stress and tubular necrotic effects of CDDP. L-Arginine showed greater antioxidant properties while glycine showed a greater antinecrotic effect. Moreover, the nephroprotective effect was mediated through lowering the platinum uptake by RCS. However, they could not counteract the inhibition of gluconeogenesis induced by CDDP. In conclusion, the present study sheds light on the mechanisms involved in glycine and L-arginine nephroprotection.

Keywords: Cisplatin (CDDP), nephrotoxicity, glycine, L-arginine, renal cortical slices (RCS), lactate dehydrogenase (LDH)

*Address correspondence to:
Dr. Ebtehal El-Demerdash, Department of Pharmacology & Toxicology, Faculty of Pharmacy, Ain Shams University, Abasia, Cairo, Egypt.
e-mail: ebtehal_dm@yahoo.com

1. Introduction

Cisplatin (*cis*-diamminedichloroplatinum; CDDP) is an effective chemotherapeutic agent and is successfully used in the treatment of a wide range of tumors (*1*). Its chief limit to greater efficacy, however, is its nephrotoxicity. Clinically, CDDP nephrotoxicity is often seen after 10 days of CDDP administration and is manifested as lower renal blood flow and glomerular filtration rate, high serum creatinine, and reduced serum magnesium and potassium levels (*2*). The mechanism by which CDDP produces renal injury is not well understood. It is probably related to its preferential uptake by the proximal tubular cells especially in the S3 segment (*3*). The renal microenvironmental changes following CDDP treatment is a complex process and could be broadly categorized into two distinct pathophysiological mechanisms. The first mechanism includes primary promoters of cellular damage such as inhibition of protein synthesis and depletion of glutathione and other protein-thiols while the secondary sequelae of established cell damage includes inactivation of transport proteins, lipid peroxidation and mitochondrial damage (*4,5*). In addition, the changes in renal hemodynamics were also found to play an important role in CDDP-induced nephrotoxicity (*6*). CDDP toxicity in proximal tubules is characterized by tubular cell damage and subsequently, the injured renal tubules lose the ability to reabsorb water which lead to dehydration and loss of body weight (*7*).

Several strategies have emerged to ameliorate CDDP nephrotoxicity. Concomitant administration of chemoprotective agents becomes an important approach (*8*). For two decades, it has been proved that amino acids (*9*) and peptides derived from protein (*10*) possess vasodilatory effects on renal vessels and increase renal blood flow and glomerular filtration rate. Among nephroprotecive amino acids, glycine and L-arginine are of great importance. It was reported that glycine exerted a cytoprotective effect in various forms of acute renal injury; it protected against hypoxic injury to rabbit renal proximal tubular cells (*11*), ouabain-induced injury in proximal tubule cells (*12*) and cyclosporine-induced cellular necrosis (*13*). Similarly,

L-arginine, a nitric oxide (NO) precursor, has been previously reported to have protective effects in drug induced renal injury where it was shown to attenuate renal dysfunction and oxidative stress in indomethacin (*14*), gentamicin (*15*), cyclosporin (*16*), and iron (*17*) induced renal impairment in rats.

Regarding CDDP nephrotoxicity, few studies tried to ameliorate its nephrotoxicity using either glycine (*18,19*) or L-arginine (*20,21*) and they reported a hemodynamic nephroprotective mechanism involving NO production. However, this hemodynamic mechanism may not be the sole one, since the nephroprotective effects were partially blocked by co-administration of the NO synthase inhibitor; N^G-nitro-L-arginine methyl ester (*21*). In addition, D-arginine, which is not a substrate for NO and has no vasodilating effect, is also reported to ameliorate the renal dysfunction that is induced by CDDP (*19,22*). Thus, glycine and L-arginine might have nephroprotective effects against CDDP nephrotoxicity independent of their renal hemodynamic actions.

Therefore, the present study was designed to elucidate and compare the role of non hemodynamic mechanisms in protective actions afforded by both glycine and L-arginine against CDDP-induced nephrotoxicity. We have investigated the possible modulatory effect of glycine and L-arginine on oxidative stress induced by CDDP as well as on CDDP uptake by kidney. We used a renal cortical slices (RCS) model because it is easily prepared, manipulated and contains populations of cells targeted by platinum anticancer agents; furthermore it is not influenced by uncontrollable hormonal, neurogenic and hemodynamic factors (*23,24*).

2. Materials and Methods

2.1. *Chemicals*

CDDP was obtained from Merk Ltd., Cairo, Egypt. L-Arginine and glycine were obtained from Sigma-Aldrich, St Louis, MO, USA. Concentrations of the drugs used were selected as previously reported (*25*) as well as from pilot experimental trials of the present study. *n*-butanol, dimethyl sulfoxide (DMSO), 3-(4,5-dimethylthiazol-2-yl)-2,5-diphenyltetrazolium bromide (MTT), 5,5'-dithio-bis-2-nitrobenzoicacid (DTNB), ethylenediamine tetraacetic acid disodium salt (EDTA), D-glucose, *N*-(2-hydroxyethyl) piperazine-*N'*-2-ethanesulfonic acid (HEPES), 1,1',3,3'-tetramethoxypropane, potassium dihydrogen phosphate, reduced glutathione (GSH), trichloroacetic acid (TCA), thiobarbituric acid (TBA), and Triton X-100 were purchased from Sigma-Aldrich. All these chemicals were dissolved in incubation medium prior to use. Other chemicals were analytical reagents.

2.2. *Animals*

Male Sprague Dawley rats were obtained from the Nile Co. for Pharmaceuticals and Chemical industries, Cairo, Egypt. Animals were kept in the animal house of Faculty of Pharmacy, Ain Shams University, under suitable laboratory conditions on a standard diet and water *ad libitum*. The standard diet pellets were obtained from El-Nasr Chemical Company, Cairo, Egypt. Animals were handled under a protocol of care of Animal Research Ethics Committee (Ain Shams University).

2.3. *Preparation and incubation of RCS*

RCS were prepared as described previously (*25*). After fasting overnight, the animal was killed by decapitation, then kidneys were rapidly removed, decapsulated and placed into ice-cold saline. The slices (0.3-0.5 mm thickness) were prepared with a razor blade on a Petri plate in an ice-bath. The slices weighing 150-200 mg were loaded into an incubation flask with cap. Each flask contained 5 mL incubation medium (134 mM NaC1, 5.9 mM KCl, 1.5 mM CaCl$_2$, 1.2 mM MgCl$_2$, 11.5 mM glucose, and 5.8 mM HEPES buffer), gassed with pure oxygen. CDDP was added to the incubation medium to a final concentration of 2 mM. The medium for control slices was free of CDDP. The RCS were incubated at 37°C on a horizontal shaker (100 cycle/min).

2.4. *Experimental design*

In order to establish the optimal experimental conditions, a time course study of CDDP nephrotoxicity as well as a dose response study of glycine and L-arginine nephroprotection was carried out by assessing membrane integrity using a lactate dehydrogenase (LDH) leakage test. Then, based on data obtained from the preliminary study, the mechanisms of nephroprotection of glycine and L-arginine were studied using 6 groups of RCS.

2.5. *Time course study of CDDP-induced nephrotoxicity in rat RCS using LDH leakage method*

RCS were incubated with 2 mM CDDP for different time intervals: 0.5, 1, 2, 3, 4, and 6 h. LDH leakage was assessed in the incubation medium according to the method described by Tietz (*26*) by measuring the rate of conversion of lactate to pyruvate and subsequent increase in the absorbance of nicotinamide adenine dinucleotide reduced form (NADH) formed at 340 nm.

2.6. *Determination of the protective concentrations of glycine and L-arginine against CDDP-induced LDH leakage*

RCS were incubated for 1 h with either glycine or L-arginine at different concentrations: 1, 2 and 4 mM. Then, 2 mM CDDP was added and the slices were incubated for 4 h to choose the optimum concentration of amino acid to be used in further studies.

2.7. *Assessment of protective mechanisms of glycine and L-arginine against CDDP-induced renal injury*

Rat RCS were classified into 6 groups (five sets/group); control, CDDP (2 mM), glycine (1 mM), L-arginine (1 mM), CDDP + glycine, CDDP + L-arginine. Amino acids were added 1 h before CDDP.

2.7.1. *Assessment of CDDP-induced cytotoxicity in RCS*

CDDP-induced cytotoxicity in RCS was examined by MTT assay (*27*). Briefly, after 4 h of CDDP incubation, the slices were blotted with filter paper and incubated in 4 mL of a second incubation medium containing MTT (1.25 mg/mL; 3 mM final concentration) at 37°C for 30 min. The slices were homogenized in 5 mL distilled water at 7,000 rpm for 1 min and centrifuged at 5,000 rpm for 5 min to remove particulate matter. An aliquot (0.25 mL) of the resulting supernatant of each group was added to a microcentrifuge tube and 0.5 mL DMSO was added to each tube followed by 0.5 mL glycine buffer (pH 10.5) containing 0.2 M glycine and 0.1 M NaCl. After mixing, the absorbances were measured at 570 nm. The results were expressed as optical density OD/mg wet tissue.

2.7.2. *Determination of lipid peroxides and GSH content in RCS*

After incubation, RCS were removed, rinsed, blotted, and homogenized with saline at a ratio of 1:10 (w/v). Lipid peroxides were assessed by measuring malonaldehyde content using TBA assays (*28*). Briefly, an aliquot of 0.5 mL of the homogenate was pipetted into a 10-mL centrifuge tube followed by the addition of 2.5 mL of 20% TCA and 1 mL of 0.67% TBA. The mixture was heated for 15 min in a boiling water bath. After cooling, 4 mL of *n*-butanol was added and mixed vigorously. After centrifugation, the supernatant was read at 532 nm spectrophotometrically. Malonaldehyde concentration was calculated using a standard curve of 1,1,3,3-tetraethoxypropane and was expressed as nmol/g tissue. To determine GSH, 0.5 mL of homogenate was added to a tube with 0.5 mL 10% TCA. The tubes were gently shaken intermittently for 15 min followed by centrifugation at 2,000 rpm for 5 min. A 0.2 mL aliquot of the resulting supernatant was added to a tube containing 1.7 mL phosphate buffer and 0.1 mL 5,5'-dithio-bis-(2-nitrobenzoic acid), then mixed and read at 412 nm within 5 min (*29*).

2.7.3. *Measurement of pyruvate stimulated gluconeo-genesis in RCS*

The slices were incubated in an incubation medium which contained 10 mM pyruvate instead of glucose according to the study of Zhang *et al.* (*25*). After incubation, the slices were removed from the medium and blotted. The medium glucose content was spectrophotometrically determined using the glucose oxidase enzymatic assay (glucose assay kit) and expressed as mg/g tissue.

2.7.4. *Determination of platinum content in RCS*

Platinum content in RCS was determined as described previously (*30*). After incubation of the slices, 1 mL of incubation medium of each sample was pipetted into a 10-mL centrifuge tube, and the volume of each sample was brought to 1.1 mL with bidistilled water. The solutions were diluted with four equal volumes (4.4 mL) of 1% Triton X-100 solution. After vortex-mixing for 30 sec, 20 μL of the diluted sample was injected into the furnace using the autosampler. The apparatus used was a model 975 flameless atomic absorption spectrophotometer. A wavelength of 265.9 nm with a lamp current of 10 mA and spectral bandwidth of 0.2 nm was employed. Also, a background correction was utilized.

2.7.5. *Histopathological examination of RCS*

After incubation, RCS were fixed in 10% formol saline for 24 h and then washed in tap water. Serial dilutions of alcohol (methyl, ethyl and absolute ethyl) were used for dehydration. Specimens were cleared in xylene and embedded in paraffin at 56°C in a hot air oven for 24 h. Paraffin bees wax tissue blocks were prepared for sectioning at 4-μm thickness using a slidge microtome. The tissue sections obtained were collected on glass slides, deparaffinized, and stained with hematoxylin and eosin stains for histopathological examinations with a light microscope.

2.8. *Statistical analysis*

Data are presented as mean ± S.E.M. An unpaired *t*-test was used to compare two different treatment groups. Multiple comparisons for more than two treatment groups were carried out using one way analysis of variance (ANOVA) followed by the Tukey-Kramer test as post-hoc analysis. Statistical significance was acceptable at a level of $p < 0.05$. Analysis of data was performed using GraphPad INSTAT. Tables and graphs were prepared using Prism software ver. 5 (GraphPad Software, San Diego, CA, USA).

3. Results

3.1. *Cytotoxicity markers*

First, CDDP-induced toxicity to the slices was determined by measuring LDH leakage from RCS. There was a time-dependent increase in LDH leakage and it was significantly increased as early as 1 h of

CDDP incubation. After 4 and 6 h of incubation, LDH leakage was significantly increased by about 2-fold as compared to the control value and therefore, the time interval 4 h was chosen for further studies (Figure 1). Preincubation of the slices with different concentrations (1, 2, and 4 mM) of either glycine or L-arginine, 1 h before CDDP addition, nearly normalized the values of LDH leakage. The protective effect of glycine and L-arginine was not concentration-dependant as there is no significant difference between the effects of different concentrations of amino acids (Table 1). Therefore, the lowest concentration (1 mM) was chosen for further studies.

Second, the MTT assay was used to assess cell damage as shown in Figure 2. After 4 h, CDDP significantly decreased the ability of the slices to reduce MTT and the absorbance was decreased to 56% of the control value. On the other hand, the slices incubated with L-arginine alone showed a significant increase in the ability of the RCS to reduce MTT and the absorbance was increased to 121% of the control value.
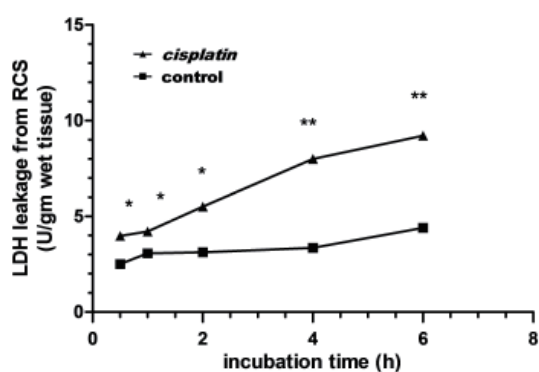

Figure 1. Time course study of the effect of 2 mM CDDP on the release of LDH from rat RCS. Values given are the mean of 5 observations ± S.E.M. * Significantly different from the corresponding control at $p < 0.05$ using unpaired student *t*-test. ** Extremely significantly different from the corresponding control at $p < 0.01$ using unpaired student *t*-test.

Table 1. Effect of glycine and L-arginine on CDDP-induced LDH enzyme leakage in the incubation medium of RCS

Treatments	LDH leakage (U/g wet weight)
Control	3.25 ± 0.13
CDDP (2 mM)	6.45 ± 0.50^a
Glycine (1 mM) + CDDP	3.66 ± 0.24^b
Glycine (2 mM) + CDDP	4.28 ± 0.22^b
Glycine (4 mM) + CDDP	4.06 ± 0.25^b
L-Arginine (1 mM) + CDDP	3.17 ± 0.29^b
L-Arginine (2 mM) + CDDP	2.74 ± 0.19^b
L-Arginine (4 mM) + CDDP	3.23 ± 0.21^b

RCS were incubated at 37°C in medium containing CDDP (2 mM) with or without different concentrations of glycine or L-arginine. Amino acids were added 1 h prior to CDDP. For the control group, the RCS were incubated in the medium without any drugs. LDH leakage was measured after 4 h of CDDP addition. Each value represents a mean of 5 sets of rat RCS ± S.E.M. ^{a} and ^{b} are significantly different from control or CDDP group, respectively, at $p < 0.05$ using ANOVA followed by Tukey-Kramer as a post Hoc test.

Incubation of RCS with glycine alone did not show any significant change in MTT reduction as compared to the control group. Pre-incubation of RCS with either glycine or L-arginine, 1 h before CDDP addition, significantly counteracted the decrease in MTT reduction induced by CDDP reaching approximately 70% of the control value.

3.2. *Oxidative stress markers*

RCS content of GSH for the control group was 5.5 ± 0.07 μmol/g wet tissue (Table. 2). Incubation of RCS with either glycine or L-arginine alone revealed no significant change in GSH content as compared to the control group. On the other hand, incubation of RCS with CDDP alone for 4 h significantly depleted GSH content to 58% of the control value. Pre-incubation of the slices with 1 mM glycine or L-arginine for 1 h before CDDP addition, significantly counteracted the effect of CDDP. Glycine and L-arginine increased the GSH content to about 76% and 90% of the control group, respectively (Table 2).

Regarding kidney lipid peroxides, the control level was 44.5 ± 0.56 nmol/g wet tissue (Table 2). Incubation of RCS with CDDP significantly increased the level of lipid peroxides reaching 131% of the control group. Pre-incubation of RCS with either glycine or L-arginine significantly normalized the level of lipid peroxides to 110 and 108% of the control group, respectively (Table 2). The RCS incubated with either glycine or L-arginine alone revealed no significant change in lipid peroxides level compared to the control group.

Co-incubation of RCS with pyruvate, a substrate of gluconeogenesis, in the presence of CDDP
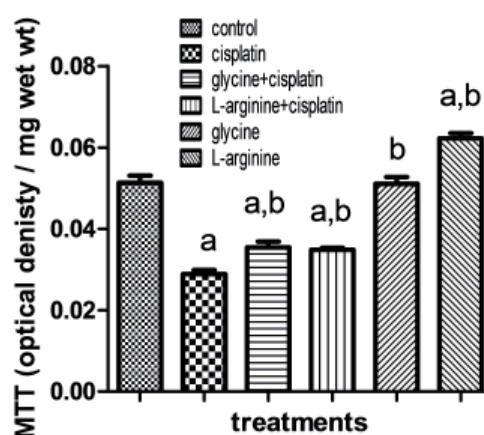
Figure 2. Effect of glycine or L-arginine on CDDP-induced cytotoxicity to RCS as percentage of control group using MTT assay. RCS were incubated at 37°C in medium containing CDDP (2 mM) and/or glycine or L-arginine (1 mM). Amino acids were added 1 h prior to CDDP. For control group, RCS were incubated in the medium without any drugs. MTT reduction was measured after 4 h of CDDP addition. Values given are the mean of 5 observations ± S.E.M. a and b: Significantly different from control or CDDP group, respectively, at $p < 0.05$ using ANOVA followed by Tukey-Kramer as a post Hoc test.

Table 2. Effect of CDDP and/or glycine or L-arginine on lipid peroxides, GSH, and pyruvate-stimulated gluconeogenesis in RCS

Treatments	Lipid peroxides (nmol/g wet tissue)	GSH (μmol/g wet tissue)	Glucose (mg/g wet tissue)
Control	44.5 ± 0.6	5.51 ± 0.07	7.81 ± 0.50
CDDP	58.4 ± 1.2[a]	3.22 ± 0.06[a]	2.64 ± 0.18[a]
Glycine + CDDP	48.9 ± 1.9[b]	4.16 ± 0.06[a,b]	2.32 ± 0.11[a]
L-Arginine + CDDP	47.9 ± 0.9[b]	4.97 ± 0.13[a,b]	1.92 ± 0.13[a]
Glycine	46.4 ± 1.4[b]	5.38 ± 0.17[b]	6.23 ± 0.32[b]
L-Arginine	45.8 ± 1.2[b]	5.67 ± 0.13[b]	6.44 ± 0.36[b]

RCS were incubated at 37°C in medium containing CDDP (2 mM) and/or glycine or L-arginine (1 mM). Amino acids were added 1 h prior to CDDP. For the control group, RCS were incubated in the medium without any drugs. Lipid peroxides, GSH and glucose were measured after 4 h of CDDP addition. Each value represents the mean of 5 sets of rat RCS ± S.E.M. [a] and [b] are significantly different from control or CDDP group, respectively, at *p* < 0.05 using ANOVA followed by Tukey-Kramer as a post Hoc test.

showed a marked depression of pyruvate-stimulated gluconeogenesis to 34% of the control value (Table 2). On the other hand, neither glycine nor L-arginine had a significant effect on the gluconeogenic capacity of RCS. Addition of either glycine or L-arginine 1 h before CDDP did not show any protective effect on CDDP-induced inhibition of gluconeogenesis.

3.3. *CDDP uptake by renal cortical slices*

In order to know whether the studied amino acids influenced uptake of CDDP by RCS, CDDP concentration in the medium was determined and subtracted from the original amount of CDDP added to the medium. The platinum content in the RCS incubated with CDDP alone was 2.23 ± 0.07 mg/g wet tissue. Preincubation of RCS with either glycine or L-arginine significantly decreased the kidney content of platinum to 86 and 91% compared to the CDDP group (Figure 3).

3.4. *Histopathological examination of RCS*

Histopathological examination of kidney specimens revealed normal renal glomeruli and tubules in the control group (Figures 4A and 4B). Also, RCS incubated with either glycine or L-arginine alone did not show any significant histopathological changes compared to the control group. On the other hand, RCS incubated with CDDP for 4 h showed tubular degeneration which varied according to kidney zone. Coagulative necrosis was observed in the tubular lining epithelium at the cortex and corticomedullary junction (++++) (Figures 4C and 4D). Coagulative necrosis is an irreversible grade of necrotic cell death and tubular cells could not regenerate after removal of toxic insult (Table 3).

Pre-incubation of slices with glycine 1 h prior to CDDP addition ameliorated the histopathological changes induced by CDDP. Most of the renal tubules and glomeruli in the cortex were intact while other few tubules showed nuclear pyknosis at the cortex (++) as well as the corticomedullary junction (+) and medulla (Figures 4E and 4F). Pyknosis is the first stage in tubular degeneration, in which nuclei showed chromatin condensation without chromatolysis. Also, pre-incubation
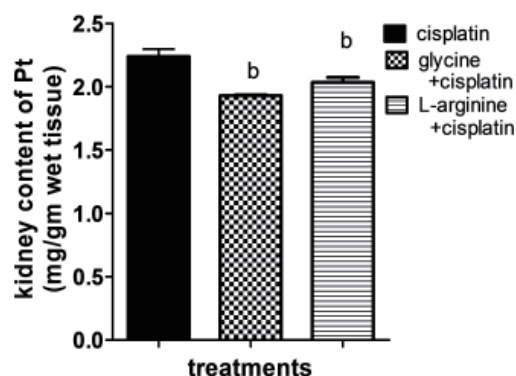
Figure 3. Effect of glycine or L-arginine on CDDP uptake by rat RCS expressed as kidney content of platinum. RCS were incubated at 37°C in medium containing CDDP (2 mM) and/or glycine or L-arginine (1 mM). Amino acids were added 1 h prior to CDDP. Platinum content was measured after 4 h of CDDP addition. Values given are the mean of 5 observations ± S.E.M. b: significantly different from CDDP group at *p* < 0.05 using ANOVA followed by Tukey-Kramer as a post Hoc test.

of slices with L-arginine 1 h prior to CDDP addition showed nephroprotective and antinecrotic effects but to a less degree as compared to the glycine effect (Table 3; Figures 4G and 4H).

4. Discussion

The present study was designed to elucidate and compare the role of non hemodynamic mechanisms in protective actions afforded by glycine and L-arginine against CDDP-induced nephrotoxicity. The first point discussed was assessment of CDDP nephrotoxicity using LDH leakage; a sensitive indicator for cell damage (*23*). It was found that both glycine and L-arginine significantly protected against CDDP-induced LDH leakage and loss of cell viability as measured by the MTT assay. These findings add further evidence for the potential cytoprotective effects of these amino acids. Since MTT is mainly reduced by the mitochondrial dehydrogenases (*27*), enzymes that were inhibited directly by CDDP after incubation with RCS (*31*), our findings give evidence that both amino acids could ameliorate CDDP-induced mitochondrial toxicity.
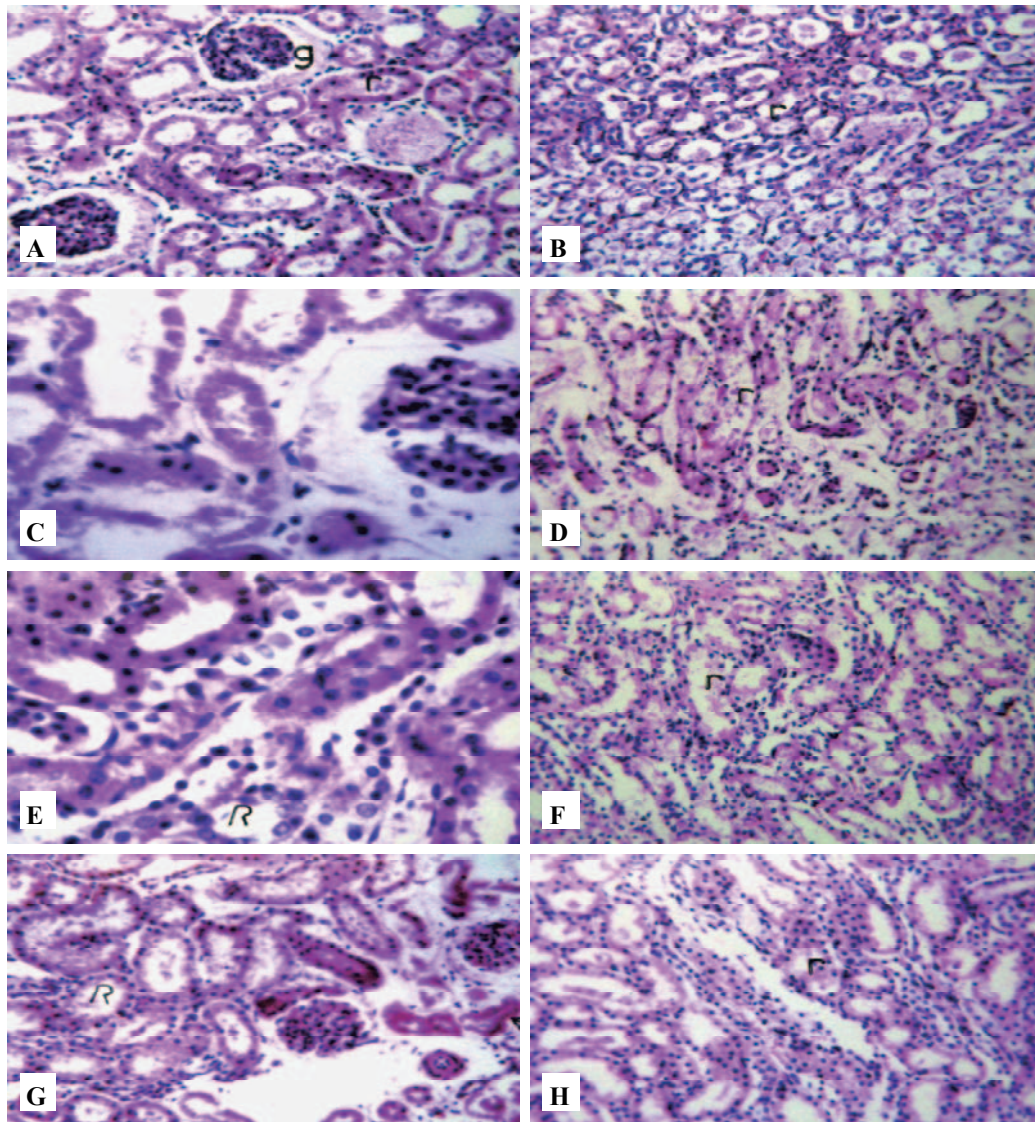
Figure 4. Photomicrographs of sections in the kidneys stained with hematoxylin-eosin stain. A and **B**: Sections taken from RCS of control group and show normal glomeruli (g) and tubules (r) at the cortex portion **(A)**, and normal renal tubules (r) at corticomedulary portion **(B)**. Original magnification, ×64. **C** and **D**: Sections taken from RCS of CDDP group and show coagulative necrosis in the tubular lining epithelium (r) of the cortical region graded as ++++ **(C)**, and also the corticomedular region graded as ++++ **(D)**. Original magnification, ×160 and ×64 for **C** and **D**, respectively. **E** and **F**: Sections taken from RCS of glycine + CDDP group and show most of the renal tubules and glomeruli in the cortex were intact with mild degenerative changes while a few other tubules showed nuclear pyknosis and complete absence of their nuclei with intact basement membrane graded as ++ at the cortex **(E)** and as + at corticomedulary junction **(F)**. Original magnification, ×160 and ×64 for **E** and **F**, respectively. **G** and **H**: Sections taken from RCS of L-arginine + CDDP group and show intact glomeruli with coagulative necrosis in multiple numbers of renal tubules and other tubules show complete loss of the lining epithelium while the basement membrane is still intact **(G)** and pyknosis of the nuclei of the lining epithelial cells at the corticomedulary junction graded as + **(H)**. Original magnification, ×64.

Table 3. Histopathological alterations in RCS

Histopathological alterations	Control group			CDDP group			Glycine + CDDP			L-Arginine + CDDP			Glycine			L-Arginine		
	C	CM	M	C	CM	M	C	CM	M	C	CM	M	C	CM	M	C	CM	M
1-Coagulative necrosis	–	–	–	++++	++++	–	–	–	–	++++	–	–	–	–	–	–	–	–
2-Pyknosis of the nuclei of the tubules	–	–	–	–	–	–	++	+	+	–	+	–	–	–	–	–	–	–
3-Degeneration of the tubular lining epithellium	–	–	–	–	–	–	–	–	++	–	–	+	–	–	–	–	–	–
4-Atrophic glomeruli	–	–	–	–	–	–	–	–	–	–	–	–	–	–	–	–	–	–

(Degree of tubular injury ↑)

C, cortex; CM, corticomedullary portion; M, medulla.

It is well known that the cellular response toward CDDP induced damage could lead to cell death either by apoptosis or necrosis. The type of cellular injury induced by CDDP depends on the extent of damage to proteins or molecules involved in the apoptotic pathway (*32*). To clarify the protective role of glycine and L-arginine in CDDP induced cell death, histopathological examination was performed and revealed that CDDP produced marked coagulative necrosis in the tubular epithelium of the cortex and corticomedullary region and these results are in accordance with previous studies (*24,33*). Furthermore, histopathological examination did not reveal apoptosis or apoptotic bodies, a finding that may indicate sever cellular damage of proteins or molecules involved in the apoptotic pathway resulting in unfinished apoptosis or necrosis (*32,34*). Regarding amino acids, glycine was found to be more effective than L-arginine in protection against CDDP induced necrosis at the cortex as glycine was capable of converting CDDP induced damage from coagulative necrosis to tubular degeneration and the first stage of nuclear necrosis; pyknosis. At the tubular degeneration stage, the kidney can regenerate its normal structure after CDDP treatment stoppage. In contrast, both of these amino acids have the same effect in the corticomedullary region.

Despite the fact that the underlying mechanism of CDDP-induced nephrotoxicity is still not clear, the avidity of platinum for sulphur containing ligands has been proposed in the hypothetical mechanisms explaining the nephrotoxicity of CDDP. The depletion of mitochondrial GSH is considered as an early and critical event during CDDP-induced lipid peroxidation and subsequent toxicity (*25,35*). In the present study, it was found that, CDDP induced a significant depletion of GSH concomitant with a significant elevation of lipid peroxides, which is in accordance with previous *in-vitro* studies (*31,36*); these findings add further evidence for the role of oxidative stress in CDDP-induced renal toxicity. Pre-incubation of RCS with either glycine or L-arginine significantly counteracted the effect of CDDP and restored the normal level of both GSH and lipid peroxides. The antioxidant properties of glycine (*37,38*) and L-arginine (*21,39*) had been previously reported in several oxidative stress situations. Although, glycine is a direct precursor of GSH, L-arginine showed a significant protective effect on GSH as compared to glycine effect. In an experiment with hypoxic proximal tubular cells, Weinberg and co-workers (*40*) observed that cytoprotection provided by glycine was accompanied by a preservation of cellular GSH and ATP levels. However, the depletion of GSH content or ATP levels of renal tubular cells did not reduce the cytoprotective activity of glycine. Therefore, they suggested that glycine might have a direct cytoprotective effect.

Besides the oxidative stress markers; pyruvate-stimulated gluconeogenesis was measured in RCS.

Co-incubation of RCS with pyruvate, a substrate of gluconeogenesis, in the presence of CDDP showed marked depression of pyruvate-stimulated gluconeogenesis which reached 32% of the control value and theses results are in accordance with other previous studies performed *in vitro* (*25*). Addition of either glycine or L-arginine 1 h before CDDP did not show any protective effect on CDDP-induced inhibition of gluconeogenesis. Although glycine and L-arginine are gluconeogenic amino acids in kidney metabolism leading to a precursor for gluconeogenesis (*41,42*), in the present study, they did not show any protective effect against CDDP induced inhibition of gluconeogenesis. These findings may indicate the existence of different mechanisms of CDDP induced nephrotoxicity beside free radical formation and oxidative stress. Indeed, previous studies are controversial concerning the role of oxidative stress in gluconeogensis and whether we can use the inhibition of gluconeogensis as a marker of oxidative stress or not. Zhang *et al.* (*25*) proposed that GSH depletion might be responsible for inhibition of the activities of the relevant gluconeogenic enzymes, *e.g.* phosphoenolpyruvate carboxykinase, glycerol-3-phosphate dehydrogenase, and glucose-6-phosphatase. On the other hand, Hannmann and Baumann in two serial studies (*43,44*), proposed that direct inhibition of the gluconeogenic enzyme glucose-6-phosphatase by CDDP or its metabolites might play a role in inducing the decrease of gluconeogenesis away from GSH depletion and oxidative stress effects of CDDP.

Finally, we tried to answer the question of whether nephroprotection can be achieved by inhibiting CDDP uptake by RCS in the presence of amino acids, either glycine or L-arginine. Since several investigators have observed a correlation between platinum levels and *in-vitro* toxicity (*45*), it is believed that the targeted inhibition of CDDP accumulation in renal cells could lead to a new therapeutic approach to preventing CDDP nephrotoxicity. In the present study, CDDP concentration in the medium was determined and subtracted from the original amount of CDDP added to the medium. The platinum content in the RCS incubated with CDDP alone was 2.23 ± 0.07 mg/g wet tissue. Our results are in agreement with Zhang *et al.* (*25*) and Saleh *et al.* (*46*). Preincubation of RCS with glycine or L-arginine 1 h before CDDP addition showed a significant decrease in the kidney content of platinum to be 86 and 91%, respectively, as compared to the CDDP group, a finding that reflects the possible inhibition of CDDP uptake in the putative mechanisms of nephroprotection afforded by both glycine and L-arginine.

Indeed, transporter mediated uptake is likely the major pathway in renal cells. The organic cation transporter (OCT 2) is the critical transporter for CDDP uptake in proximal tubules in both animals and humans (*47*). They mediate the basolateral-to-apical transport of

several cationic compounds in renal tubular cells (*48*). On the basis of active transport of CDDP, cimetidine, an inhibitor of OCTs, could prevent CDDP-induced proximal tubule cell cytotoxicity or apoptosis (*49*). One study has been conducted on glycine, Heymen *et al.* (*50*) reported that the infusion of glycine into the rats 15 min before CDDP injection attenuated the early accumulation of platinum in the kidney, and may explain the protective effect of glycine. The results of this study confirmed the role of a hemodynamic effect of glycine, possibly through increasing renal blood flow and glomerular filtration rate and so accelerating CDDP excretion. Although, glycine is also actively transported by renal cells (*51*), it is not known whether it utilizes the OCT or not. As we mentioned before, RCS is a good model for studying CDDP nephrotoxicity because it contains populations of cells targeted by platinum anticancer agents and is not influenced by uncontrollable hormonal, neurogenic and hemodynamic factors. Therefore, the present study demonstrated that the decrease in CDDP uptake could be a direct effect of glycine on CDDP transportation. Further studies are warranted to explore whether glycine can affect the OCT carrier. On the other hand, in reviewing the literature, nothing concerning the effect of L-arginine on CDDP uptake by kidney has been reported. Thus, the findings of the present study add another new mechanism for L-arginine nephroprotection by reducing CDDP uptake. It is important to mention that L-arginine uptake was proven to be mediated through the cationic amino acid transporter (*52*) and so, it might interfere with CDDP uptake by the cationic transporters.

In conclusion, the present study clearly demonstrates that glycine and L-arginine could be promising drugs as nephroprotectors against CDDP-induced nephrotoxicity. Furthermore, this study sheds light on the mechanisms involved in their nephroprotection. They guard against oxidative stress induced by CDDP by restoring cellular defense mechanisms, replenishing kidney GSH content and normalizing lipid peroxidation. Also, the nephroprotective effect was mediated through lowering platinum uptake by the kidney tissue. Furthermore, they could ameliorate necrosis or renal tubule damage induced by CDDP. L-Arginine showed greater antioxidant properties while glycine showed greater antinecrotic effects. Further investigations are clearly warranted to establish the clinical applicability of these amino acids in patients with nephrotoxicity associated with CDDP administration and to explore possible interference of the antitumor activity of CDDP.

Acknowledgement

References

1. Rosenberg B. Platinum complexes for the treatment of cancer: Why the search goes on. In: Ciplatin. Chemistry and biochemistry of a leading anticancer drug (Lippert B, ed.). Wiley-VCH, Basel, Switzerland. 1999; pp. 3-27.
2. Arany I, Safirstein RL. Cisplatin nephrotoxicity. Semin Nephrol. 2003; 23:460-464.
3. Andersson A, Fagerberg J, Lewensohn R, Ehrsson H. Pharmacokinetics of cisplatin and its monohydrated complex in humans. J Pharm Sci. 1996; 85:824-827.
4. Lau AH. Apoptosis induced by cisplatin nephrotoxic injury. Kidney Int. 1999; 56:1295-1298.
5. Kuhlmann MK, Burkhardt G, Köhler H. Insights into potential cellular mechanisms of cisplatin nephrotoxicity and their clinical application. Nephrol Dial Transplant. 1997; 12:2478-2480.
6. Winston JA, Safirstein R. Reduced renal blood flow in early cisplatin-induced acute renal failure in the rat. Am J Physiol. 1985; 249:F490-F496.
7. Ali BH, Al-Moundhri M, Tageldin M, Al Husseini IS, Mansour MA, Nemmar A, Tanira MO. Ontogenic aspects of cisplatin-induced nephrotoxicity in rats. Food Chem Toxicol. 2008; 46:3355-3359.
8. Hospers GA, Eisenhauer EA, de Vries EG. The sulfhydryl containing compounds WR-2721 and glutathione as radio- and chemoprotective agents. A review, indications for use and prospects. Br J Cancer. 1999; 80:629-638.
9. Brezis M, Silva P, Epstein FH. Amino acids induce renal vasodilatation in isolated perfused kidney: Coupling to oxidative metabolism. Am J Physiol. 1984; 247:H999-H1004.
10. Rodríguez-Iturbe B, Herrera J, García R. Relationship between glomerular filtration rate and renal blood flow at different levels of protein-induced hyperfiltration in man. Clin Sci (Lond). 1988; 74:11-15.
11. Weinberg JM, Davis JA, Abarzua M, Rajan T. Cytoprotective effects of glycine and glutathione against hypoxic injury to renal tubules. J Clin Invest. 1987; 80:1446-1454.
12. Weinberg JM, Davis JA, Abarzua M, Smith RK, Kunkel R. Ouabain-induced lethal proximal tubule cell injury is prevented by glycine. Am J Physiol. 1990; 258:F346-F355.
13. Thurman RG, Zhong Z, von Frankenberg M, Stachlewitz RF, Bunzendahl H. Prevention of cyclosporin-induced nephrotoxicity with dietary glycine. Transplantation. 1997; 63:1661-1667.
14. Basivireddya J, Jacob M, Pulimooda AB, Balasubramanian KA. Indomethacin-induced renal damage: Role of oxygen free radicals. Biochem Pharmacol. 2004; 67:587-599.
15. Secilmia MA, Karatas Y, Yorulmaza O, Buyukafşar K, Singirik E, Doran F, Inal TC, Dikmen A. Protective effect of L-arginine intake on the impaired renal vascular responses in the Gentamicin-treated rats. Nephron Physiol. 2005; 100:13-20.
16. Kuruş M, Eşrefoğlu M, Bay A, Oztürk F. Protective effect of oral L-arginine supplementation on cyclosporine induced nephropathy in rats. Int Urol Nephrol. 2005; 37:587-594.
17. Gupta A, Chander V, Sharma S, Chopra K. Sodium nitroprusside and L-arginine attenuates ferric nitrilotriacetate-induced oxidative renal injury in rats. Toxicology. 2007; 232:183-191.
18. Heyman SN, Rosen S, Silva P, Spokes K, Egorin MJ, Epstein FH. Protective action of glycine in cisplatin

nephrotoxicity. Kidney Int. 1991; 40:273-279.

19. Li Q, Bowmer CJ, Yates MS. The protective effect of glycine in cisplatin nephrotoxicity: Inhibition with NG-nitro-L-arginine methyl ester. J Pharm Pharmacol. 1994; 46:346-351.

20. Cernadas MR, López-Farré A, Riesco A, Gallego MJ, Espinosa G, Digiuni E, Hernando L, Casado S, Caramelo C. Renal and systemic effect of amino acids administered separately: Comparison between L-arginine and non-nitric oxide donor amino acids. J Pharm Exp Ther. 1992; 263:1023-1029.

21. Saleh S, El-Demerdash E. Protective effects of L-arginine against cisplatin-induced renal oxidative stress and toxicity: Role of nitric oxide. Basic Clin Pharmacol Toxicol. 2005; 97:91-97.

22. Li Q, Bowmer C, Yates MS. Effect of arginine on cisplatin-induced acute renal failure in rat. Biochem Pharmacol. 1994; 47:2298-2301.

23. Smith JH. The use of renal cortical slices from the Fischer 344 rat as an *in-vitro* model to evaluate nephrotoxicity. Fundam Appl Toxicol. 1988; 132-142.

24. Vickers AE, Rose K, Fisher R, Saulnier M, Sahota P, Bentley P. Kidney slices of human and rat to characterize cisplatin-induced injury on cellular pathways and morphology. Toxicologic Pathol. 2004; 32:577-590.

25. Zhang JG, Zhong LF, Zhang M, Xia YX. Protection effects of procaine on oxidative stress and toxicities of renal cortical slices from rats caused by cisplatin *in vitro*. Arch Toxicol. 1992; 66:354-358.

26. Tietz NW. Clinical guide to laboratory tests. 3rd ed., W.B. Saunders Co., Philadelphia, PA, 1995.

27. Mosmann T. Rapid colorimetric assay for cellular growth and survival: Application to proliferation and cytotoxicity assays. J Immunol Methods. 1983; 65:55-63.

28. Buege JA, Aust SD. Microsomal lipid peroxidation. Methods Enzymol. 1978; 52:302-310.

29. Ellman GL. Tissue sulfhydryl groups. Arch Biochem Biophys. 1959; 82:70-77.

30. el-yazigi A, Al-Saleh I. Rapid determination of platinum by flameless atomic absorption spectrophotometry following the administration of cisplatin to cancer patients. Ther Drug Monit. 1986; 8:318-320.

31. Zhang JG, Lindup WE. Role of mitochondria in cisplatin-induced oxidative damage exhibited by rat renal cortical slices. Biochem Pharmacol. 1993; 45:2215-2222.

32. Gonzalez VM, Fuertes MA, Alonso C, Perez JM. Is Cisplatin-induced cell death always produced by apoptosis? Mol Pharmacol. 2001; 59:657-663.

33. Cristofori P, Zanetti E, Fregona D, Piaia A, Trevisan A. Renal proximal tubule segment-specific nephrotoxicity: An overview on biomarkers and histopathology. Toxicologic Pathol. 2007;35:270-275.

34. Delmastro DA, Li J, Vaisman A, Solle M, Chaney SG. DNA damage inducible-gene expression following platinum treatment in human ovarian carcinoma cell lines. Cancer Chemother Pharmaco. 1997; 39:245-253.

35. Mora Lde O, Antunes LM, Francescato HD, Bianchi Mde L. The effects of oral glutamine on cisplatin-induced nephrotoxicity in rats. Pharmacol Res. 2003; 47:517-522.

36. Yoshida M, Itzuka K, Hara M, Nishijima H, Shimada A, Nakada K, Satoh Y, Akama Y, Terada A. Prevention of

nephrotoxicity of cisplatin by repeated oral administration of ebslenin rats. Tohoku J Exp Med. 2000; 191:209-220.

37. Sobage K, Roeser NF, Venkatachalam MA, Weinberg JM. Differential cytoprotection by glycine against oxidant damage to proximal tubule cells. Kidney Int. 1996; 50:845-854.

38. Shaikh ZA, Tang W. Protection against chronic cadmium toxicity by glycine. Toxicology. 1999; 132:139-146.

39. Mansour M, Daba MH, Gado A, Al-Rikabi A, Al-Majed A. Protective effect of L-arginine against nephrotoxicity induced by cyclosporine in normal rats. Pharmacol Res. 2002; 45:441-446.

40. Weinberg JM, Davis JA, Abarzua M, Kiani T. Relationship between cell adenosine triphosphate and glutathione content and protection by glycine against hypoxic proximal tubule cell injury. J Lab Clin Med. 1989; 113:612-622.

41. Krebs HA, Yoshida T. The gluconeogenic capacity of the kidney cortex of various species. Biochem J. 1963; 89:398-400.

42. Hetenyi G Jr, Anderson PJ, Raman M, Ferrarotto C. Gluconeogenesis from glycine and serine in fasted normal and diabetic rats. Biochem J. 1988; 253:27-32.

43. Hannemann J, Baumann K. Nephrotoxicity of cisplatin, carboplatin and transplatin, a comparative *in vitro* study. Arch Toxicol. 1990; 64:393-400.

44. Hannemann J, Baumann K. Cisplatin-induced lipid peroxidation and decrease of gluconeogenesis in rat kidney cortex: Different effects of antioxidants and radical scavengers. Toxicology. 1988; 51:119-132.

45. Yao X, Panichpisal K, Kurtzman N, Nugent K. Cisplatin Nephrotoxicity: A review. Am J Med Sci. 2007; 334:115-124.

46. Saleh S, Ain-Shoka AA, El-Demerdash E, Khalef MM. Prevention of cisplatin-induced nephrotoxicity by an angiotensin-II receptor blocker, losratan. Chemotherapy. 2009; 55:399-406

47. Kröning R, Lichtenstein AK, Nagami GT. Sulfur-containing amino acids decrease cisplatin cytotoxicity and uptake inrenal tubule epithelial cell lines. Cancer Chemother Pharmacol. 2000; 45:43-49.

48. Pabla N, Dong Z. Cisplatin nephrotoxicity: Mechanisms and renoprotective strategies. Kidney Int. 2008; 73:994-1007.

49. Ludwig T, Riethmüller C, Gekle M, Schwerdt G, Oberleithner H. Nephrotoxicity of platinum complexes is related to basolateral organic cation transport. Kidney Int. 2004; 66:196-202.

50. Heymen SN, Spokes K, Egorin MJ, Epstein FH. Glycine reduces early renal parenchymal uptake of cisplatin. Kidney Int. 1993; 43:1226-1228.

51. Scallera V, Corcelli A, Frassanito A, Storelli C. Chloride dependence of the sodium-dependent glycine transport in pig kidney cortex brush border membrane vesicles. Biochim Biophys Acta. 1987; 903:1-10.

52. Kim JW, Closs EI, Albritton LM, Cunningham JM. Transport of cationic amino acids by the mouse ecotropic retrovirus receptor. Nature. 1991; 352:725-728.

Validated spectrophotometric methods for determination of some oral hypoglycemic drugs

Maha Farouk[1], Osama Abdel-Satar[2], Omar Abdel-Aziz[1,*], Maya Shaaban[3]

[1] *Faculty of Pharmacy, Ain Shams University, Cairo, Egypt;*
[2] *National Organization of Drug Control and Research, Giza, Egypt;*
[3] *Faculty of Pharmacy, Egyptian Russian University, Helwan, Egypt.*

ABSTRACT: Four accurate, precise, rapid, reproducible, and simple spectrophotometric methods were validated for determination of repaglinide (RPG), pioglitazone hydrochloride (PGL) and rosiglitazone maleate (RGL). The first two methods were based on the formation of a charge-transfer purple-colored complex of chloranilic acid with RPG and RGL with a molar absorptivity 1.23×10^3 and 8.67×10^2 l·mol^{-1}·cm^{-1} and a Sandell's sensitivity of 0.367 and 0.412 μg·cm^{-2}, respectively, and an ion-pair yellow-colored complex of bromophenol blue with RPG, PGL and RGL with molar absorptivity 8.86×10^3, 6.95×10^3, and 7.06×10^3 l·mol^{-1}·cm^{-1}, respectively, and a Sandell's sensitivity of 0.051 μg·cm^{-2} for all ion-pair complexes. The influence of different parameters on color formation was studied to determine optimum conditions for the visible spectrophotometric methods. The other spectrophotometric methods were adopted for demtermination of the studied drugs in the presence of their acid-, alkaline- and oxidative-degradates by computing derivative and pH-induced difference spectrophotometry, as stability-indicating techniques. All the proposed methods were validated according to the International Conference on Harmonization guidelines and successfully applied for determination of the studied drugs in pure form and in pharmaceutical preparations with good extraction recovery ranges between 98.7-101.4%, 98.2-101.3%, and 99.9-101.4% for RPG, PGL, and RGL, respectively. Results of relative standard deviations did not exceed 1.6%, indicating that the proposed methods having good repeatability and reproducibility. All the obtained results were statistically compared to the official method used for RPG analysis and the manufacturers methods used for PGL and RGL analysis, respectively, where no significant differences were found.

1. Introduction

For many years pharmacological agents such as sulphonylureas and biguanides were the mainstay of oral treatment for type II diabetes. Target control is achieved with these medications for some patients only, however; secondary failure is relatively common. Thus, the introduction of newer agents such as meglitinides (repaglinide; RPG) and thiazolidinediones (pioglitazone and rosiglitazone) has been welcomed (*1*). RPG acts by stimulating insulin secreation of β-cells of the pancreas, while both pioglitazone hydrochloride (PGL) and rosiglitazone maleate (RGL), which exert their glucose-lowering effect by binding to peroxisome proliferator-activated γ receptors, thus increasing the receptor sensitivity to insulin (*2*). Structures of RPG, PGL, and RGL are illustrated below.

Repaglinide

Pioglitazone hydrochloride

Rosiglitazone maleate
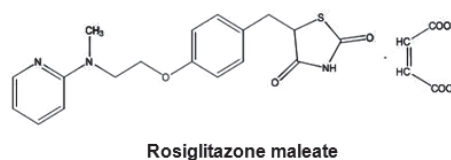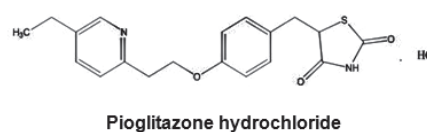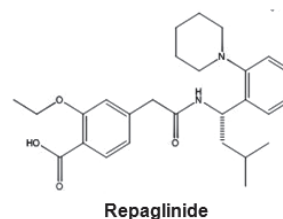
*Address correspondence to:
Dr. Omar Abdel-Aziz, Faculty of Pharmacy, Ain Shams University, Cairo, Egypt.
e-mail: dr_omarghonim@hotmail.com

Many analytical methods have been reported for the quantitative estimation of RPG in pharmaceutical preparations and biological samples (*3-5*) which include visible spectrophotometric (*6,7*), HPLC (*8,9*) and electrochemical methods (*10*). PGL and its metabolites have been determined in biological fluids and pharmaceutical preparations by HPLC with UV detection (*11-13*), reversed phase TLC (*14*), liquid chromatography coupled with mass spectrometry (*15*), and spectrometry (*16*). On the other hand, RGL in pharmaceutical preparations and human plasma has been determined by HPLC with UV detection (*17-21*), HPTLC (*22*), TLC (*23*), and liquid chromatography coupled with mass spectrometry (*24*).

The aim of this study is to develop and validate simple, rapid, sensitive, and reliable spectrophotometric methods for accurate quantitation of RPG, PGL, and RGL *via* 'charge-transfer and ion-pair' complexation reactions and stability-indicating assays using 'derivative and pH-induced difference spectrophotometry'. All the proposed methods were successfully applied for routine quality control analysis of the mentioned drugs in raw material and in their pharmaceutical preparations unaffected by interference from excipients.

2. Materials and Methods

2.1. *Chemicals and reagents*

RPG and PGL were kindly supplied by Amoun Pharmaceutical Co. (Cairo, Egypt) and certified to contain 99.99% and 99.95%, respectively. Diarol® tablets, batch number 1018, were labeled to each contain 2 mg of RPG and Actozone® tablets, batch number 3543, were labeled to each contain 45 mg of PGL. RGL was kindly supplied by Apex Pharma (Cairo, Egypt) and certified to contain 99.99%. Rosizone® tablets, batch number MT0410208, were labeled to each contain 4 mg of RGL.

Methanol and acetonitrile were purchased from Honeywell Riedel-de Haen, Seelze, Germany. Chloranilic acid, bromophenol blue, hydrochloric acid (35.4%), sodium hydroxide, potassium hydrogen phthalate, chloroform, hydrogen peroxide (30%), and ethanol were from BDH Chemicals, Poole, UK. All chemicals and reagents used throughout this work were spectroscopic analytical grade. Bi-distilled water was used throughout the whole work and indicated by the word "water".

2.2. *Instruments*

A Hewlett-Packard HP 8452A Diode Array Spectrophotometer (Hewlett-Packard, Palo Alto, CA, USA) connected to an IBM compatible computer and HP laser printer was used. The bundled software was UV-Visible ChemStation Rev. A.08.03, Agilent

Technologies, Santa Clara, CA, USA. The spectral bandwidth was 0.2 nm and the wavelength scanning speed was 2,800 nm·min^{-1}. The absorption spectra of the reference and the test solutions were recorded in 1.0-mL quartz cells at 25.0°C using conditions of '$\Delta\lambda$ = 4 nm and scaling factor of 10 for first derivative (D^1)' and '$\Delta\lambda$ = 8 nm and scaling factor of 100 for second and third derivative (D^2 and D^3, respectively)'. A sonicator (Model RK 100H DVE GS; Bandelin Sonorex, Berlin, Germany) and a pH-meter equipped with a combined glass electrode (Jenway, Essex, UK) were used.

2.3. *Standard solutions*

2.3.1. *Standard solutions of drugs studied*

For the charge-transfer method, RPG and RGL stock standard solutions with a concentration of 1.0 mg·mL^{-1} in acetonitrile were prepared, which were also used as working standard solutions. For the other three spectrophotometric methods, stock standard solutions of RPG, PGL, and RGL with concentrations of 1.0 mg·mL^{-1} in methanol were prepared, which were further diluted with methanol to obtain concentrations of 0.1 mg·mL^{-1} to be used as working standard solutions.

2.3.2. *Standard solutions of reagents used for charge-transfer and ion-pair methods*

0.1% (w/v) chloranilic acid (CLA) in acetonitrile was used for the charge-transfer method and 0.1% (w/v) bromophenol blue (BPB) and phthalate buffers, pH 2.4 and 2.2, (*25*) were for the ion-pair method.

2.3.3. *Standard solutions of degradates for stability-indicating spectrophotometric methods*

Three standard solutions of degradates, *i.e.* acid-, alkaline-, and oxidative degradation products of RPG, PGL, and RGL, were prepared. Ten mg of each compound were mixed with 50 mL of 2 M HCl, 2 M NaOH, and 30% H_2O_2 for acid-, alkaline-, and oxidative degradation, respectively, followed by heating in a thermostatic water-bath at 80°C for 24 h. After cooling, the mixtures for the acid- and alkaline-degradated-solutions were neutralized with 5 M NaOH and 5 M HCl, respectively. The final concentrations of all the degradated-solutions were adjusted to 0.1 mg·mL^{-1} with methanol.

2.4. *Charge-transfer method*

Aliquots of RPG and RGL working standard solutions were mixed with 3.0 and 2.0 mL of 0.1% CLA in a series of 10-mL volumetric flasks and then diluted with acetonitrile to obtain a concentration range of 50-325 and 50-300 µg·mL^{-1}, respectively. The absorbance of

the produced purple-colored charge-transfer complex was measured at 518 nm against a reagent-blank at room temperature. Calibration curves were constructed and the regression equation was then computed.

2.5. Ion-pair method

Into three separating funnels, aliquots of RPG, PGL, and RGL working standard solutions were separately transferred and mixed with 4.0 mL of phthalate buffer, pH 2.4 for RPG and PGL, and pH 2.2 for RGL. The solutions were then mixed with 3.0 mL of 0.1% BPB reagent solution. The produced yellow-colored ion-pair complexes were extracted twice with 4 mL chloroform and allowed to stand for clear separation of the two phases. The chloroformic layer was then passed through anhydrous sodium sulfate and diluted with chloroform in 10-mL volumetric flasks to obtain a concentration range of 5-35 $\mu g \cdot mL^{-1}$. The absorbance of the produced colored-complexes was measured at 414 nm, 416 nm and 415 nm, respectively, against a reagent blank at room temperature. Calibration curves were constructed and the regression equation was then computed.

2.6. Stability-indicating spectrophotometric methods

2.6.1. Derivative spectrophotometric (D^n) method

From standard working solutions, aliquots were transferred into a series of 10 mL-volumetric flasks and diluted with methanol. RPG was determined in a concentration range of 5-75 $\mu g \cdot mL^{-1}$ in the presence of its acid-, alkaline- and oxidative-degradates, where the values of the first derivative (D^1) amplitudes were computed at 263.79, 264.33 and 304.84 nm, respectively. PLG was determined in a concentration range of 5-60 $\mu g \cdot mL^{-1}$ in the presence of its acid- and alkaline-degradates, where the values of the first derivative (D^1) were computed at 253.35 and 284.05 nm, respectively, and the values of the second derivative (D^2) were computed at 276.31 nm in a concentration range of 5-75 $\mu g \cdot mL^{-1}$ in the presence of its oxidative-degradates. RGL was determined in a concentration range of 5-70 $\mu g \cdot mL^{-1}$ in the presence of its acid-, alkaline- and oxidative-degradates, where the values of the second derivative (D^2) amplitudes were computed at 307.95, 287.73, and 325.67 nm, respectively. Calibration curves were constructed and the regression equation was then computed.

2.6.2. pH-induced difference spectrophotometric (DD^n) method

From standard working solutions, aliquots were transferred into two sets of 10-mL volumetric flasks and diluted with either 0.1 M HCl or 0.1 M NaOH. ΔA spectra were computed by placing the acid solution in the

reference beam and the alkaline solution in the sample beam. RPG was determined in a concentration range of 5-65 $\mu g \cdot mL^{-1}$ in the presence of its acid- and alkaline-degradates, where the values of the first derivative of ΔA spectra (DD^1) were computed at 258.04 and 261.82 nm, respectively, while the second derivative of ΔA spectra (DD^2) values were computed at 252.80 nm in a concentration range of 5-75 $\mu g \cdot mL^{-1}$ in the presence of its oxidative-degradates. PGL was determined in a concentration range of 5-80 $\mu g \cdot mL^{-1}$ in the presence of its acid- and alkaline-degradates, where the values of the first derivative of ΔA spectra (DD^1) were computed at 242.81 and 243.41 nm, respectively, and the values of the second derivative ΔA spectra (DD^2) were computed at 253.12 nm in a concentration range of 5-75 $\mu g \cdot mL^{-1}$ in the presence of its oxidative-degradates. RGL was determined in a concentration range of 5-70 $\mu g \cdot mL^{-1}$ in the presence of its acid-, alkaline-, and oxidative-degradates, where the values of second derivative ΔA spectra (DD^2) were computed at 272.00 nm in the presence of its alkaline-degradates and those of the third derivative of ΔA spectra (DD^3) amplitudes were computed at 275.90 and 267.40 nm in the presence of its acid- and oxidative-degradates, respectively. Calibration curves were constructed and the regression equation was then computed.

2.7. Assays of the pharmaceutical preparations by the proposed methods and application of standard addition techniques

Sixty tablets of Diarol®, 10 tablets of Actozone®, and 30 tablets of Rosizone® were individually weighed to get the average weight of the tablets, respectively. For the charge-transfer method, a sample of the powdered tablets containing 50 mg of RPG or RGL was transferred to 50-mL volumetric flasks and sonicated for 20 min with 30 mL acetonitrile. The solution was brought to 50 mL with the same solvent and then filtered to prepare stock working solutions with a concentration of 1.0 mg·mL^{-1}. Aliquots of the filtrate were further diluted with the same solvent and then subjected to the procedure for the charge-transfer method as described above. For other spectrophotometric methods, a sample of the powdered tablets containing 25 mg of RPG, PGL, or RGL was transferred to 250-mL volumetric flasks and sonicated for 20 min with 200 mL methanol. The solution was brought to 250 mL with the same solvent and then filtered to prepare stock working solutions with a concentration of 0.1 mg·mL^{-1}. Aliquots of the filtrate were further diluted with the same solvent and then subjected to the procedures for ion-pair and stability-indicating spectrophotometric methods as described above.

To check the validity of the proposed methods, the standard addition technique was applied. For the

charge-transfer method, a sample of the powdered tablets containing 5 mg of RPG or RGL was accurately weighed and mixed with 5, 10, 15, 20, and 25 mg of the corresponding pure drug. Each spiked sample of RPG and RGL was transferred to a 25-mL volumetric flask, and sonicated for 20 min with 20 mL acetonitrile. The mixtures were diluted with the same solvent and filtered to get five spiked solutions from each pharmaceutical preparation in a concentration range of 0.4-1.2 mg•mL^{-1}. From each spiked solution, 2.5 mL was transferred to a 10-mL volumetric flask and then subjected to the procedure for the charge-transfer method as described above. For ion-pair and stability-indicating spectrophotometric methods, a sample of the powdered tablets containing 5 mg of RPG, PGL, or RGL was accurately weighed and mixed with 5, 10, 15, 20, 25 mg of the corresponding pure drug. Each spiked sample of RPG, PGL, and RGL was transferred to a 100-mL volumetric flask, and sonicated for 20 min with 75 mL methanol. The mixtures were then diluted with the same solvent and filtered to get five spiked solutions from each pharmaceutical preparation in a concentration range of 0.1-0.3 mg•mL^{-1}. One mL each and 1.5 mL each of spiked solutions was subjected to the procedure for the ion-pair method and stability-indicating spectrophotometric methods, respectively, as described above.

3. Results

3.1. *Development of charge-transfer and ion-pair methods*

3.1.1. *Absorption spectra*

Absorption spectra of charge-transfer complexes formed by RPG and CLA (Figure 1A) and RGL and CLA (Figure 1B) and those of ion-pair complexes formed by RPG and BPB (Figure 1C), PGL and BPB (Figure 1D), and RGL and BPB (Figure 1E) were measured against reagent-blanks. Both charge-transfer complexes showed maximum absorbance at 518 nm (Figures 1A and 1B). In contrast, the ion-pair complexes showed maximum absorbance at 414, 416, and 415 nm for RPG-BPB, PGL-BPB, and RGL-BPB, respectively. The influence of different parameters on color formation was studied to determine optimum conditions for the visible spectrophotometric methods.

3.1.2. *Choice of solvent*

In order to select the suitable solvent for charge-transfer complex formation, the reaction of RPG and RGL with CLA was performed in different solvents. Acetonitrile showed super priority over chloroform, 2-propanol, dichloroethane, 1,4-dioxan, methanol, and ethanol, as the complex formed in these solvents had a

low molar absorptivity. Furthermore, acetonitrile was considered as an ideal solvent for CLA (π-acceptor), because it offered a maximum sensitivity which was attributed to its high dielectric constant that promotes maximum yield of the complex (*26*). For the ion-pair method, the effect of several organic solvents such as chloroform, carbon tetrachloride, ethyl acetate, diethylether, toluene, and dichloromethane were tried for effective extraction of the colored species from the aqueous phase. Chloroform was found to be the most suitable solvent for extraction of ion-pair complexes from the aqueous solutions. It yielded maximum absorbance intensity and considerably lower extraction ability for the reagent blank and it was also observed that only double extraction was adequate to achieve a quantitative recovery of the complex.
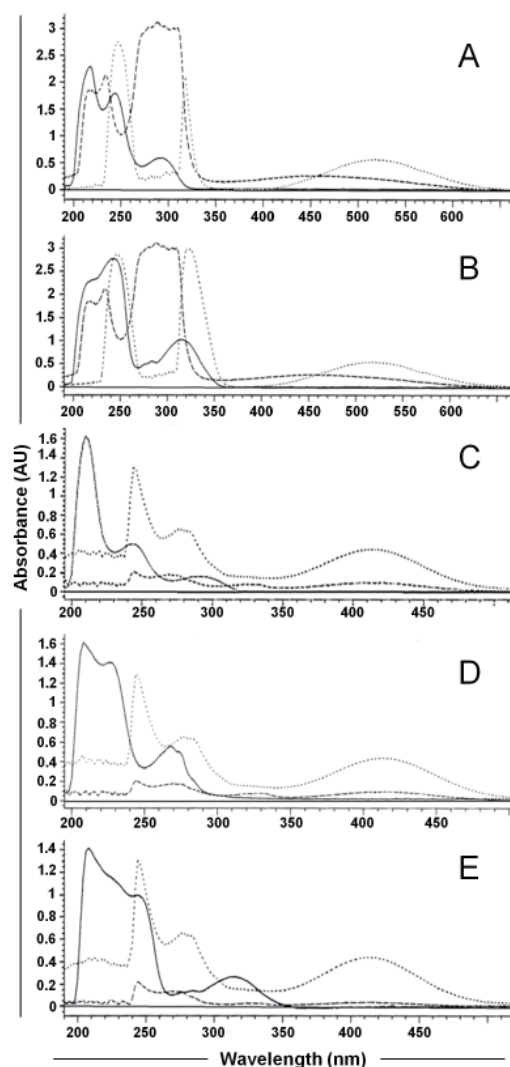
Figure 1. Absorption spectra of various charge-transfer and ion-pair complexes examined. (A) RPG, solid line; CLA, dashed line; RPG-CLA charge-transfer complex, dotted line. **(B)** RGL, solid line; CLA, dashed line; RGL-CLA charge-transfer complex, dotted line. **(C)** RPG, solid line; BPB, dashed line; RGL-BPB ion-pair complex, dotted line. **(D)** PGL, solid line; BPB, dashed line; PGL-BPB ion-pair complex, dotted line. **(E)** RGL, solid line; BPB, dashed line; RGL-BPB ion-pair complex, dotted line.

3.1.3. *Reagent concentration*

Figure 2A shows the effect of CLA concentration (by volume) on the quantitativeness of its reaction with RPG and RGL. It was found that, when various concentrations (by volume) of CLA solution were added to fixed concentrations of the studied drugs, 3.0 and 2.0 mL of 0.1% (w/v) CLA solutions were found to be effective volumes for quantitative determination of RPG and RGL, respectively. Figure 2B shows the effect of BPB concentration (by volume) on the intensity of the color-developed when reacted with RPG, PGL, and RGL. It was found that, when various concentrations (by volume) of BPB solution were added to fixed concentrations of the studied drugs, 3.0 mL of 0.1% (w/v) BPB solution was adequate to obtain a stable product for quantitative determination of RPG, PGL, and RGL.

3.1.4. *Effect of reaction time and temperature*

Optimum reaction time was investigated by following color development at ambient temperature. As shown in Figure 3A, the relationship between time and absorbance showed that the reaction was instantaneous and stable up to 2 h for the produced charge-transfer complexes. For ion-pair complexes, complete color intensity was attained after 2 min of mixing with chloroform and stable up to 2 h (Figure 3B). Figures 3C and 3D shows the relationship between temperature and absorbance, where raising the temperature to 30°C had no effect on the formation of both charge-transfer and ion-pair complexes, but the absorbance started to decay above 30°C.

3.1.5. *Effect of pH and volume of phthalate-buffer on the ion-pair complex formation*

The effect of pH on ion-pair complex formation was studied by extracting the yellow-colored complexes in

the presence of phthalate-buffer at various pH between 2.0-4.0. As shown in Figure 4A, the relationship between pH and the absorbance showed maximum color intensity and consequently a higher absorbance at pH 2.4 for RPG and PGL and at pH 2.2 for RGL. Also, the stability of the formed color-complexes was achieved without affecting the absorbance by using 4.0 mL of phthalate buffers at the chosen pH-values, where maximum absorbance and reproducible results were obtained (Figure 4B).
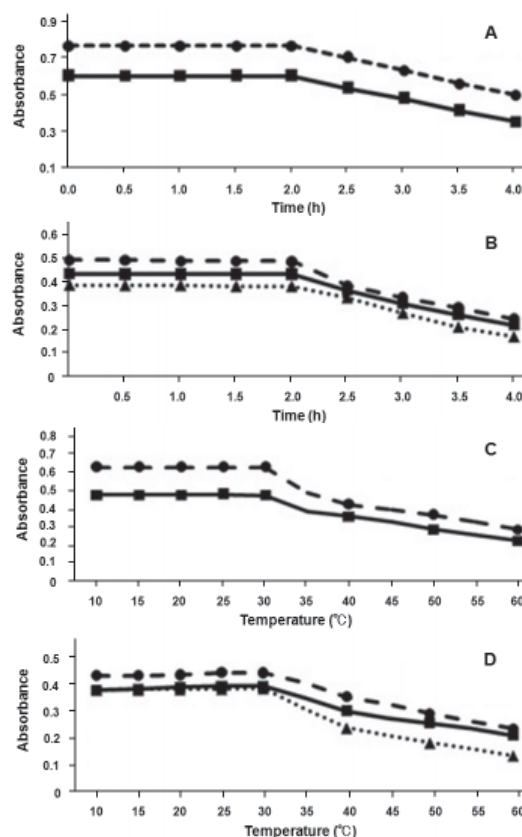
Figure 3. Effect of reaction time or temperature to form various complexes. (A and **C)** Charge-transfer complex formation of RPG (dashed line) and RGL (solid line); (**B** and **D)** Ion-pair complex formation with RPG (dashed line), PGL (dotted line), and RGL (solid line).

Figure 2. Effect of CLA and BPB volumes in reaction mixtures for complex formation with RPG, PGL and RGL. (A) Effect of CLA volume for charge-transfer complex formation with RPG (dashed line) and RGL (solid line). **(B)** Effect of BPB volume for ion-pair complex formation with RPG (dashed line), PGL (dotted line), and RGL (solid line).
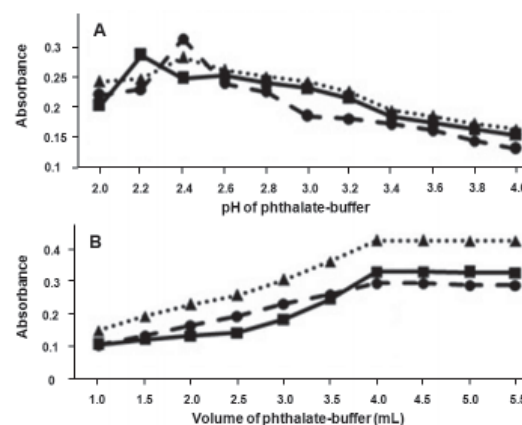
Figure 4. Effect of pH (A) and volume (B) of phthalate-buffer on ion-pair complex formation. Dashed line, RPG; dotted line, PGL; solid line, RGL.

3.1.6. *Stoichiometric relationship*

Job's method of continuous variation (*27*) was applied in order to ascertain the stoichiometry of the reactions of charge-transfer and ion-pair complex formation, where equimolar solutions (1.0×10^{-3}) of each drug, of CLA and BPB were used.

As shown in Figure 5A, the results obtained from Job's method suggested that 1:1 (drug:π-acceptor) charge-transfer complexes were formed through complete electron transfer from RPG or RGL as an electron donor to CLA as an electron acceptor with the formation of intensely colored radical ions in the polar solvent acetonitrile. The deduced scheme is shown in Figure 5C. This finding was anticipated by the presence of one basic electron-donating center (nitrogen atom) present in RPG and RGL structures, while PGL lacks this basic center and consequently failed to form a charge transfer complex when reacted with CLA as a π-acceptor.

Reaction-stoichiometry for ion-pair complexes was found to be a good 1:1 approximation (drug:reagent) ratio which were formed through the electrostatic attraction between positive protonated RPG^+, PGL^+, or RGL^+ and negative BPB^- (Figure 5B). The deduced extraction equilibrium is shown in Figure 5D. In this scheme, $Drug^+$ and BPB^- represent the protonated oral hypoglycemic drugs studied and the anion of the dye, respectively, and the subscripts (aq) and (org) refer to the aqueous and organic phases, respectively.

Figure 5. Job's method graphs for charge-transfer and ion-pair complex formations (A, B); Deduced scheme of charge-transfer and ion-pair complex formation and the extraction equilibrium (C, D). A, charge-transfer complex formation of RPG (dashed line) and RGL (solid line); **B**, ion-pair complex formation with RPG (dashed line), PGL (dotted line), and RGL (solid line); **C**, charge-transfer complex formation; **D**, Ion-pair complex formation.

3.2. *Development of stability-indicating spectrophotometric methods*

3.2.1. *Derivative spectrophotometry method (D^n)*

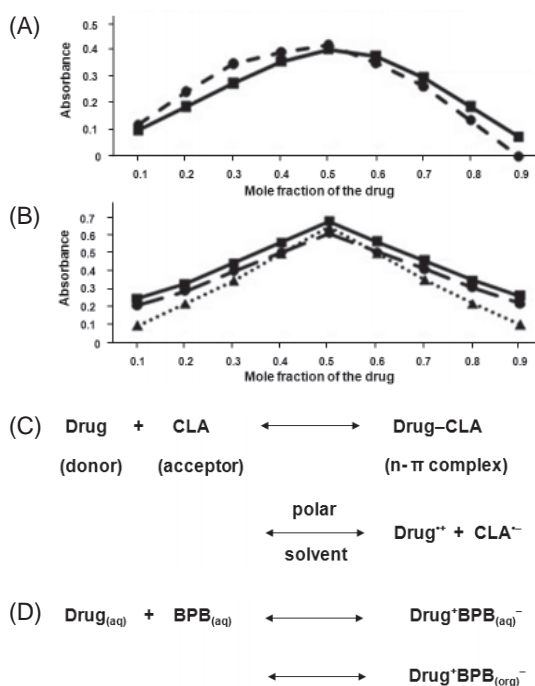The UV-spectra of the oral hypoglycemic drugs under study and their acid-, alkaline- and oxidative-degradates are shown in Figure 6AI-6II, where zero order determination for the drugs was not permitted in the presence of their degradates. Therefore, derivative spectrophotometric methods were adopted, where zero-crossing points for acid-, alkaline-, and oxidative-degradates of each studied drug are indicated. The first derivative spectrophotometric method (D^1) permitted a selective determination of RPG in the presence of its acid-, alkaline-, and oxidative-degradates at 263.8, 264.3, and 304.8 nm, respectively (Figures 6AII-6CII), and PGL in the presence of its acid- and alkaline-degradates at 253.4 and 284.1 nm, respectively (Figures 6DII and 6EII). Also, the second derivative spectrophotometric method (D^2) permitted an excellent determination of PGL in the presence of its oxidative-degradates at 276.3 nm (Figure 6FII), and RGL in the presence of its acid-, alkaline-, and oxidative-degradates at 308.0, 287.7, and 325.7 nm, respectively (Figures 6GII-6III).

3.2.2. *pH-induced difference spectrophotometric method (DD^n)*

Change in the absorption spectra of the intact drugs under investigation, by using acid and alkaline media, was used as a stability-indicating study. The direct UV measurement of ΔA spectra were not suitable for assaying the studied drugs in the presence of their degradates, since there was severe overlap between spectra of the drugs and the degradates (Figure 7AI-7II). Thus, first, second, and third derivative of ΔA spectra were adopted, where zero-crossing points for the acid-, alkaline-, and oxidative-degradates of each studied drug are indicated, respectively. First derivative [DD^1] of ΔA spectra was computed for determination of RPG in the presence of its acid- and alkaline-degradates at 258.0 and 261.8 nm, respectively (Figures 7AII and 7BII), and PGL in the presence of its acid- and alkaline-degradates at 242.8 and 243.4 nm, respectively (Figures 7DII and 7EII). Second derivative of ΔA spectra [DD^2] was computed for determination of RPG and PGL in the presence of their oxidative-degradates at 252.8 and 253.1, respectively (Figures 7CII and 7FII). RGL was also determined in the presence of its acid- and oxidative-degradates at 275.9 and 267.4 nm by computing third derivative [DD^3] of ΔA spectra (Figures 7GII and 7HII) and in the presence of its alkaline-degradates at 272.0 nm by computing second derivative [DD^2] of ΔA spectra (Figure 7III).

Figure 6. (I) UV-spectra of RPG, PGL, RGL, and their acid-, alkaline-, and oxidative-degradates. AI, RPG (solid line) and its acid-degradate (dashed line); **BI**, RPG (solid line) and its alkaline-degradate (dashed line); **CI**, RPG (solid line) and its oxidative-degradate (dashed line); **DI**, PGL (solid line) and its acid-degradate (dashed line); **EI**, PGL (solid line) and its alkaline-degradate (dashed line); **FI**, PGL (solid line) and its oxidative-degradate (dashed line); **GI**, RGL (solid line) and its acid-degradate (dashed line); **HI**, RGL (solid line) and its alkaline-degradate (dashed line); **II**, RGL (solid line) and its oxidative-degradate (dashed line). **(II) First (D^1) or second (D^2) derivative spectra of RPG, PGL, RGL, and their acid-, alkaline-, and oxidative-degradates. AII**, first (D^1) derivative spectra of RPG (solid line) and its acid-degradate (dashed line); **BII**, first (D^1) derivative spectra of RPG (solid line) and its alkaline-degradate (dashed line); **CII**, first (D^1) derivative spectra of RPG (solid line) and its oxidative-degradate (dashed line); **DII**, first (D^1) derivative spectra of PGL (solid line) and its acid-degradate (dashed line); **EII**, first (D^1) derivative spectra of PGL (solid line) and its alkaline-degradate (dashed line); **FII**, second (D^2) derivative spectra of PGL (solid line) and its oxidative-degradate (dashed line); **GII**, second (D^2) derivative spectra of RGL (solid line) and its acid-degradate (dashed line); **HII**, second (D^2) derivative spectra of RGL (solid line) and its alkaline-degradate (dashed line); **III**, second (D^2) derivative spectra of RGL (solid line) and its oxidative-degradate (dashed line).
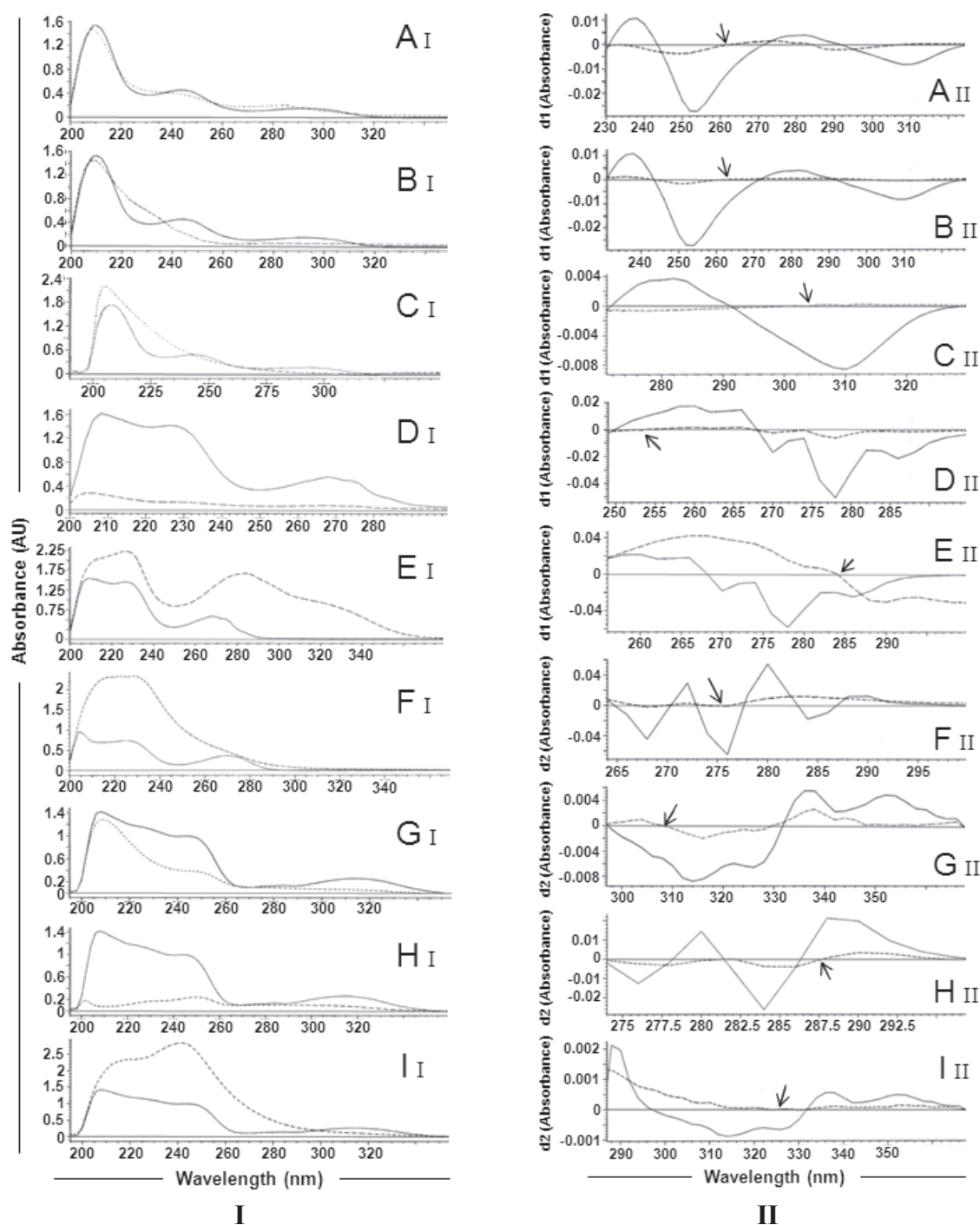
Figure 7. (I) ΔA spectra of RPG, PGL, RGL, and their acid-, alkaline-, and oxidative-degradates. AI, RPG (solid line) and its acid-degradate (dashed line); **B**I, RPG (solid line) and its alkaline-degradate (dashed line); **C**I, RPG (solid line) and its oxidative-degradate (dashed line); **D**I, PGL (solid line) and its acid-degradate (dashed line); **E**I, PGL (solid line) and its alkaline-degradate (dashed line); **F**I, PGL (solid line) and its oxidative-degradate (dashed line); **G**I, RGL (solid line) and its acid-degradate (dashed line); **H**I, RGL (solid line) and its alkaline-degradate (dashed line); **I**I, RGL (solid line) and its oxidative-degradate (dashed line). **(II) First (DD^1), second (DD^2), or third (DD^3) derivative of ΔA spectra of RPG, PGL, RGL, and their acid-, alkaline-, and oxidative-degradates. A**II, first (DD^1) derivative of ΔA spectra of RPG (solid line) and its acid-degradate (dashed line); **B**II, first (DD^1) derivative of ΔA spectra of RPG (solid line) and its alkaline-degradate (dashed line); **C**II, second (DD^2) derivative of ΔA spectra of RPG (solid line) and its oxidative-degradate (dashed line); **D**II, first (DD^1) derivative of ΔA spectra of PGL (solid line) and its acid-degradate (dashed line); **E**II, first (DD^1) derivative of ΔA spectra of PGL (solid line) and its alkaline-degradate (dashed line); **F**II, second (DD^2) derivative of ΔA spectra of PGL (solid line) and its oxidative-degradate (dashed line); **G**II, third (DD^3) derivative of ΔA spectra of RGL (solid line) and its acid-degradate (dashed line); **H**II, third (DD^3) derivative of ΔA spectra of PGL (solid li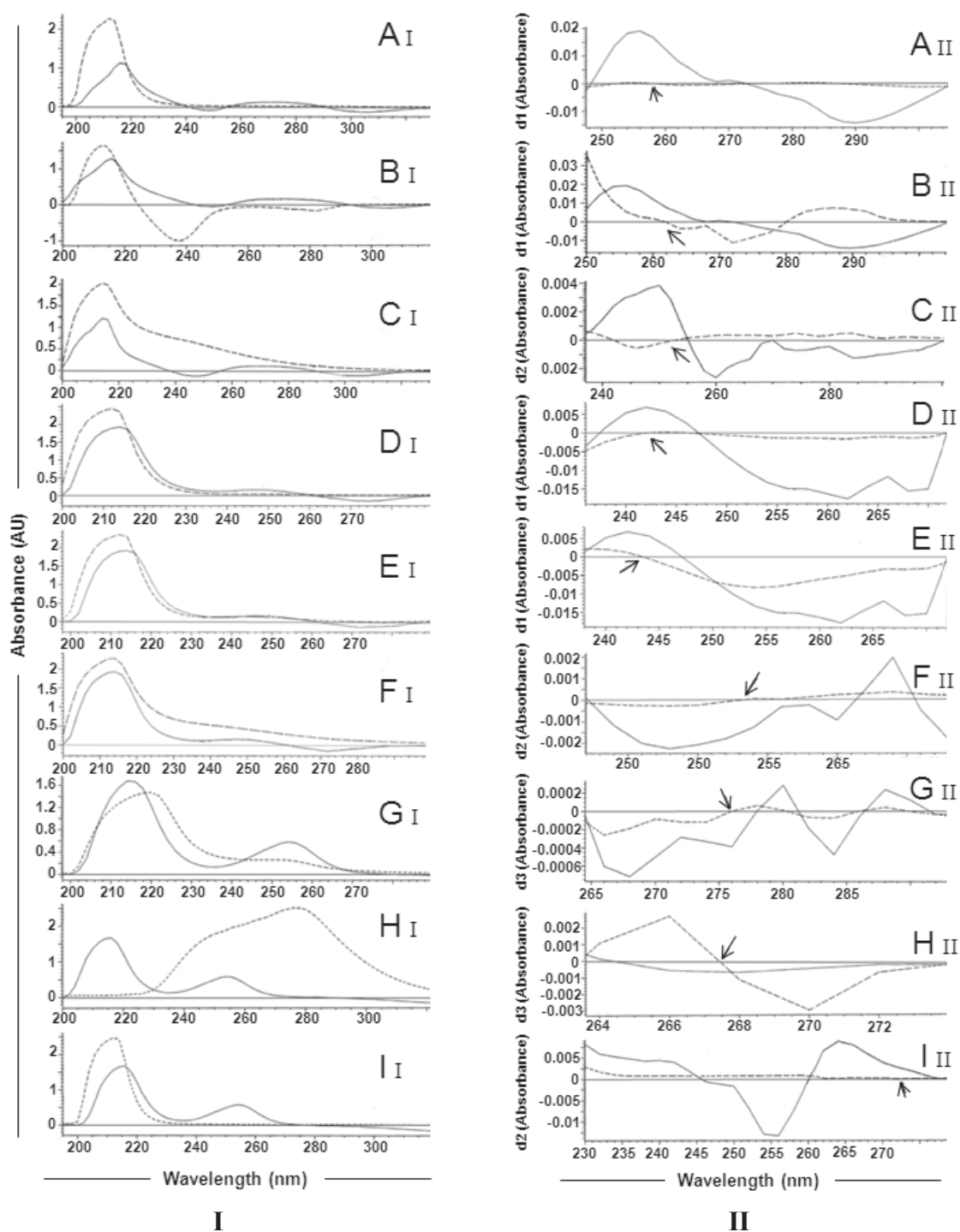ne) and its oxidative-degradate (dashed line); **I**II, second (DD^2) derivative of ΔA spectra of PGL (solid line) and its alkaline-degradate (dashed line).

3.3. *Method validation*

Validation parameters according to International Conference on Harmonization (ICH) guidelines (*28*) are summarized in Tables 1-2. In the adopted spectrophotometric methods, the limits of detection (LOD) and limits of quantitation (LOQ) were determined using the formula: LOD or LOQ = κSDa/b, where κ = 3.3 for LOD and 10 for LOQ. SDa is the standard deviation of the intercept, and b is the slope. Three different concentrations of each studied drug (in the linear range) were analyzed by the proposed

Table 1. Validation parameters for charge-transfer and ion-pair spectrophotometric methods

Validation parameters	Charge-transfer method		Ion-pair method		
	RPG; 518.00 nm	RGL; 518.00 nm	RPG; 414.00 nm	PGL; 416.00 nm	RGL; 415.00 nm
Linearity ($\mu g \cdot mL^{-1}$)	50-325	50-300	5-35	5-35	5-35
Slope	0.00273	0.00243	0.01958	0.01950	0.01957
Intercept	0.01426	0.04705	0.05515	0.05229	0.03418
Correlation coefficient (*r*)	0.9998	0.9996	0.9997	0.9998	0.9997
LOD ($\mu g \cdot mL^{-1}$)	4.22	5.96	0.49	0.47	0.56
LOQ ($\mu g \cdot mL^{-1}$)	12.80	18.06	1.50	1.42	1.76
Precision					
Intra-day Mean (%)	99.46	99.52	99.87	98.82	100.85
R.S.D. (%)	0.396	1.558	0.881	1.565	0.662
Inter-day Mean (%)	99.45	99.62	99.82	98.84	100.70
R.S.D. (%)	0.431	1.520	1.124	1.591	0.549
Ruggedne [R.S.D. (%)]	0.755	0.716	0.710	0.607	1.340
Robustness [R.S.D. (%)]	0.539	0.581	0.760	0.725	1.493

Table 2. Validation parameters for the proposed stability-indicating spectrophotometric methods. A, Validation parameters for derivative spectrophotometric method (D^n); **B**, Validation parameters for pH-induced difference spectrophotometric (DD^n) method.

Table 2A

Validation parameters	RPG			PGL			RGL		
	D^1 at 263.79 nm	D^1 at 264.33 nm	D^1 at 304.84 nm	D^1 at 253.35 nm	D^1 at 284.05 nm	D^2 at 276.31 nm	D^2 at 307.95 nm	D^2 at 287.73 nm	D^2 at 325.67 nm
Linearity ($\mu g \cdot mL^{-1}$)	5-75	5-75	5-75	5-60	5-60	5-75	5-70	5-70	5-70
Slope	0.00046	0.00043	0.00037	0.00052	0.00119	0.00021	0.00003	0.00010	0.00004
Intercept	−0.00040	−0.00056	−0.00029	−0.00121	−0.00376	0.00093	0.00005	−0.00020	−0.00012
Correlation coefficient (*r*)	0.9998	0.9998	0.9998	0.9998	0.9999	0.9997	0.9999	0.9997	0.9997
LOD ($\mu g \cdot mL^{-1}$)	0.90	0.88	0.78	0.83	0.53	0.95	0.55	1.02	0.98
LOQ ($\mu g \cdot mL^{-1}$)	2.73	2.66	2.37	2.52	1.60	2.88	1.67	3.10	2.98
Precision									
Intra-day Mean (%)	100.29	100.93	99.13	99.02	99.33	99.12	100.70	100.58	100.33
R.S.D. (%)	0.987	1.248	0.286	0.221	0.728	1.143	0.167	0.129	0.771
Inter-day Mean (%)	100.27	100.75	98.99	99.72	99.06	98.98	100.61	100.80	100.36
R.S.D. (%)	1.142	1.315	0.237	0.539	0.861	1.007	0.570	0.963	1.514
Ruggedness [R.S.D. (%)]	0.404	0.634	0.802	0.460	0.770	0.845	0.663	0.412	0.429

Table 2B

Validation parameters	RPG			PGL			RGL		
	DD^1 at 258.04 nm	DD^1 at 261.82 nm	DD^2 at 252.80 nm	DD^1 at 242.81 nm	DD^1 at 243.41 nm	DD^2 at 253.12 nm	DD^3 at 275.90 nm	DD^2 at 272.00 nm	DD^3 at 267.40 nm
Linearity ($\mu g \cdot mL^{-1}$)	5-65	5-65	5-75	5-80	5-80	5-75	5-70	5-70	5-70
Slope	0.00083	0.00038	0.00010	0.00035	0.00033	0.00007	0.00002	0.00008	0.00004
Intercept	0.00016	0.00032	0.00016	-0.00053	-0.00053	0.00008	-0.00005	0.00013	-0.00002
Correlation coefficient (*r*)	0.9997	0.9996	0.9997	0.9997	0.9997	0.9998	0.9997	0.9997	0.9997
LOD ($\mu g \cdot mL^{-1}$)	0.98	1.08	1.02	1.09	0.96	0.73	0.92	1.04	1.04
LOQ ($\mu g \cdot mL^{-1}$)	2.98	3.26	3.08	3.30	2.90	2.22	2.78	3.14	3.16
Precision									
Intra-day Mean (%)	100.63	101.30	100.30	100.02	99.53	98.94	99.79	101.51	100.65
R.S.D. (%)	0.853	0.499	1.623	0.967	0.797	0.367	0.615	0.144	0.914
Inter-day Mean (%)	100.30	101.01	100.10	98.68	99.56	98.93	100.16	101.56	100.76
R.S.D. (%)	0.841	0.723	1.636	0.163	0.849	0.364	0.880	0.281	0.950
Ruggedness [R.S.D. (%)]	0.410	0.489	0.355	0.479	0.630	0.338	0.477	0.590	0.710
Ruggedness [R.S.D. (%)]	0.435	0.316	0.250	0.457	0.642	0.355	0.413	0.434	0.556

spectrophotometric methods in three independent series on the same day (intra-day precision) and three consecutive days (inter-day precision) within each series and every concentration was examined three times. The R.S.D.% values of intra- and inter-day studies showed that the intermediate precision of the proposed methods were satisfactory (Tables 1-2). When ruggedness of the adopted spectrophotometric methods was assessed by applying the procedures using two different sources of solvents, *i.e.* methanol and acetonitrile, and results obtained were found to be reproducible since R.S.D.% did not exceed 2%. Robustness of the spectrophotometric procedures was determined by evaluating the influence of small variations of experimental variables: CLA concentration (charge-transfer method), BPB concentration and pH of phthalate buffer (ion-pair method) and HCl and NaOH concentration used in pH-induced difference spectrophotometric method; where the capacity of the method remained unaffected by small deliberate variations. The results obtained from both ruggedness and robustness provided an indication of the reliability of the proposed methods during routine work.

Solution stability was evaluated, in which the standard solutions and the reagents solutions were subjected to long term (8 days) stability studies. The stability of the solutions kept at 4°C or room temperature was studied by comparing their recoveries with freshly prepared solutions. It was found that solutions kept at 4°C were stable up to 7 days while those kept at room temperature were stable for only 3 days (data not shown).

Degradation behaviors of the studied drugs were investigated by the proposed stability-indicating spectrophotometric methods, where RPG, PGL, and RGL were determined in solutions containing different amounts of their acid-, alkaline-, and oxidative-degradates by D^n and DD^n spectrophotometric methods. The recovery% and R.S.D.% proved a high specificity of the adopted stability-indicating methods (Table 3), where the studied hypoglycemic drugs could be determined in the presence of their degradates (up to 90%).

Molar absorptivity values of the charge-transfer method for RPG and RGL with CLA were found to be 1.23×10^3 and 8.67×10^2 l·mol^{-1}·cm^{-1}, respectively, and those of the ion-pair method for RPG, PGL, and RGL with BPB were found to be 8.86×10^3, 6.95×10^3, and 7.06×10^3 l·mol^{-1}·cm^{-1}, respectively. Sandell's sensitivity (S) represents the number of micrograms of the determinant per milliliter of a solution having an absorbance (A) of 0.001 for a path length (l) of 1-cm (*29*). Thus, $S = 10^{-3}/a = \mu g \cdot cm^{-2}$ where, a is the specific absorptivity and its value (in mL·g^{-1}·cm^{-1}) corresponds to determination in a cuvette with a path length of 1-cm. Also, a = (b/molecular weight of the drug under study) $\times$ 1,000, where b = molar absorptivity = A/Cl, where C is the molar concentration of the determinant and l = 1-cm path length. Sandell's sensitivity was found to be 0.367 and 0.412 $\mu g \cdot cm^{-2}$ for the charge-transfer method of RPG and RGL with CLA, respectively, and 0.051 $\mu g \cdot cm^{-2}$ for the ion-pair method for all hypoglycemic drugs under study with BPB.

Table 3. Specificity of the proposed stability-indicating spectrophotometric methods. A, Specificity of the proposed derivative spectrophotometric (D^n) method; **B**, Specificity of the proposed pH-induced difference spectrophotometric (DD^n) method.

Table 3A

Laboratory-prepared mixture		% Recovery[b] of RPG			% Recovery[b] of PGL			% Recovery[b] of RGL		
Intact drug (μg·mL^{-1})	Degradate[a] (μg·mL^{-1})	D^1 at 263.79 nm	D^1 at 264.33 nm	D^1 at 304.84 nm	D^1 at 253.35 nm	D^1 at 284.05 nm	D^2 at 276.31 nm	D^2 at 307.95 nm	D^2 at 287.73 nm	D^2 at 325.67 nm
45.00	5.00	98.34	98.14	98.79	101.23	99.68	99.33	100.78	100.42	100.46
35.00	15.00	99.13	98.38	99.07	101.00	99.47	98.93	101.09	100.62	99.72
25.00	25.00	99.25	98.50	99.17	101.43	99.70	99.52	101.72	101.97	100.25
15.00	35.00	99.26	99.12	99.27	101.36	99.87	99.59	101.94	100.09	99.11
5.00	45.00	99.38	99.44	101.01	101.27	100.20	98.51	101.62	101.13	99.86
Mean (%)		99.07	98.71	99.46	101.26	99.78	99.18	101.43	100.84	99.88
R.S.D. (%)		0.423	0.543	0.890	0.163	0.272	0.456	0.473	0.726	0.522

Table 3B

Laboratory-prepared mixture		% Recovery[b] of RPG			% Recovery[b] of PGL			% Recovery[b] of RGL		
Intact drug (μg·mL^{-1})	Degradate[a] (μg·mL^{-1})	DD^1 at 258.04 nm	DD^1 at 261.82 nm	DD^2 at 252.80 nm	DD^1 at 242.81 nm	DD^1 at 243.41 nm	DD^2 at 253.12 nm	DD^3 at 275.90 nm	DD^2 at 272.00 nm	DD^3 at 267.40 nm
45.00	5.00	98.95	101.12	98.64	98.16	98.18	100.41	99.87	101.02	101.70
35.00	15.00	99.69	101.45	99.51	98.51	98.10	100.05	100.40	101.44	100.60
25.00	25.00	99.77	101.50	99.86	98.50	98.38	99.62	101.91	101.16	101.57
15.00	35.00	99.85	101.84	100.44	98.45	98.34	99.73	101.63	100.91	101.77
5.00	45.00	100.98	100.82	101.38	98.55	98.20	100.40	101.51	99.86	101.02
Mean (%)		99.85	101.35	99.97	98.44	98.24	100.04	101.06	100.88	101.33
R.S.D. (%)		0.730	0.384	1.027	0.162	0.119	0.365	0.871	0.598	0.499

[a] In presence of acid, alkaline and oxidative-degradates of each studied oral hypoglycemic drug, respectively.
[b] Mean of three determinations.

The accuracy of the proposed methods was demonstrated by recovery experiments, using a standard addition technique, where the percentage of R.S.D.s can be considered to be very satisfactory. The analytical results of the pharmaceutical preparations and the standard addition technique of the studied drugs by the proposed spectrophotometric methods are summarized in ¶Tables S1-S4, suggesting that there is no interference from any excipients present normally in tablets.

All the obtained results were statistically compared to the official method used for RPG analysis and the manufacturer methods used for PGL and RGL analysis, respectively. As shown in ¶Table S5, no significant differences were found.

4. Discussion

The aim of this study was to develop simple, fast, validated, and economical methods for analysis of RPG, PGL, and RGL in pure forms and in their pharmaceutical preparations. Two selective, simple, and less time consuming spectrophotometric methods were described for analyzing RPG and RGL using CLA reagents and RPG, PGL, and RGL using BPB reagents. The proposed stability-indicating methods (derivative and pH-induced difference spectrophotometry) provided accurate, specific, and reproducible quantitative analysis of the studied drugs in the presence of their acidic, alkaline, and oxidative degradation products. ICH guidelines were followed throughout the study for method validation and stress testing. The high recovery percentage and low relative standard deviation suggested high accuracy and precision of the proposed methods. Moreover, the adopted methods are easy, applicable to a wide range of concentration, besides being less time consuming, highly cost-effective and depending on simple and available reagents, thus offering economical and acceptable methods for the routine quality control analysis of drugs in bulk powder and in their pharmaceutical preparations without interference from common excipients.

References

1. Gumieniczek A, Hopkala H, Berecka A, Kowalczuk D. Normal- and reversed-phase thin-layer chromatography of seven oral antidiabetic agents. J Planar Chromatogr Mod TLC. 2003; 16:271-275.
2. Venkatesh P, Harisudhan T, Choudhury H, Mullangi R, Srinivas N. Simultaneous estimation of six anti-diabetic drugs-glibenclamide, gliclazide, glipizide, pioglitazone, repaglinide and rosiglitazone: Development of a novel HPLC method for use in the analysis of pharmaceutical formulations and its application to human plasma assay. Biomed Chromatogr. 2006; 20:1043-1048.
3. Gandhimathi M, Ravi TK, Renu SK. Determination of repaglinide in pharmaceutical formulations by HPLC with UV detection. Anal Sci. 2003; 19:1675-1677.
4. The United States Pharmacopoeia. 2005; 28:1710.
5. The British Pharmacopoeia. 2005; 1719.
6. Goyal A, Singhvi I. Visible spectrophotometric methods for estimation of repaglinide in tablet formulation. Indian J Pharm Sci. 2006; 68:656-657.
7. Jain S, Agrawal G, Jain N. Spectrophotometric determination of repaglinide in tablet dosage forms. Indian J Pharm Sci. 2005; 67:249-251.
8. Ruzilawati AB, Wahab MS, Imran A, Ismail Z, Gan SH. Method development and validation of repaglinide in human plasma by HPLC and its application in pharmacokinetic studies. J Pharm Biomed Anal. 2007; 43:1831-1835.
9. Khan R, Talegaonkar S, Singh R, Mathur S, Shiv R, Singh G. A simple HPLC method for quantitation of repaglinide in tablet dosage form. Indian Drugs. 2007; 44:428-433.
10. El-Ries MA, Mohamed GG, Attia AK. Electrochemical determination of the antidiabetic drug repaglinide. Yakugaku Zasshi. 2008; 128:171-177.
11. Radhakrishna T, Sreenivas Rao D, Om Reddy G. Determination of pioglitazone hydrochloride in bulk and pharmaceutical formulations by HPLC and MEKC methods. J Pharm Biomed Anal. 2002; 29:593-607.
12. Yamashita K, Murakami H, Okuda T, Motohashi M. High performance liquid chromatographic determination of pioglitazone and its metabolites in human serum and urine. J Chromatogr B Biomed Appl. 1996; 677:141-146.
13. Zhong WZ, Lakings DB. Determination of pioglitazone in dog serum using solid-phase extraction and high-performance liquid chromatography with ultraviolet (229 nm) detection. J Chromatogr. 1989; 490:377-385.
14. Gumieniczek A, Hopkala H, Berecka A. Reversed-phase thin-layer chromatography of three new oral antidiabetics and densitometric determination of pioglitazone. J Liq Chromatogr Relat Technol. 2004; 27:2057-2070.
15. Sane RT, Menon SN, Inamdar S, Mote M, Menezes A. Simultaneous determination of pioglitazone and glimepiride by high-performance thin-layer chromatography. J Planar Chromatogr Mod TLC. 2004; 17:154-156.
16. Lin ZJ, Ji W, Desai-Krieger D, Shum L. Simultaneous determination of pioglitazone and its two active metabolites in human plasma by LC-MS/MS. J Pharm Biomed Anal. 2003; 33:101-108.
17. Sankar D, Kumar J, Reddy M. Extractive spectrophotometric determination of Pioglitazone hydrochloride using both acidic and basic dyes. Asian J Chem. 2004; 16:251-254.
18. Mamidi RN, Benjamin B, Ramesh M, Srinivas NR. Simple method for the determination of rosiglitazone in human plasma using a commercially available internal standard. Biomed Chromatogr. 2003; 17:417-420.
19. Radhakrishna T, Satyanarayana J, Satyanarayana A. LC determination of rosiglitazone in bulk and pharmaceutical formulation. J Pharm Biomed Anal. 2002; 29:873-880.
20. Gomes P, Sippel J, Jablonski A, Steppe M. Determination of rosiglitazone in coated tablets by MEKC and HPLC methods. J Pharm Biomed Anal. 2004; 36:909-913.
21. Kim KA, Park JY. Simple and extractionless high-performance liquid chromatographic determination of rosiglitazone in human plasma and application to pharmacokinetics in humans. Biomed Chromatogr. 2004; 18:613-615.

22. Sane RT, Francis M, Moghe A, Khedkar S, Anerao A. High-performance thin-layer chromatographic determination of rosiglitazone in its dosage form. J Planar Chromatogr Mod TLC. 2005; 15:192-194

23. Gumeiniczek A, Berecka A, Hopkala H, Mroczek T. Rapid HPTLC determination of rosiglitazone in pharmaceutical formulations. J Liq Chromatogr Relat Technol. 2003; 26:3307-3314.

24. Ho EN, Yiu KC, Wan TS, Stewart BD, Watkins KL. Detection of anti-diabetics in equine plasma and urine by liquid chromatography-tandem mass spectrometry. J Chromatogr B Analyt Technol Biomed Life Sci. 2004; 811:65-73.

25. Gouda AA, Shafey ZE, Hossny N, El-Azzazy R. Spectrophotometric determination of hyoscine butylbromide and famciclovir in pure form and in pharmaceutical formulations. Spectrochim Acta A Mol Biomol Spectrosc. 2008; 70:785-792.

26. Vogel's, Textbook of Practical Organic Chemistry. 5th ed., Longman Group UK Ltd., UK, 1989; pp. 1442-1444.

27. Yoe, J, Jones A. Ind. Eng. Chem., Prod. Res. Dev., Anal. Ed., 1944; 16: p. 111.

28. International Conference on Harmonization (ICH) Topic Q1A(R2) Stability Testing of new Drug Substances and Products. 2003. Available from: *http://www.ich.org/cache/ compo/363-272-1.html#Q1A(R2)*

29. Onal A. Spectrophotometric and HPLC determinations of anti-diabetic drugs, rosiglitazone maleate and metformin hydrochloride, in pure form and in pharmaceutical preparations. Eur J Med Chem. 2009; 44:4998-5005.

Matrix type transdermal therapeutic systems of glibenclamide: Formulation, *ex vivo* and *in vivo* characterization

Asgar Ali[1], Anupam Trehan[1], Zabih Ullah[2], Mohammed Aqil[1,*], Yasmin Sultana[1]

[1] *Department of Pharmaceutics, Faculty of Pharmacy, Hamdard University, New Delhi, India;*
[2] *Department of Pharmaceutical Medicine, Faculty of Pharmacy, Hamdard University, New Delhi, India.*

ABSTRACT: Matrix type transdermal therapeutic systems (TTS) of glibenclamide were formulated using polymers Eudragit RL 100, ethyl cellulose, PVP K-30, and polyvinyl acetate, and citral was used as the penetration enhancer. The polymer films were formulated with Eudragit RL 100 and PVP K-30 in different ratios and subsequently subjected to *ex vivo* studies (drug permeation through rat skin) followed by interaction studies, skin irritation studies, accelerated stability analysis, and *in vivo* studies (determination of blood glucose level in rabbits). The drug content of the formulations was found to be 99.1-99.2%. The cumulative percentages of drug permeated through rat skin from the three selected formulations in 48 h were 95.3%, 98.8%, and 99%, respectively. A plot between cumulative percent of drug permeated and square root of time exhibited linear curves, which suggests the Higuchian matrix mechanism of drug release. The formulation containing Eudragit RL 100 and PVP K-30 showed better improvement in hypoglycemic activity in rabbits (56.2-60.8% reduction in blood glucose level, *p* < 0.05). There were fewer fluctuations in blood glucose level as compared to oral therapy due to controlled release of the active pharmaceutical ingredient, and no interaction was found between the drug and excipients of the formulation. Accelerated stability analysis showed that the formulation was stable up to 5.5 years, with negligible skin irritation. The formulation precluded severe hypoglycemic reactions (side effect of sulfonylureas) and was effective for management of diabetes mellitus up to 48 h, with a single TTS.

Keywords: Matrix type transdermal therapeutic system, glibenclamide

*Address correspondence to:
Dr. Mohammed Aqil, Department of Pharmaceutics, Faculty of Pharmacy, Hamdard University, New Delhi 110062, India.
e-mail: aqilmalik@yahoo.com

1. Introduction

Diabetes mellitus is a metabolic disorder characterized by high blood glucose level (fasting plasma glucose > 7.0 mM, or plasma glucose > 11.1 mM 2 h after meal) (*1*). In total diabetic patients more than 90% suffer from type 2 diabetes (*2*). Globally, the burden of type 2 diabetes is rising fast. The global prevalence of diabetes among adults was estimated at 150 million in 1995, and this is projected to rise up to 300 million by 2025 (*3*). Developing countries may experience the largest proportional increase in diabetes (*4*). Type 2 diabetes is caused by insulin deficiency in the body due to partial or incomplete inactivation/destruction of β cells of pancreas and often associated with insulin resistance (*5,6*). The blood glucose rises because of impaired hepatic glucose output and reduced uptake of glucose by skeletal muscles. When the renal threshold for glucose reabsorption increases, it leads to glycosurea (glucose in urine) and osmotic diuresis which leads to dehydration, thirst, and increased drinking (*7*). The treatment of type 2 diabetes includes life style changes, drugs that reduce intestinal glucose uptake and hepatic gluconeogenesis, and drugs that increase insulin secretion from the pancreas (*e.g.* sulfonylurea) (*8*).

Glibenclamide, a sulfonylurea, has short term and long term pharmacological actions. During short term treatment it increases insulin secretion from functioning pancreatic islet β cells (pancreatic effect) where as during long term treatment its main action appears to be enhancement of insulin action on peripheral tissues and reduction of glucose output from the liver (extra-pancreatic effect). In short term treatment glibenclamide causes degranulation of the β cells in pancreas (*9*). The evoked release of insulin from the pancreas is very rapid and sulfonylureas appear to stimulate calcium influx into islet cells (*10,11*), as glibenclamide is a hydrophobic/lipophilic molecule and acts on sulfonylurea receptors from within the hydrophobic phase of the cell membrane (*12*). The treatment of non-insulin dependent diabetes mellitus (NIDDM) with glibenclamide is associated with severe and some fatal hypoglycemic reactions (*13,14*) with

symptoms like cold sweats, cool pale skin, tremors, anxious feelings, unusual tiredness or weakness, confusion, difficulty in concentration, excessive hunger, temporary vision changes, headache or nausea (*1*). These side effects occur because of high interindividual variation with glibenclamide therapy. These incidences are related to the potency and duration of action of the active agent, and these incidences mostly occur with chlorpropamide and glibenclamide, so glibenclamide is avoided in the elderly and in patients with renal failure because of the risk of hypoglycemia (*6*). Whereas when glibenclamide is administered through a transdermal therapeutic system (TTS), it provides controlled release of the active pharmaceutical ingredient (API), and thus minimizes plasma fluctuation of the drug, reduces the intensity of action and thus reduces the side effect (hypoglycemia) associated with its oral therapy (*12,13*). Patient compliance is also increased because antidiabetic drugs have to be taken for a long period (*15*). The various properties of glibenclamide are very suitable for a TTS, *i.e.*, molecular weight 494 Da (*16*), variable biological half life 0.1-10 h, an effective plasma concentration 30-50 µg/L (*17*), and a reasonable partition coefficient (octanol/water) 4.23 (*18*). Thus transdermal formulation provides many advantages over its oral counterpart, including reduced side effects, easy termination of medication when necessary, improved patient compliance, elimination of first pass metabolism, and controlled drug delivery (*19*). The skin permeation profile of glibenclamide has been previously reported, which suggests that it significantly permeates rat skin and reduces blood glucose level (*20*).

In the present study, we have formulated the matrix type of TTS for glibenclamide delivery; a matrix type system was taken into consideration because of the high dose of the drug. The matrix type system was prepared using the polymer combination of Eudragit® RL 100, PVP K-30, and polyvinyl acetate. PEG-400 was used as plasticizer and citral as a penetration enhancer. The TTS was subjected to *ex vivo* skin permeation studies through rat skin, and *in vivo* studies in rabbit models. The formulation was also tested for drug excipients interaction studies, skin irritation studies, and accelerated stability analysis to determine the shelf life of the formulation.

2. Materials and Methods

2.1. *Materials*

Glibenclamide I.P. was purchased from Hoechst Marion Roussel Ltd., Mumbai, India. Eudragit RL100 and PVP K-30 were from Pharmax India, Mumbai, India. Ethyl cellulose was from Loba Cheme, Mumbai, India. Polyvinyl acetate was from Ranbaxy Laboratories, Gurgaon, India. Eudragit RS PO was obtained from Crossland India Mumbai, India. Eudragit RL 30D was

from Rohm Pharma, Darmstadt, Germany. PEG-400 and oleic acid were from CDH, Mumbai, India. All other ingredients were obtained from E. Merck (India) Ltd. (Mumbai, India) and S. D. Fine Chemicals (Mumbai, India) and were of analytical grade.

2.2. *Preparation of polymer films*

Transdermal films were cast on an aluminum surface, and the aluminum pockets were made using two glass rings such that the external diameter of one is equal to the internal diameter of other ring. Aluminium foil was placed between these rings and the internal ring was pressed and then taken out to form a pocket. The internal diameter of the aluminium pocket was 6.4 cm and its depth was 5 mm. The formed aluminium pocket was placed on a Petri dish which was placed in an oven on a flat surface parallel to the horizon. The polymer, plasticizer, drug, and penetration enhancer were accurately weighed and dissolved in different proportions of solvent systems using a magnetic stirrer (Table 1). The resulting solution was poured carefully into the aluminium pocket. The solvent was allowed to evaporate undisturbed in an oven at an elevated temperature (55 ± 5°C) condition. An inverted funnel was placed over the Petri dish to prevent rapid evaporation of the solvent. The film dried up in approximately 2-3 h. A backing film was applied on one side of the film and a release liner on the other side. The resulting films were evaluated for physicochemical properties *viz.*, thickness, weight, folding endurance, and percent elongation at break.

2.3. *Ex vivo skin permeation studies*

For *ex vivo* skin permeation studies, a vertical diffusion cell was used consisting of donor and receiver compartment. The capacity of the receiver cell was 50 mL. The full thickness abdomen skin of an albino rat was taken and treated with depilatory to remove hair and after that the fat were removed with the help of isopropyl alcohol, and the skin was mounted between two compartments with the stratum corneum facing

Table 1. Formulas for optimized TTS formulations of glibenclamide

Ingredients	Formulation code with quantities		
	A	B	C
Eudragit RL 100 (mg)	600	400	900
PVP K-30 (mg)	400	600	–
Polyvinyl acetate (mg)	–	–	100
Glibenclamide (mg)	47.7	47.7	47.7
PEG-400 (%, w/w)	5	5	10
Citral (mL)	5	5	5
Dichloromethane (mL)	5	5	5
Ethanol (mL)	3	3	3

towards the donor compartment whereas the dermis faced the receiver compartment. The donor cell was kept empty while the receptor compartment was filled with 30% (v/v) isopropanolol in isotonic phosphate buffer, pH 7.4 (IPH). The receiver fluid was stirred with a magnetic stirrer at a speed of 500 rpm and the assembled apparatus was placed in a hot air oven preset at 37 ± 2°C. The buffer solution was replaced every 30 min to stabilize the skin (*21*). After applying the transdermal formulation, the samples were withdrawn from the receiver compartment at different time intervals up to 48 h, and an equal volume of permeation medium was added to the receptor compartment to maintain the sink condition. The withdrawn samples were analyzed for drug content.

2.4. *In vivo studies*

Optimized formulations which yielded satisfactory *in vitro* drug release and skin permeation results were subjected to *in vivo* studies. Initial blood glucose values of all rabbits were determined and the TTS was then placed on the back of the rabbit, which was previously cleared of hair with scissors and depilatory, within an area sufficient for application of the transdermal patch (*22*). Blood glucose was estimated at 0, 2, 4, 6, 8, 12, 24, 28, 32, 36, 48, 52, 56, 60, and 72 h.

For these studies, healthy male albino rabbits weighing between 1.5-2 kg were used for better assessment of blood glucose. Rabbits were selected as test animals because the permeability of rabbit skin matches to a great extent that of human skin (*23*). The blood glucose determinations were carried out in 18 normoglycemic rabbits in 3 groups of 6 each for transdermal therapeutic formulations (A, B and C). For the collection of blood, the hair from the area around the marginal ear vein was cut short with scissors to make the vein clear. After applying xylene, a No. 26 disposable needle was used and a prick was given to the marginal ear vein. After discarding the first drop, 20 μL of blood was taken directly into a 20 μL micropipette and put into tubes containing tetrachloric acid, and further analyzed for glucose estimation by the glucose oxidase-peroxidase method (*24*). The method involved the use of 4-aminophenazone as a color coupler with sulphonated 2,4-dichlorophenol for determination of hydrogen peroxide produced from glucose with glucose oxidase. The sensitivity of the method was such that 20 μg of glucose in a final volume of 4 mL gave an optical density of 0.61 at 515 nm with 10-mm cells, which corresponds to a molecular absorption of 22,000.

2.5. *Analysis of glibenclamide in TTS*

The transdermal film was dissolved in a small volume of isopropanol to produce 10 mL of solution A and filtered through Whatman filter paper No. 42. Then 1

mL of solution A was diluted to 10 mL with isopropanol to give solution B. One mL of the solution B was further diluted with isopropanol to produce solution C and it was analyzed at 238 nm using isopropanol as blank. Solution C had a dilution factor of 100. The concentration (μg/mL) of drug was read from the standard curve of the drug in isopropanol. The content of drug (in mg) was calculated as follows:

$$\text{Drug content (mg)} = \frac{\text{Concentration (μg/mL)} \times \text{Dilution factor}}{1000}$$

2.6. *Interaction studies*

Interaction between the excipients and drug were analyzed by ultraviolet (UV) scanning, drug assay, Fourier transform infrared (FT-IR) spectral analysis, and thin layer chromatography (TLC). The transdermal formulation was dissolved in isopropanol, the solution was filtered and scanned for UV absorption between 200-400 nm. The transdermal formulation was assayed using the assay method reported in analytical methodology and the drug content was calculated to estimate the percentage recovery of the loaded drug (*25*). FT-IR (Perkin Elmer, Rodgau, Germany) spectra of the dried medicated films were taken in the range of 400-4,000 cm^{-1}. TLC analysis was conducted using a silica gel GF$_{250}$ plate with chloroform/cyclohexane/ethanol/glacial acetic acid (45:45:5:5, v/v) as a mobile phase and a UV chamber for visualization (*26*).

2.7. *Skin irritation studies*

The possibility of skin irritation arising from the application of the transdermal patches was assessed using a modified score test in rabbits by Draize *et al.* and Aqil *et al.* (*27,28*). The intact and abraded skin of rabbits were used for this purpose. The patches were placed on four areas, 10 cm apart (two intact and two abraded) on the back of the rabbit. The patches were placed on the rabbit with the help of adhesive to prevent patch removal due to animal movement. The rabbit was placed in an animal holder ensuring minimal movement during the 24 h patch exposure. Upon removal of the patches, the resulting reactions were also recorded after 72 h and the final skin irritation score represents an average of the 24 and 72 h reading. The score for erythma and edema formation (none = 0, very slight = 1, well defined = 2, moderate = 3, severe = 4) were estimated by visual inspection. The exercise was repeated three times for each formulation.

2.8. *Accelerated stability analysis*

Formulation C which produced satisfactory *ex vivo* and *in vivo* results was used for accelerated stability

studies (*29*). Sufficient replicates of formulation C were prepared, packed in aluminium foil and stored in petridis at different temperatures of 40 ± 0.5°C, 50 ± 0.5°C, and 60 ± 0.5°C for 60 days. Three samples were withdrawn at intervals of 20, 40, and 60 days and analyzed for drug content by the assay method reported previously (*29*). The logarithms of percent drug remaining were plotted against time in days. The graph was plotted between percent drug remaining and time in days. This gave straight lines suggesting that the drug degradation followed first order kinetics. The degradation rate constant was calculated using the following formula.

$$slope = \frac{-K}{2.303}$$

where K is the degradation rate constant. K_{25} value was determined by Arrhenius plot and the shelf life was calculated by substituting the value of K_{25} in the following equation.

$$t_{0.9} = \frac{0.1054}{K_{25}}$$

2.9. *Statistical analysis*

Statistical analysis of the experimental data was performed by applying student's *t*-tests using GraphPad InStat 3.0 software (GraphPad Software, La Jolla, CA, USA). A *p* value of < 0.05 was considered significant.

3. Results

3.1. *Physicochemical parameters of polymer films*

The prepared polymeric films had an internal diameter of 2.93 cm and surface area of 6.74 cm^2. Physicochemical properties of the films were as follows: thickness was 250 ± 5, 256 ± 5, and 243 ± 5 μm for formulation A, B, and C respectively; weight was 247 ± 3, 242 ± 3, 221 ± 3 mg for formulations A-C, respectively; folding endurance was 268 ± 6, 163 ± 2, 208 ± 6 for formulations A-C, respectively; and percent elongation at break was 79 ± 2, 69 ± 1, 84 ± 2% for formulations A-C, respectively (data not shown).

3.2. *Ex vivo skin permeation studies*

The *ex vivo* skin permeation profile of glibenclamide TTS is shown in Figure 1. The cumulative percentages of drug permeated through rat skin from the three formulations in 48 h were 95.3, 98.8, and 99% for formulations A-C, respectively. After an initial lag period, permeation was observed to be gradually approaching a constant for the rest of the time, thus illustrating the controlled release behavior of these

systems. In the graph between cumulative percent drug permeated *vs.* square root of time almost linear curves were obtained for all three optimized formulations A-C. This suggests that the formulation follows the Higuchian matrix mechanism of drug release (*11*). The result of kinetic analysis of *ex vivo* data showed a significantly lower coefficient of variation in the case of zero order *vs.* first order permeation kinetics except in formulation B in which the difference was not significant. Therefore, it is concluded that the permeation of the drug from the TTS followed zero order kinetics.

3.3. *In vivo studies*

Normoglycemic rabbits were used instead of hyperglycemic as hyperglycemia is induced by injecting streptozotocin which causes death in a large number of cases (*30*), however, in normoglycemic subjects, a dose dependent fall in blood glucose level was seen on transdermal administration of glibenclamide (*9*). As shown in Figure 2, a sufficiently high reduction in blood glucose level was obtained within 2 h for all formulations. The reduced level remained almost constant with a slight rise in blood glucose level on administration of food (Figure 2). These observations corroborated the *ex vivo* release pattern of the drug.

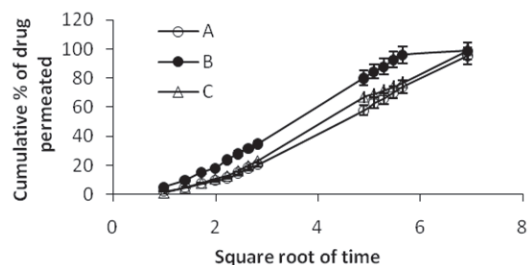**Figure 1. Cumulative percent of glibenclamide permeated in *ex vivo* study through rat skin from matrix type TTS. A**, Eudragit RL 100 (600 mg) + PVP K-30 (400 mg); **B**, Eudragit RL 100 (400 mg) + PVP K-30 (600 mg); **C**, Eudragit RL 100 (900 mg) + polyvinyl acetate (100 mg). Data are the mean ± S.D. (*n* = 3).
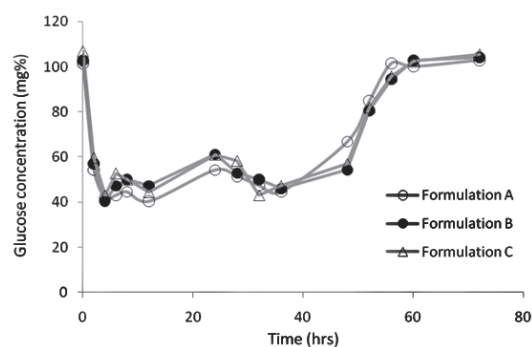

Figure 2. Effect of formulation A, B and C on blood glucose level of albino rabbits.

Normal glucose levels were restored in approximately 8 h after the removal of the transdermal system. There was insignificant variation ($p > 0.05$) in the blood glucose level when the placebo formulations were applied on the skin of albino rabbits, *vis-à-vis* the baseline values of normoglycemic rabbits (data not shown). Only slight variation on administration of food was observed.

3.4. *Interaction studies*

In the interaction studies, the UV spectra revealed that the transdermal formulation and pure drug (API) solution exhibited the same absorption maxima at 246 nm (data not shown), but there was a slight deviation in the absorption pattern of formulations due to the combined effect of API and excipients. The assay of drug from TTS (percentage recovery) was found to be in the range of 99.1 to 99.2% (data not shown). Formulation C was selected for FT-IR spectral analysis and it showed an identical spectral pattern compared to that of pure drug, although it showed a less intense peak to that of API (Figure 3). A few peaks were merged in the spectrum of the formulation and this might be due
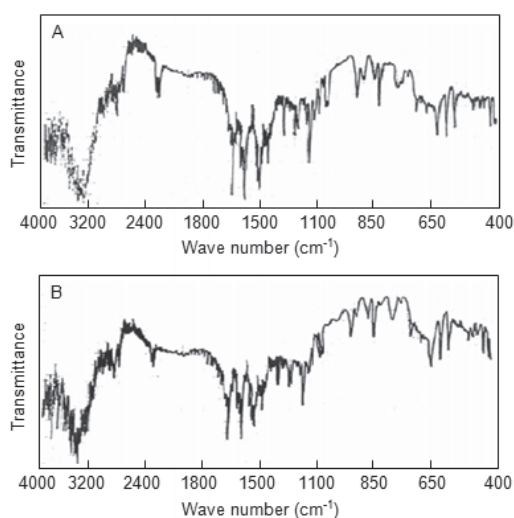

Figure 3. FT-IR spectra of pure drug (A) and formulation C (B).

to physical but not chemical interaction between the drug and polymer. In TLC studies, almost the same R_f values and single spots were observed for the API and the drug in formulation (data not shown). From the results of all these interaction studies, it can be inferred that the glibenclamide remained intact in the TTS and no chemical interaction seemed to occur between API and the excipients therein.

3.5. *Skin irritation studies*

On performing the visual score test (*27,28*), the combined average for intact and abraded rabbit skin irritation score for the test formulations was found to be less than one (Table 2). The compound producing a score of 2 or less at 24 h was considered negative for irritation. Since the test formulation fulfilled the above condition, it was concluded that the TTS was devoid of skin irritation potential and could be well tolerated during the course of treatment.

3.6. *Accelerated stability analysis*

The formulation was subjected to accelerated stability analysis. On the basis of first order degradation kinetics the shelf life ($t_{0.9}$) was calculated to be 5.5 years (data not shown), which predicts very high stability of the drug in the TTS. The result conformed to the extremely high stability of the API with only 1% degradation in 3 years (data not shown). Various physical characteristics, thickness, weight, folding endurance, and percent elongation at break varied to negligible proportions and drug content declined insignificantly in 12 weeks (data not shown).

4. Discussion

Glibenclamide is a potent hypoglycemic drug indicated in the management of NIDDM**.** However, the drug shows an erratic absorption pattern due to interpatient and formulation factors resulting in variable oral biological half life. Also the erratic absorption of the

Table 2. Skin irritation data of formulation A, B and C

Formulations	Intact skin (i)			Abraded skin (ii)			Combined average (i + ii)
	24 h	72 h	Average	24 h	72 h	Average	
A	1	0	0.33	2	1	0.67	0.50
	0	0		0	0		
	1	0		1	0		
B	1	1	0.33	1	1	0.83	0.58
	0	0		1	0		
	0	0		1	1		
C	1	0	0.50	2	0	0.83	0.66
	1	1		1	1		
	0	0		1	0		

Criteria of scores for visual observation were as follows. Erythma scale: none, 0; very slight, 1; well defined, 2; moderate, 3; severe, 4. Edema scale: none, 0; very slight, 1; well defined, 2; moderate, 3; severe, 4.

drug leads to its major side effect, *i.e.*, hypoglycemia which is an extension of the pharmacological response (*31*). Also there is no controlled release formulation of the drug available in the market. These factors prompted us to develop Glibenclamide TTS to provide for the controlled and sustained release of the drug for a period of 48 h. The drug sample (API) was characterized on the basis of physicochemical and spectral analysis; the result confirmed it to be the pure sample of glibenclamide (*32*).

Since the amount of drug to be incorporated in the system was higher, monolithic matrix type TTS were fabricated by a film casting technique on an aluminum surface (*33*). Methyl alcohol/dichloromethane (3:5, v/v) was found to be an ideal solvent system for film formation (*34*). An elevated temperature condition was selected for solvent evaporation as the time required was reduced and complete removal of solvent was achieved. The polymer selected were non adhesive, therefore, a micro porous tape which forms an adhesive rim which could be stuck onto the skin was used. The Eudragit polymer based placebo films which yielded satisfactory results on physical characterization (thickness, weight, folding endurance, and % elongation at break) were selected for incorporation of the drug and the penetration enhancer.

Due to a moderate skin permeation rate of glibenclamide by passive diffusion (*32*), different chemical methods of permeation enhancement were used with various penetration enhancers such as dimethyl sulfoxide, propylene glycol, *N,N*-dimethylformamide, citral, and oleic acid. In the preliminary study, Tween 20 and turpentine oil were tried (data not shown). It was found that citral was the most effective enhancer for glibenclamide yielding 5.0-fold enhancements in permeability coefficients over controls. In conclusion, 5% citral was selected as enhancer for incorporation in medicated patches.

An apparatus similar to Keshary-Chein's diffusion cell (*35*) was fabricated for the evaluation of *ex vivo* skin permeation of the drug from the formulations. Formulations containing Eudragit RL polymer exhibited satisfactory results. These formulations were modified in quest of improved performance. The modified patches were coded as A, B and C containing Eudragit RL100/ PVP K-30 (6:4), Eudragit RL100/PVP K-30 (4:6), and Eudragit RL100/PVP K-30 (8:2), respectively. The formulation containing the maximum ratio of RL100 and minimum ratio of PVP K-30 shows the maximum permeation (99%) of the drug, it suggests that the release pattern of drug from formulation "C" is more favorable. Whereas formulation A containing polymer ratio 6:4 showed poor permeability (95.3%) in comparison to formulation C (Figure 1). After an initial lag period permeation was observed to be gradually approaching a constant for the rest of the time, which exhibited the controlled release behavior of these systems.

The plots of cumulative percentage drug permeated (Q) *vs*. square root of time showed an almost linear curve for the three optimized formulations which endorsed the Higuchi matrix diffusion mechanism of drug release for these formulations.

The *in vivo* studies on selected transdermal formulation (A, B and C) containing 0.46 mg/kg of drug were carried out by determining the reduction in blood glucose level of albino rabbits. Sufficiently high reduction in blood glucose level ($p < 0.05$) was obtained within 2 h for all formulations. The reduced levels were maintained almost constant with a slight rise in blood glucose level on administration of food. Normal glucose levels were restored in approximately 8 h, after the removal of the transdermal system. There was no reduction in blood glucose level when the placebo formulations were applied on the skin of albino rabbits ($p > 0.05$). Only slight variation in glucose level was observed on administration of food.

The result of the interaction studies indicates that the drug remained intact in the formulation and there was no chemical interaction between the drug and excipient therein. The fabricated system produced no or very mild skin irritation, which could be well tolerated during the course of therapy. The accelerated stability studies at elevated temperature and humidity (*29*) revealed that the developed TTS held promise for high stability ($t_{0.9} = 5.5$ years) and satisfactory performance if stored at optimum temperature and humidity conditions.

5. Conclusion

On the basis of above *ex vivo* and *in vivo* evaluations, it could be concluded that glibenclamide, a potent hypoglycemic drug, could be administered successfully from the matrix type monolithic TTS for controlled and sustained management of NIDDM for a period of 48 h. The systems were free of any hazardous skin irritation. Further work needs to be done to establish the therapeutic utility of these systems through long term pharmacokinetic and pharmacodynamic studies on healthy human subjects and patients.

Acknowledgement

References

1. Davis SN, Granner DK. Insulin, oral hypoglycemic agents, and the pharmacology of the endocrine pancreas. In: Goodman & Gilman's the Pharmacological Basis of Therapeutics (Hardman JG, Limbird LE, Molinoff PB, *et al.*, eds.). 9th ed., McGraw-Hill, New York, NY, USA, 1996; pp. 1487-1517.
2. Adeghate E, Schattner P, Dunn E. An update on the

etiology and epidemiology of diabetes mellitus. Ann N Y Acad Sci. 2006; 1084:1-29.

3. Cooper RS, Rotimi CN, Kaufman JS, Owoaje EE, Fraser H, Forrester T, Wilks R, Riste LK, Cruickshank JK. Prevalence of NIDDM among populations of the African diaspora. Diabetes Care. 1997; 20:343-348.

4. Olatunbosun ST, Ojo PO, Fineberg NS, Bella AF. Prevalence of diabetes mellitus and impaired glucose tolerance in a group of urban adults in Nigeria. J Natl Med Assoc. 1998; 90:293-301.

5. Nolte MS, Karam JH. Pancreatic hormone and antidiabetic drugs. In: Basic and Clinical Pharmacology, Lang Medical Books (Katzung BG, ed.). 8th ed., McGraw-Hills Publishing Division, New York, NY, USA, 2001; pp. 711-734.

6. Rang HP, Dale MM, Ritter JM, Moore PK. Pharmacology. 5th ed., Churchill-Livingstone, New York, NY, USA, 2003; pp. 385-392.

7. Nolte MS, Karam JH. Pancreatic harmone and antidiabetic drugs. In: Basic and Clinical Pharmacology, Lang Medical Books (Katzung BG, ed.). 9th ed., McGraw-Hills Publishing Division, New York, NY, USA, 2001; pp. 693-715.

8. American Diabetes Association. Standards of medical care in diabetes – 2007. Diabetes Care. 2007; 30 (Suppl 1):S4-S41.

9. Beck-Nielsen H, Hother-Nielsen O, Pedersen O. Mechanism of action of sulphonylureas with special reference to the extrapancreatic effect: An overview. Diabet Med. 1988; 5:613-620.

10. Dollery C. Therapeutic Drugs. Churchil Livingstone, New York, NY, USA, 1991; Vol. II: G21-G26.

11. Weston AH, Bray KM, Duty S. Glibenclamide: A review. Drugs. 1971; 1:116-140.

12. Barrett-Jolley R, Davies NW. Kinetic analysis of the inhibitory effect of glibenclamide on KATP channels of mammalian skeletal muscle. J Membr Biol. 1997; 155:257-262.

13. Gorus FK, Schuit FC, In't Veld PA, Gepts W, Pipeleers DG. Interaction of sulfonyl ureas with pancreatic beta-cells. A study with gliburide. Diabetes. 1988; 37:1090-1095.

14. Ikegami H, Shima K, Tanaka A, Tahara Y, Hirota M, Kumahara Y. Interindividual variation in the absorption of glibenclamide in man. Acta Endocrinol (Copenh). 1986; 111:528-532.

15. Takahshi Y, Furuya K, Iwata M, Onishi H, Machida Y, Shirotake S. Trial for transdermal administration of sulfonylureas. Yakugaku Zasshi. 1997; 117:1022-1027. (in Japanese)

16. British Pharmacopoeia. Glibenclamide. H.M.S.O., London, UK, 1988; p. 269.

17. Coppack SW, Lant AF, McIntosh CS, Rodgers AV. Pharmacokinetic and pharmacodynamic studies of glibenclamide in non-insulin dependent diabetes mellitus. Br J Clin Pharmacol. 1990; 29:673-684.

18. Siluk D, Kaliszan R, Haber P, Petrusewicz J, Brzozowski Z, Sut G. Antiaggregatory activity of hypoglycaemic sulphonylureas. Diabetologia. 2002; 45:1034-1037.

19. Kanikkannan N, Andega S, Burton S, Babu RJ, Singh M. Formulation and *in vitro* evaluation of transdermal patches of melatonin. Drug Dev Ind Pharm. 2004; 30:205-212.

20. Yamamoto T, Katakabe K, Akiyoshi K, Kan K, Asano T, Okumura M. Topical application of the hypoglycemic agent glibenclamide and changes in blood glucose, plasma insulin (IRI) levels and plasma concentration of glibenclamide in normal rats. Diabetes Res Clin Pract. 1990; 8:19-22.

21. Jaiswal J, Poduri R, Panchagnula R. Transdermal delivery of naloxone: *Ex vivo* permeation studies. Int J Pharm. 1999; 179:129-134.

22. Rao PR, Reddy MN, Ramakrishna S, Diwan PV. Comparative *in vivo* evaluation of propranolol hydrochloride after oral and transdermal administration in rabbits. Eur J Pharm Biopharm. 2003; 56:81-85.

23. Nicoli S, Cappellazzi M, Colombo P, Santi P. Characterization of the permselective properties of rabbit skin during transdermal iontophoresis. J Pharm Sci. 2003; 92:1482-1488.

24. Barham D, Trinder P. An improved colour reaction for the determination of blood glucose by the oxidase system. Analyst. 1972; 42:142-144.

25. Aqil M, Ali A. Monolithic matrix type transdermal drug delivery systems of pinacidil monohydrate: *In vitro* characterisation. Eur J Pharm Biopharm. 2002; 54:161-164.

26. Bandisode MS, Boshell BR. Clinical experience with glibenclamide in long-term treatment of diabetes mellitus. Curr Ther Res Clin Exp. 1976; 19:237-241.

27. Aqil M, Ali A, Sultana Y, Parvez N. Matrix type transdermal drug delivery system of metoprolol tartrate, skin toxicity and *in vivo* characterization. Eth Pharm J. 2004; 22:50-55.

28. Draize JH, Woodard G, Calvery HO. Methods for the study of irritation and toxicology of substances applied topically to the skin and mucous membrane. J Pharmacol Exp Ther. 1944; 82:377-390.

29. Carstensen JT. Drug Stability: Principle and Practices. 3rd ed., Marcel Dekker Inc., New York, NY, USA, 1990; 43:19-55.

30. Rerup CC. Drug producing diabetes through damage of the insulin secreting cells. Pharmacol Rev. 1970; 22:485-518.

31. Hoffman A, Fischer Y, Gilhar D, Raz I. The effect of hyperglycaemia on the absorption of glibenclamide in patients with non-insulin-dependent diabetes mellitus. Eur J Clin Pharmacol. 1994; 47:53-55.

32. Mutalik S, Udupa N. Formulation development, *in vitro* and *in vivo* evaluation of membrane controlled transdermal systems of glibenclamide. J Pharm Pharm Sci. 2005; 8:26-38.

33. Kandavilli S, Nair V, Panchagnula R. Polymers in transdermal drug delivery systems. Pharmaceutical Technology. 2002; 62-80.

34. Aqil M, Sultana Y, Ali A, Dubey K, Najmi A, Pillai K. Transdermal drug delivery system of a beta blocker: Design, *in vitro* and *in vivo* characterization. Drug Deliv. 2004; 11:27-31.

35. Aqil M, Ali A. Monolithic matrix type transdermal drug delivery systems of pinacidil monohydrate: *In vitro* characterisation. Eur J Pharm Biopharm. 2002; 54:161-164.

DD&T
Drug Discoveries & Therapeutics

Guide for Authors

1. Scope of Articles

Drug Discoveries & Therapeutics welcomes contributions in all fields of pharmaceutical and therapeutic research such as medicinal chemistry, pharmacology, pharmaceutical analysis, pharmaceutics, pharmaceutical administration, and experimental and clinical studies of effects, mechanisms, or uses of various treatments. Studies in drug-related fields such as biology, biochemistry, physiology, microbiology, and immunology are also within the scope of this journal.

2. Submission Types

Original Articles should be well-documented, novel, and significant to the field as a whole. An Original Article should be arranged into the following sections: Title page, Abstract, Introduction, Materials and Methods, Results, Discussion, Acknowledgments, and References. Original articles should not exceed 5,000 words in length (excluding references) and should be limited to a maximum of 50 references. Articles may contain a maximum of 10 figures and/or tables.

Brief Reports definitively documenting either experimental results or informative clinical observations will be considered for publication in this category. Brief Reports are not intended for publication of incomplete or preliminary findings. Brief Reports should not exceed 3,000 words in length (excluding references) and should be limited to a maximum of 4 figures and/or tables and 30 references. A Brief Report contains the same sections as an Original Article, but the Results and Discussion sections should be combined.

Reviews should present a full and up-to-date account of recent developments within an area of research. Normally, reviews should not exceed 8,000 words in length (excluding references) and should be limited to a maximum of 100 references. Mini reviews are also accepted.

Policy Forum articles discuss research and policy issues in areas related to life science such as public health, the medical care system, and social science and may address governmental issues at district, national, and international levels of discourse. Policy Forum articles should not exceed 2,000 words in length (excluding references).

Case Reports should be detailed reports of the symptoms, signs, diagnosis, treatment, and follow-up of an individual patient. Case reports may contain a demographic profile of the patient but usually describe an unusual or novel occurrence. Unreported or unusual side effects or adverse interactions involving medications will also be considered. Case Reports should not exceed 3,000 words in length (excluding references).

News articles should report the latest events in health sciences and medical research from around the world. News should not exceed 500 words in length.

Letters should present considered opinions in response to articles published in Drug Discoveries & Therapeutics in the last 6 months or issues of general interest. Letters should not exceed 800 words in length and may contain a maximum of 10 references.

3. Editorial Policies

Ethics: Drug Discoveries & Therapeutics requires that authors of reports of investigations in humans or animals indicate that those studies were formally approved by a relevant ethics committee or review board.

Conflict of Interest: All authors are required to disclose any actual or potential conflict of interest including financial interests or relationships with other people or organizations that might raise questions of bias in the work reported. If no conflict of interest exists for each author, please state "There is no conflict of interest to disclose".

Submission Declaration: When a manuscript is considered for submission to Drug Discoveries & Therapeutics, the authors should confirm that 1) no part of this manuscript is currently under consideration for publication elsewhere; 2) this manuscript does not contain the same information in whole or in part as manuscripts that have been published, accepted, or are under review elsewhere, except in the form of an abstract, a letter to the editor, or part of a published lecture or academic thesis; 3) authorization for publication has been obtained from the authors' employer or institution; and 4) all contributing authors have agreed to submit this manuscript.

Cover Letter: The manuscript must be accompanied by a cover letter signed by the corresponding author on behalf of all authors. The letter should indicate the basic findings of the work and their significance. The letter should also include a statement affirming that all authors concur with the submission and that the material submitted for publication has not been published previously or is not under consideration for publication elsewhere. The cover letter should be submitted in PDF format. For example of Cover Letter, please visit http://www.ddtjournal.com/downcentre.php (Download Centre).

Copyright: A signed JOURNAL PUBLISHING AGREEMENT (JPA) must be provided by post, fax, or as a scanned file before acceptance of the article. Only forms with a hand-written signature are accepted. This copyright will ensure the widest possible dissemination of information. A form facilitating transfer of copyright can be downloaded by clicking the appropriate link and can be returned to the e-mail address or fax number noted on the form (Please visit Download Centre). Please note that your manuscript will not proceed to the next step in publication until the JPA form is received. In addition, if excerpts from other copyrighted works are included, the author(s) must obtain written permission from the copyright owners and credit the source(s) in the article.

Suggested Reviewers: A list of up to 3 reviewers who are qualified to assess the scientific merit of the study is welcomed. Reviewer information including names, affiliations, addresses, and e-mail should be provided at the same time the manuscript is submitted online. Please do not suggest reviewers with known conflicts of interest, including participants or anyone with a stake in the proposed research; anyone from the same institution; former students, advisors, or research collaborators (within the last three years); or close personal contacts. Please note that the Editor-in-Chief may accept one or more of the proposed reviewers or may request a review by other qualified persons.

Language Editing: Manuscripts prepared by authors whose native language is not English should have their work proofread by a native English speaker before submission. If not, this might delay the publication of your manuscript in Drug Discoveries & Therapeutics.

The Editing Support Organization can provide English proofreading, Japanese-English translation, and Chinese-English translation services to authors who want to publish in Drug Discoveries & Therapeutics and need assistance before submitting a manuscript. Authors can visit this organization directly at http://www.iacmhr.com/iac-eso/support.php?lang=en. IAC-ESO was established to facilitate manuscript preparation by researchers whose native language is not English and to help edit works intended for international academic journals.

4. Manuscript Preparation

Manuscripts should be written in clear, grammatically correct English and submitted as a Microsoft Word file in a single-column format. Manuscripts must be paginated and typed in 12-point Times New Roman font with 24-point line spacing. Please do not embed figures in the text. Abbreviations should be used as little as possible and should be explained at first mention unless the term is a well-known abbreviation (*e.g.* DNA). Single words should not be abbreviated.

Title page: The title page must include 1) the title of the paper (Please note the title should be short, informative, and contain the major key words); 2) full name(s) and affiliation(s) of the author(s), 3) abbreviated names of the author(s), 4) full name, mailing address, telephone/fax numbers, and e-mail address of the corresponding author; and 5) conflicts of interest (if you have an actual or potential conflict of interest to disclose, it must be included as a footnote on the title page of the manuscript; if no conflict of interest exists for each author, please state "There is no conflict of interest to disclose"). Please visit Download Centre and refer to the title page of the manuscript sample.

Abstract: A one-paragraph abstract consisting of no more than 250 words must be included. The abstract should briefly state the purpose of the study, methods, main findings, and conclusions. Abbreviations must be kept to a minimum and non-standard abbreviations explained in brackets at first mention. References should be avoided in the abstract. Key words or phrases that do not occur in the title should be included in the Abstract page.

Introduction: The introduction should be a concise statement of the basis for the study and its scientific context.

Materials and Methods: The description should be brief but with sufficient detail to enable others to reproduce the experiments. Procedures that have been published previously should not be described in detail but appropriate references should simply be cited. Only new and significant modifications of previously published procedures require complete description. Names of products and manufacturers with their locations (city and state/country) should be given and sources of animals and cell lines should always be indicated. All clinical investigations must have been conducted in accordance with Declaration of Helsinki principles. All human and animal studies must have been approved by the appropriate institutional review board(s) and a specific declaration of approval must be made within this section.

Results: The description of the experimental results should be succinct but in sufficient detail to allow the experiments to be analyzed and interpreted by an independent reader. If necessary, subheadings may be used for an orderly presentation. All figures and tables must be referred to in the text.

Discussion: The data should be interpreted concisely without repeating material already presented in the Results section. Speculation is permissible, but it must be well-founded, and discussion of the wider implications of the findings is encouraged. Conclusions derived from the study should be included in this section.

Acknowledgments: All funding sources should be credited in the Acknowledgments section. In addition, people who contributed to the work but who do not meet the criteria for authors should be listed along with their contributions.

References: References should be numbered in the order in which they appear in the text. Citing of unpublished results, personal communications, conference abstracts, and theses in the reference list is not recommended but these sources may be mentioned in the text. In the reference list, cite the names of all authors when there are fifteen or fewer authors; if there are sixteen or more authors, list the first three followed by *et al*. Names of journals should be abbreviated in the style used in PubMed. Authors are responsible for the accuracy of the references. Examples are given below:

Example 1 (Sample journal reference):
Nakata M, Tang W. Japan-China Joint Medical Workshop on Drug Discoveries and Therapeutics 2008: The need of Asian pharmaceutical researchers' cooperation. Drug Discov Ther. 2008; 2:262-263.

Example 2 (Sample journal reference with more than 15 authors):
Darby S, Hill D, Auvinen A, *et al*. Radon in homes and risk of lung cancer: Collaborative analysis of individual data from 13 European case-control studies. BMJ. 2005; 330:223.

Example 3 (Sample book reference):
Shalev AY. Post-traumatic stress disorder: diagnosis, history and life course. In: Post-traumatic Stress Disorder, Diagnosis, Management and Treatment (Nutt DJ, Davidson JR, Zohar J, eds.). Martin Dunitz, London, UK, 2000; pp. 1-15.

Example 4 (Sample web page reference):
World Health Organization. The World Health Report 2008 – primary health care: Now more than ever. *http://www.who.int/whr/2008/whr08_en.pdf* (accessed September 23, 2010).

Tables: All tables should be prepared in Microsoft Word or Excel and should be arranged at the end of the manuscript after the References section. Please note that tables should not in image format. All tables should have a concise title and should be numbered consecutively with Arabic numerals. If necessary, additional information should be given below the table.

Figure Legend: The figure legend should be typed on a separate page of the main manuscript and should include a short title and explanation. The legend should be concise but comprehensive and should be understood without referring to the text. Symbols used in figures must be explained.

Figure Preparation: All figures should be clear and cited in numerical order in the text. Figures must fit a one- or two-column format on the journal page: 8.3 cm (3.3 in.) wide for a single column, 17.3 cm (6.8 in.) wide for a double column; maximum height: 24.0 cm (9.5 in.). Please make sure that artwork files are in an acceptable format (TIFF or JPEG) at minimum resolution (600 dpi for illustrations, graphs, and annotated artwork, and 300 dpi for micrographs and photographs). Please provide all figures as separate files. Please note that low-resolution images are one of the leading causes of article resubmission and schedule delays. All color figures will be reproduced in full color in the online edition of the journal at no cost to authors.

Units and Symbols: Units and symbols conforming to the International System of Units (SI) should be used for physicochemical quantities. Solidus notation (*e.g.* mg/kg, mg/mL, mol/mm^2/min) should be used. Please refer to the SI Guide www.bipm.org/en/si/ for standard units.

Supplemental data: Supplemental data might be useful for supporting and enhancing your scientific research and Drug Discoveries & Therapeutics accepts the submission of these materials which will be only published online alongside the electronic version of your article. Supplemental files (figures, tables, and other text materials) should be prepared according to the above guidelines, numbered in Arabic numerals (*e.g*., Figure S1, Figure S2, and Table S1, Table S2) and referred to in the text. All figures and tables should have titles and legends. All figure legends, tables and supplemental text materials should be placed at the end of the paper. Please note all of these supplemental data should be provided at the time of initial submission and note that the editors reserve the right to limit the size and length of Supplemental Data.

5. Submission Checklist

The Submission Checklist will be useful during the final checking of a manuscript prior to sending it to Drug Discoveries & Therapeutics for review. Please visit Download Centre and download the Submission Checklist file.

6. Online submission

Manuscripts should be submitted to Drug Discoveries & Therapeutics online at http://www.ddtjournal.com. The manuscript file should be smaller than 5 MB in size. If for any reason you are unable to submit a file online, please contact the Editorial Office by e-mail at office@ddtjournal.com

7. Accepted manuscripts

Proofs: Galley proofs in PDF format will be sent to the corresponding author *via* e-mail. Corrections must be returned to the editor (proof-editing@ddtjournal.com) within 3 working days.

Offprints: Authors will be provided with electronic offprints of their article. Paper offprints can be ordered at prices quoted on the order form that accompanies the proofs.

Page Charge: A page charge of $140 will be assessed for each printed page of an accepted manuscript. The charge for printing color figures is $340 for each page. The total charge may be reduced or waived in accordance with conditions in the country where the study took place.

(Revised February 2011)

JOURNAL PUBLISHING AGREEMENT (JPA)

Manuscript No:

Title:

Corresponding author:

The International Advancement Center for Medicine & Health Research Co., Ltd. (IACMHR Co., Ltd.) is pleased to accept the above article for publication in Drug Discoveries & Therapeutics. The International Research and Cooperation Association for Bio & Socio-Sciences Advancement (IRCA-BSSA) reserves all rights to the published article. Your written acceptance of this JOURNAL PUBLISHING AGREEMENT is required before the article can be published. Please read this form carefully and sign it if you agree to its terms. The signed JOURNAL PUBLISHING AGREEMENT should be sent to the Drug Discoveries & Therapeutics office (Pearl City Koishikawa 603, 2-4-5 Kasuga, Bunkyo-ku, Tokyo 112-0003, Japan; E-mail: office@ddtjournal.com; Tel: +81-3-5840-9697; Fax: +81-3-5840-9698).

1. Authorship Criteria

As the corresponding author, I certify on behalf of all of the authors that:

1) The article is an original work and does not involve fraud, fabrication, or plagiarism.

2) The article has not been published previously and is not currently under consideration for publication elsewhere. If accepted by Drug Discoveries & Therapeutics, the article will not be submitted for publication to any other journal.

3) The article contains no libelous or other unlawful statements and does not contain any materials that infringes upon individual privacy or proprietary rights or any statutory copyright.

4) I have obtained written permission from copyright owners for any excerpts from copyrighted works that are included and have credited the sources in my article.

5) All authors have made significant contributions to the study including the conception and design of this work, the analysis of the data, and the writing of the manuscript.

6) All authors have reviewed this manuscript and take responsibility for its content and approve its publication.

7) I have informed all of the authors of the terms of this publishing agreement and I am signing on their behalf as their agent.

2. Copyright Transfer Agreement

I hereby assign and transfer to IACMHR Co., Ltd. all exclusive rights of copyright ownership to the above work in the journal Drug Discoveries & Therapeutics, including but not limited to the right 1) to publish, republish, derivate, distribute, transmit, sell, and otherwise use the work and other related material worldwide, in whole or in part, in all languages, in electronic, printed, or any other forms of media now known or hereafter developed and the right 2) to authorize or license third parties to do any of the above.

   I understand that these exclusive rights will become the property of IACMHR Co., Ltd., from the date the article is accepted for publication in the journal Drug Discoveries & Therapeutics. I also understand that IACMHR Co., Ltd. as a copyright owner has sole authority to license and permit reproductions of the article.

   I understand that except for copyright, other proprietary rights related to the Work (*e.g.* patent or other rights to any process or procedure) shall be retained by the authors. To reproduce any text, figures, tables, or illustrations from this Work in future works of their own, the authors must obtain written permission from IACMHR Co., Ltd.; such permission cannot be unreasonably withheld by IACMHR Co., Ltd.

3. Conflict of Interest Disclosure

I confirm that all funding sources supporting the work and all institutions or people who contributed to the work but who do not meet the criteria for authors are acknowledged. I also confirm that all commercial affiliations, stock ownership, equity interests, or patent-licensing arrangements that could be considered to pose a financial conflict of interest in connection with the article have been disclosed.

Corresponding Author's Name (Signature):

Date:

Drug Discoveries & Therapeutics (www.ddtjournal.com)

Pearl City Koishikawa 603, 2-4-5 Kasuga, Bunkyo-ku, Tokyo 112-0003, Japan; E-mail: office@ddtjournal.com; Tel: +81-3-5840-9697; Fax: +81-3-5840-9698